

Article

Atypical Mineralization Involving Pd-Pt, Au-Ag, REE, Y, Zr, Th, U, and Cl-F in the Oktyabrsky Deposit, Norilsk Complex, Russia

Andrei Y. Barkov ^{1,*}, Ivan I. Nikulin ², Andrey A. Nikiforov ¹, Boris M. Lobastov ³, Sergey A. Silyanov ³  and Robert F. Martin ⁴

¹ Research Laboratory of Industrial and Ore Mineralogy, Cherepovets State University, 5 Lunacharsky Prospect, 162600 Cherepovets, Russia; ultramafic-rocks@mail.ru

² Norilskgeologiya OOO, 11 Grazhdansky Prospect, 195220 Saint-Petersburg, Russia; iinikulin@gmail.com

³ Institute of Mining, Geology and Geotechnology, Siberian Federal University, 79 Svobodny Prospect, 660041 Krasnoyarsk, Russia; lbm02@ya.ru (B.M.L.); silyanov-s@mail.ru (S.A.S.)

⁴ Department of Earth and Planetary Sciences, McGill University, 3450 University Street, Montreal, QC H3A 0E8, Canada; robert.martin@mcgill.ca

* Correspondence: ore-minerals@mail.ru; Tel.: +7-(8202)-55-65-97



Citation: Barkov, A.Y.; Nikulin, I.I.; Nikiforov, A.A.; Lobastov, B.M.; Silyanov, S.A.; Martin, R.F. Atypical Mineralization Involving Pd-Pt, Au-Ag, REE, Y, Zr, Th, U, and Cl-F in the Oktyabrsky Deposit, Norilsk Complex, Russia. *Minerals* **2021**, *11*, 1193. <https://doi.org/10.3390/min11111193>

Academic Editor: Liqiang Yang

Received: 28 September 2021

Accepted: 19 October 2021

Published: 27 October 2021

Publisher's Note: MDPI stays neutral with regard to jurisdictional claims in published maps and institutional affiliations.



Copyright: © 2021 by the authors. Licensee MDPI, Basel, Switzerland. This article is an open access article distributed under the terms and conditions of the Creative Commons Attribution (CC BY) license (<https://creativecommons.org/licenses/by/4.0/>).

Abstract: Highly atypical mineralization involving Pd-Pt, Au-Ag, REE, Y, Zr, U, Th, and Cl-F enriched minerals is found in zones with base metal sulfides (BMS; ~5 vol.% to 20 vol.%) in the eastern portion of the Oktyabrsky deposit in the Norilsk complex (Russia). The overall variations in Mg# index, 100 Mg/(Mg + Fe²⁺ + Mn), in host-rock minerals are 79.8 → 74.1 in olivine, 77.7 → 65.3 in orthopyroxene, 79.9 → 9.2 in clinopyroxene, and An_{79.0} → An_{3.7}. The span of clinopyroxene and plagioclase compositions reflects their protracted crystallization from early magmatic to late interstitial associations. The magnesian chromite (Mg# 43.9) trends towards Cr-bearing magnetite with progressive buildups in oxygen fugacity; ilmenite varies from early Mg-rich to late Mn-rich variants. The main BMS are chalcopyrite, pyrrhotite, troilite, and Co-bearing pentlandite, with less abundant cubanite (or isocubanite), rare bornite, Co-bearing pyrite, Cd-bearing sphalerite (or wurtzite), altaite, members of the galena-clausthalite series and nickeline. A full series of Au-Ag alloy compositions is found with minor hessite, acanthite and argentopentlandite. The uncommon assemblage includes monazite-(Ce), thorite-coffinite, thorianite, uraninite, zirconolite, baddeleyite, zircon, bastnäsite-(La), and an unnamed metamict Y-dominant zirconolite-related mineral. About 20 species of PGM (platinum group minerals) were analyzed, including Pd-Pt tellurides, bismuthotellurides, bismuthides and stannides, Pd antimonides and plumbides, a Pd-Ag telluride, a Pt arsenide, a Pd-Ni arsenide, and unnamed Pd stannide-arsenide, Pd germanide-arsenide and Pt-Cu arsено-oxysulfide. The atypical assemblages are associated with Cl-rich annite with up to 7.54 wt.% Cl, Cl-rich hastingsite with up 4.06 wt.% Cl, ferro-hornblende (2.53 wt.% Cl), chlorapatite (>6 wt.% Cl) and extensive solid solutions of chlorapatite, fluorapatite and hydroxylapatite, Cl-bearing members of the chlorite group (chamosite; up to 0.96 wt.% Cl), and a Cl-bearing serpentine (up to 0.79 wt.% Cl). A decoupling of Cl and F in the geochemically evolved system is evident. The complex assemblages formed late from Cl-enriched fluids under subsolidus conditions of crystallization following extensive magmatic differentiation in the ore-bearing sequences.

Keywords: Pd-Pt and Au-Ag mineralization; REE; Y; Zr; U and Th mineralization; platinum group minerals; base metal sulfides; fluids enriched in chlorine; basic-ultrabasic rocks; Oktyabrsky deposit; Norilsk complex; Russia

1. Introduction and Geological Context

The Norilsk complex of Permo-Triassic age hosts giant ore deposits, such as the Oktyabrsky deposit of copper, nickel and platinum group elements (PGE), developed close to the northwestern margin of the Siberian Platform in northern Russia (e.g., [1], and [4.0]).

references therein). These deposits are genetically related to large-scale sills of gabbro-dolerite and olivine gabbro-dolerite whose emplacement was largely controlled by the NNE-trending Norilsk-Kharayelakh fault (Norilsko-Kharaelakhskiy, Figure 1). They are considered to be feeders of trap basalts, which attain 3.5 km in thickness. Understandably, the Norilsk complex was (and still is) a Mecca for international teams of investigators; indeed, thousands of research articles describe various characteristics of its mineralogy, geology, petrology and geochemistry, and consider models of origin [1–10]. At the same time, there are mineralized zones of relatively low-grade ores, especially those deposited in peripheral areas or in the vicinity of external contacts, which are much less thoroughly investigated, and thus deserve more attention. In this sense, our goals are focused here on mineralogical studies of ore-bearing zones that have developed in the eastern portion and relatively close to contacts of the Oktyabrsky Cu-Ni-PGE deposit (Figure 1). Some of our findings are new and unusual, and these implications extend our insight into the geochemical evolution and ore potential of the Norilsk complex.

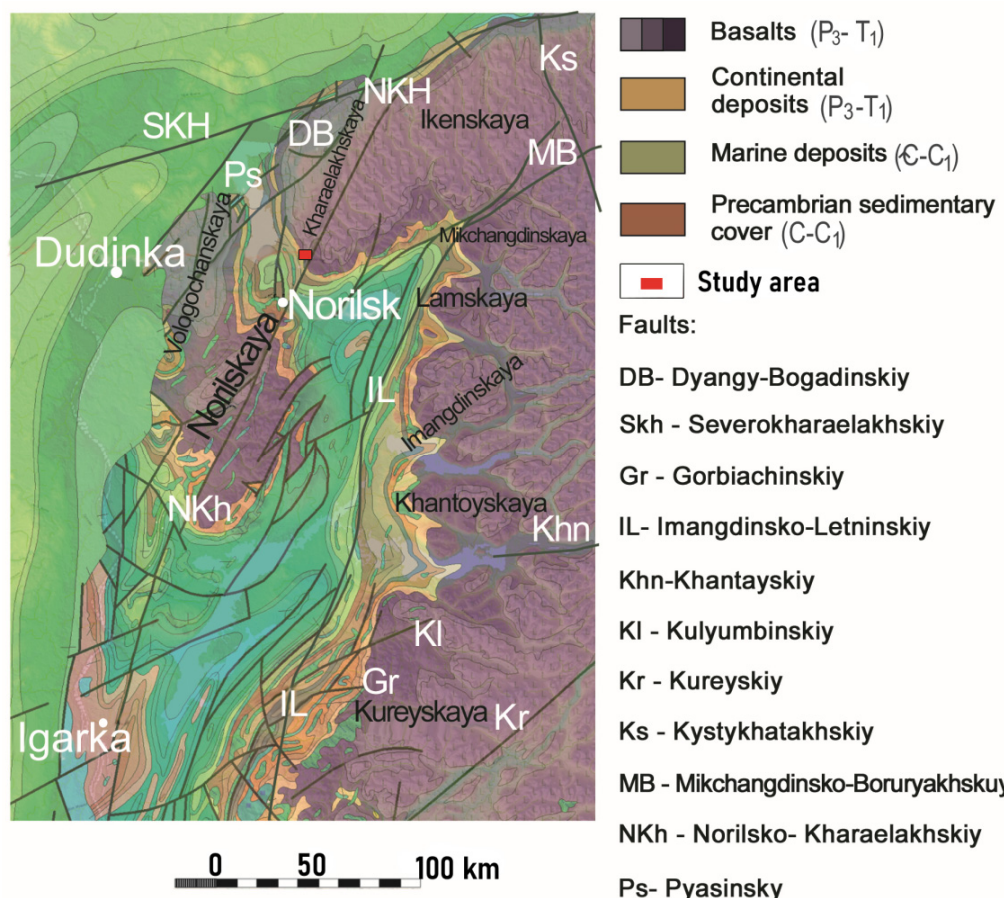


Figure 1. Generalized scheme of geology of the Norilsk area, after [1] and references therein. The labels from DB to Ps pertain to original names of the regional faults, which are used historically in the Russian literature. The study area is shown schematically by the red square symbol.

2. Materials and Methods

A total of twenty-six ore-bearing samples collected in a series of boreholes (Figure 2) were studied mineralogically. Quantitative analyses of minerals were performed at the R&D center of Norilsk Nickel at the Institute of Mining, Geology and Geotechnology of the Siberian Federal University, Krasnoyarsk, by means of scanning electron microscopy and energy-dispersive analysis (SEM-EDS) done on a Tescan Vega III SBH system (Tescan Orsay Holding, Brno, Czech Republic) equipped with an Oxford X-Act spectrometer (Oxford

Instruments Nanoanalysis, Wycombe, UK). The operating conditions were held at an accelerating voltage of 20 kV and a beam current of 1.2 nA.

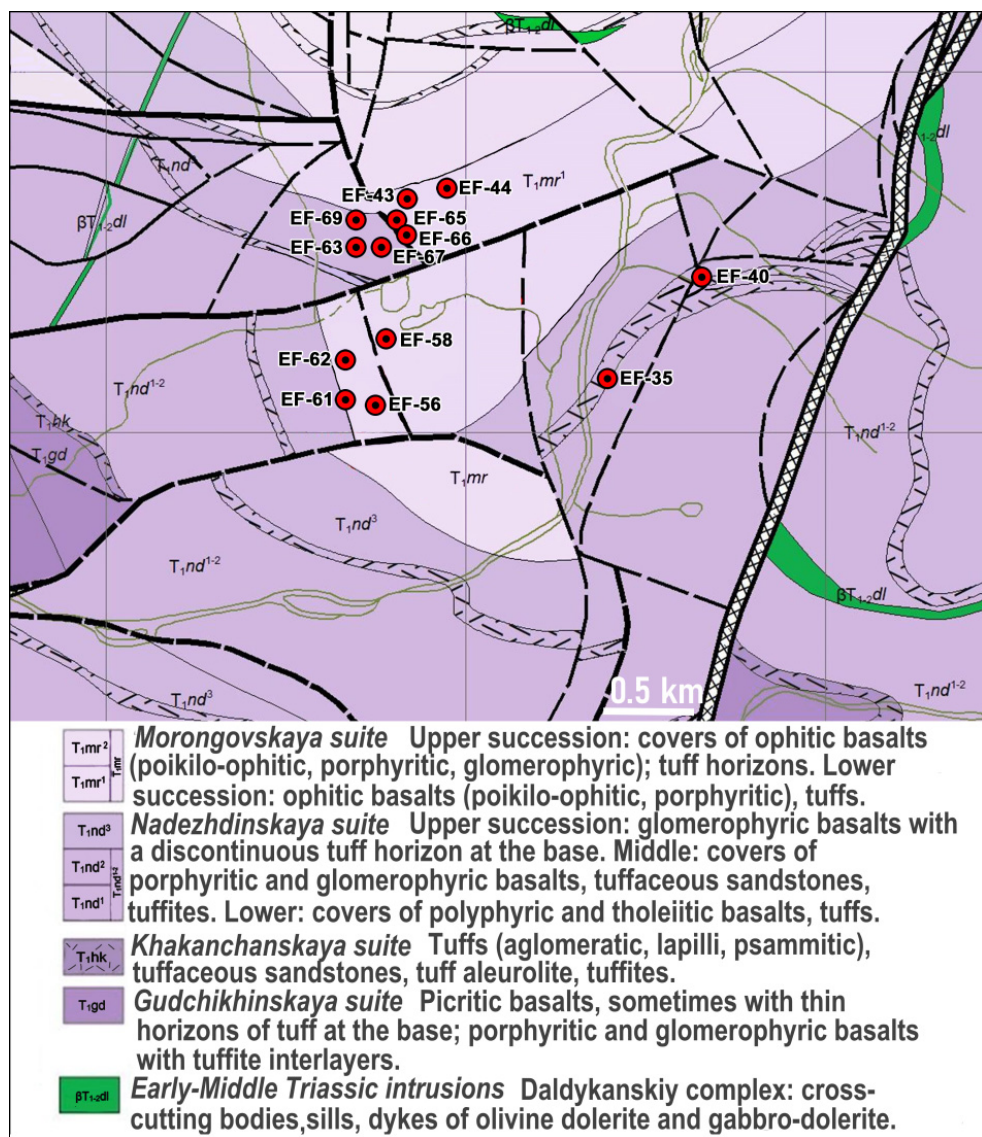


Figure 2. Geology of the area investigated, with the location of boreholes sampled in the eastern portion of the Oktyabrsky ore deposit. The study area is shown in Figure 1.

The commonly used combinations of X-ray lines were used along with a set of standards provided by Micro-Analysis Consultants Ltd. (MAC, Cambridgeshire, UK; registration no. 11192). The K line was used for oxygen, Si (quartz standard), Ca (wollastonite), K (orthoclase), Na (albite), Cu (synthetic chalcopyrite), Fe, S (pyrite and pyrrhotite) and Ni, as well as Co, Ti, V and Cr; specimens of Al_2O_3 were used for Al, MgO for Mg, pure Mn for Mn, sphalerite for Zn, and synthetic GaP for P. The F- and Cl-bearing minerals were also analyzed using the K line, with specimens of fluorite and halite as standards. Furthermore, the L line and standards of pure elements were used for Y, La, Pr, Nd, Pm, Sm, Eu, Gd, Tb, Dy, Ho, Er, Tm, and Yb. The L line and synthetic CeO_2 and LaB_6 were used for Ce and La. The L line was also used for Nb, Ag, Se and Sb (pure elements and stibnite as standards), as well as for Zr, Cd (pure Zr and Cd), Sn (pure Sn), Te (PbTe), As (arsenopyrite), and Pd and Rh (pure Pd and Rh). The M line was used for Au (pure Au), Ir (Ir), Os (Os), Pt (Pt), Bi (pure Bi), Pb (PbTe), Th (ThO_2), U (pure U), and also for Hf (pure Hf). The beam current was measured every 60 min using the MAC cobalt standard (registration no. 9941).

In total, more than two thousand SEM-EDS point-analyses were made. The analytical error for the main components did not exceed 2–3 relative percent and satisfied the requirements for a quantitative analysis. As a test, some of the ore minerals were analyzed by wavelength-dispersive spectroscopy (WDS) on a JEOL JXA-8100 electron microprobe at the Institute of Geology and Mineralogy, Siberian Branch of the Russian Academy of Sciences in Novosibirsk; the results of these tests were in good mutual agreement.

Reflectance measurements were performed using a LomoMSFU-KYu-30.54.072 microspectrophotometer (OOO “Lomo”, St. Petersburg, Russia), using a single-crystal silicon standard (KEF 4.5/0.3) provided by the S.I. Vavilov State Optical Institute, an All-Russian Research Center in St. Petersburg, Russia.

3. Results and Observations

Mineral associations and compositional variations were examined in ore-bearing samples in the differentiated sequences of picritic, “taxitic” and olivine-bearing gabbro-dolerite in the eastern portion of the Oktyabrsky deposit (Figure 2). These rocks typically contain about 5 vol. % to 20 vol. % base metal sulfide minerals (BMS) that occur as primary disseminations, angular or droplet-like grains, or as interstitial grains with an irregular shape (e.g., Figure 3a).

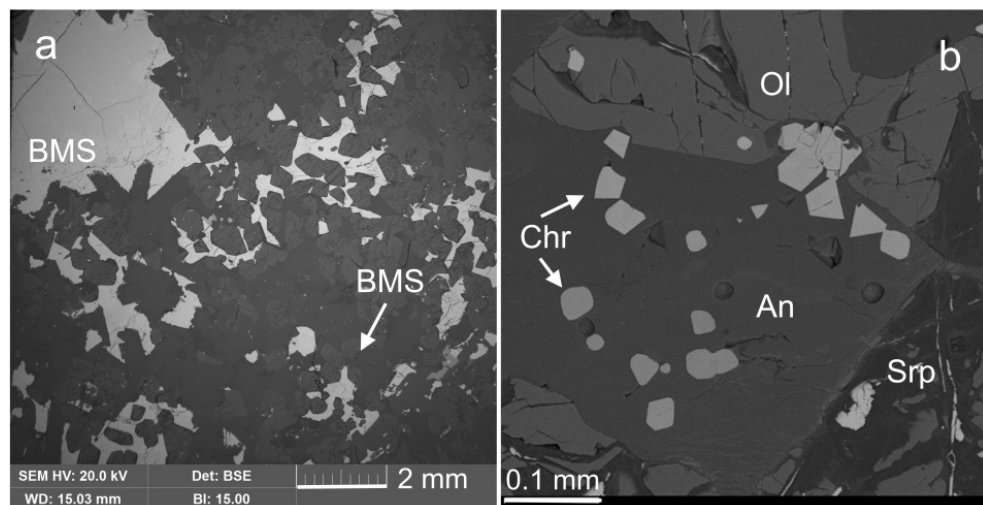


Figure 3. (a) shows the representative texture of mineralized gabbro-dolerite; it consists of large interstitial grains of base metal sulfides (BMS) hosted by a fine-grained matrix of rock-forming silicates (gray). (b) displays an aggregate of euhedral grains of chromian spinel (Chr) associated with olivine (Ol) and a calcic plagioclase (An). Srp is a member of the serpentine group. These back-scattered electron images (BEI) were obtained by scanning electron microscopy (SEM).

3.1. Rock-Forming Minerals and the Accessory Fe-Cr-(Ti) Oxides

The overall variations in the composition of rock-forming silicates are displayed in Tables 1 and 2. Olivine grains vary compositionally in the range of Mg# values, i.e., $100 \text{Mg}/(\text{Mg} + \text{Fe}^{2+} + \text{Mn})$, from 79.8 to 74.1. Grains of orthopyroxene display the range 78.0–65.3. In contrast, compositions of clinopyroxene exhibit much more extensive variations in the diopside-hedenbergite series, with Mg# values in the range 79.9–9.2. The unusually low Mg compositions formed late in the crystallization history (Table 1, Figure 4a). The compositions of plagioclase also cover an impressive range, from early An_{79.0} to Ab_{96.3}, with the sodic members of the series present in the “intercumulus” (interstitial) association (Table 2, Figure 4b).

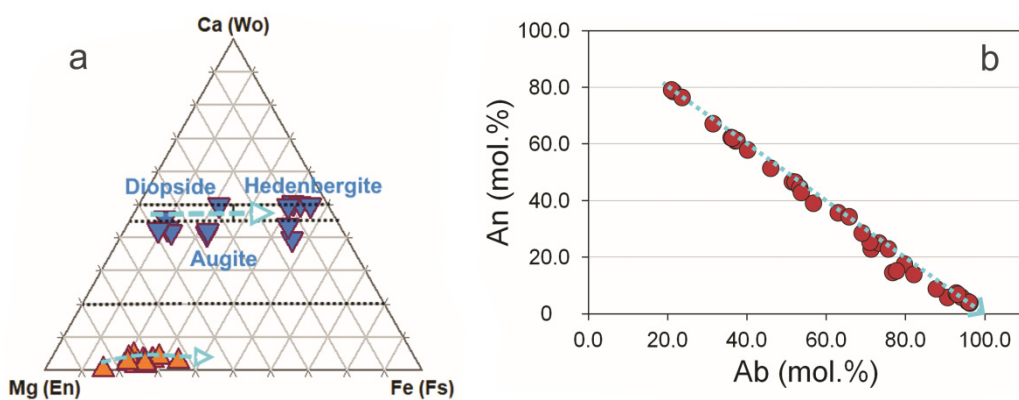


Figure 4. (a) shows the compositional ranges of monoclinic and orthorhombic pyroxenes, shown by the blue and orange symbols, respectively, in terms of a Ca-Mg-Fe plot. The samples were taken from mineralized zones in the eastern portion of the Oktyabrsky ore deposit. Labels: Wo is wollastonite; En is enstatite, and Fs is ferrosilite. The pyroxene nomenclature is after [11]. (b) displays the existence of a continuous series of compositions of plagioclase in these zones, in terms of the components albite (Ab) and anorthite (An).

Table 1. Compositions of grains of olivine and pyroxenes in the eastern portion of the Oktyabrsky ore deposit.

#	Sample		SiO ₂	TiO ₂	Al ₂ O ₃	FeO	MnO	MgO	CaO	Total (wt.%)	Mg#
1	EF0040-1706.4	Ol	39.00	0	0	21.91	0.48	38.80	0.08	100.27	75.5
2	EF0040-1706.4		38.68	0	0	22.33	0.35	39.10	0.20	100.66	75.4
3	EF0043-1748.4		39.62	0	0	23.43	0.39	38.14	0.15	101.73	74.1
4	EF0065-1714.8		39.21	0	0	21.15	0.49	39.62	0	100.47	76.5
5	EF0066-1684.4		39.92	0	0	20.88	0.45	39.90	0	101.15	76.9
6	EF0066-1684.4		40.20	0	0	18.73	0.36	42.32	0	101.61	79.8
7	EF0069-1743.6		39.09	0	0	21.68	0	38.89	0	99.66	76.2
8	EF8057-1572.3		39.22	0	0	19.96	0.35	40.49	0	100.01	78.0
9	EF0040-1706.4	Opx	54.60	0	0	18.51	0	26.86	1.51	101.48	75.6
10	EF0040-1706.4		55.45	0	0.36	15.80	0.37	27.08	0.76	99.82	73.9
11	EF0042-1722.3		52.84	0	0	17.32	0.56	25.77	1.43	97.92	74.9
12	EF0042-1722.3		56.05	0.68	0.96	14.04	0	27.03	2.18	100.94	74.3
13	EF0043-1764.3		52.52	0.68	0.77	17.69	0.48	24.13	1.82	98.09	70.4
14	EF0062-1597.4		54.64	0.37	0	15.48	0	27.73	0.57	98.79	76.1
15	EF0063-1744.3		53.36	0	0	21.09	0.87	22.77	1.25	99.34	65.3
16	EF0065-1714.8		56.97	0	0	13.69	0	28.34	1.75	100.75	76.7
17	EF0065-1714.8		54.75	0	0	16.22	0	26.73	1.44	99.14	74.9
18	EF0065-1714.8		57.01	0	0	14.87	0	28.80	1.22	101.90	77.1
19	EF67-1707.8		54.83	0	1.10	16.79	0	26.12	0.64	99.48	71.9
20	EF67-1707.8		56.29	0	0	16.31	0.39	26.81	1.36	101.16	72.9
21	EF0069-1743.6		57.33	0.45	0	13.83	0.52	29.43	1.11	102.67	77.7
22	EF0035-1553.75	Cpx	51.19	0	0	23.32	1.32	2.98	23.93	102.74	17.4
23	EF0040-1706.4		55.49	0	0	7.19	0	16.90	21.91	101.49	78.7
24	EF0043-1764.3		51.84	0	0.77	13.88	0	12.60	19.97	99.06	61.7
25	EF0061-1603.3		48.41	0	0	26.45	0.71	4.89	18.54	99.00	25.5
26	EF0065-1713.3		55.54	0	0.81	5.87	0	16.37	23.28	101.87	79.8
27	EF0066-1684.4		52.38	0	0	12.42	0.85	10.05	24.34	100.03	56.9
28	EF67-1707.8		48.99	0	0	24.25	0.87	2.35	23.14	99.60	14.5
29	EF0069-1757.8		50.47	0	0	22.54	0.85	3.53	22.85	100.24	20.2
30	EF8057-1572.3		56.52	0	0.94	5.76	0	17.81	21.74	102.77	79.9
31	EF00566-1568.7		52.82	0	0	13.30	0.65	12.57	20.67	100.01	61.1
32	EF00566-1568.7		48.24	0	0.77	23.86	2.40	1.48	22.60	99.35	9.2

Note. These results of SEM-EDS analyses are listed in weight %. Ol is olivine; Opx is orthopyroxene; and Cpx is clinopyroxene. Zero stands for “not detected” or “not analyzed”. Mg# = 100 Mg/(Mg + Fe²⁺ + Mn).

Table 2. Compositions of grains of plagioclase in the eastern portion of the Oktyabrsky ore deposit.

#	Sample	SiO ₂	Al ₂ O ₃	FeO	CaO	Na ₂ O	K ₂ O	Total (wt.%)	An (mol.%)	Ab	Or
1	EF0035-1546.2	52.95	28.89	1.51	12.22	3.91	0.29	99.77	62.2	36.0	1.8
2	EF0035-1553.75	69.25	20.09	0.57	1.12	9.81	0.61	101.45	5.7	90.6	3.7
3	EF0035-1553.75	68.67	18.71	0	0.71	10.14	0	98.23	3.7	96.3	0.0
4	EF0040-1706.4	62.70	22.56	0.49	4.39	7.59	0.95	98.68	22.8	71.3	5.9
5	EF0040-1706.4	66.08	21.58	0.39	2.94	8.59	1.49	101.07	14.5	76.7	8.8
6	EF0040-1706.4	53.23	29.59	0.81	12.61	4.23	0.31	100.78	61.1	37.1	1.8
7	EF0043-1748.4	64.27	23.85	0.59	5.12	8.33	0.30	102.46	24.9	73.3	1.7
8	EF0043-1748.4	60.93	25.32	0.67	7.18	7.00	0.22	101.32	35.7	63.0	1.3
9	EF0043-1764.3	54.60	28.81	0.62	12.79	4.33	0.24	101.39	61.2	37.5	1.4
10	EF0061-1603.3	66.98	22.28	0.32	3.11	8.83	1.23	102.75	15.1	77.7	7.1
11	EF0061-1603.3	70.26	20.52	0	0.91	11.05	0	102.74	4.4	95.6	0.0
12	EF0063-1744.3	57.04	27.13	0.85	9.47	5.88	0.25	100.62	46.4	52.1	1.5
13	EF0065-1713.3	64.52	22.64	0.53	4.44	8.13	0.24	100.50	22.8	75.7	1.5
14	EF0065-1714.8	52.31	30.91	0.60	13.73	3.56	0.25	101.36	67.1	31.5	1.5
15	EF0065-1714.8	58.21	26.68	0.58	9.46	6.28	0.39	101.60	44.4	53.4	2.2
16	EF0066-1684.4	48.95	32.14	0.42	16.19	2.45	0	100.15	78.5	21.5	0.0
17	EF0066-1726.05	58.23	25.96	0.75	8.73	6.05	0.60	100.32	42.8	53.7	3.5
18	EF67-1707.8	67.15	21.45	0.94	2.83	9.26	0.69	102.32	13.9	82.1	4.0
19	EF67-1712.0	53.08	28.53	1.26	11.53	4.42	0.33	99.15	57.9	40.2	2.0
20	EF67-1724.65	53.01	29.46	0.72	12.55	4.06	0.27	100.07	62.1	36.3	1.6
21	EF67-1724.65	59.58	25.26	0.64	7.89	6.34	0.71	100.42	39.0	56.8	4.2
22	EF0069-1743.6	61.83	23.81	0.51	5.74	7.70	0.42	100.01	28.5	69.1	2.5
23	EF0069-1743.6	49.48	32.93	0	15.71	2.31	0	100.43	79.0	21.0	0.0
24	EF0069-1743.6	51.26	32.46	0.54	15.81	2.71	0	102.78	76.3	23.7	0.0
25	EF0062-1615.4	65.81	20.35	0.78	1.37	9.75	0	98.06	7.2	92.8	0.0
26	EF0066-1717	67.75	19.54	0.54	0.78	10.43	0	99.04	4.0	96.0	0.0
27	EF0066-1717	65.79	20.20	2.47	1.75	9.61	0.57	100.39	8.8	87.7	3.4

Note: These results of SEM-EDS analyses are listed in weight %. Zero stands for “not detected” or “not analyzed”. Proportions of end members (An: anorthite; Ab: albite; and Or: orthoclase) are expressed in mol.%.

Species of Cr-Ti oxides form part of the ore assemblage (Table 3). Accessory grains and aggregates of chromite and Cr-bearing magnetite, hereafter referred to as chromian spinel (Chr) for the sake of simplicity, and ilmenite (Ilm) attain 0.1–0.2 mm in size (Figures 3b and 5a,b and Table 4). The compositions of chromian spinel display a trend of Fe³⁺ enrichment during crystallization, a reflection of the increasing amounts of the magnetite component (Figure 6a). They display a positive correlation of Al vs. Mg, with a coefficient R of 0.88 based on a total of 33 data-points ($n = 33$). Additionally, they display a gradual decrease in Mg and Al during crystallization, i.e., in the spinel component (MgAl₂O₄). Notable levels of Ti (up to 5% TiO₂; Table 4) are characteristic of the chromian spinel, as is typical of the Norilsk complex (e.g., [12]). The ilmenite contains up to 5.42 wt.% MgO, i.e., the geikielite component. In addition, grains enriched in the pyrophanite component contain up to 5.05 wt.% MnO.

Table 3. List of ore minerals in the investigated zones of mineralization in the eastern portion of the Oktyabrsky ore deposit.

#	Speciation	Mineral	Compositional Variety	Main or Common	Subordinate	Minor or Rare
1	Base metal sulfides	Pyrrhotite; Fe_{1-x}S	Ni-Cu-bearing Troilite; FeS	×		
2		Chalcopyrite; CuFeS_2		×		
3		Pentlandite ($\text{Fe},\text{Ni})_9\text{S}_8$	Co-bearing	×		
4		Cubanite (and/or isocubanite); CuFe_2S_3			×	
5		Bornite; Cu_5FeS_4				×
6		Pyrite; FeS_2	Co-bearing			×
7	Pb sulfide	Galena; PbS	Se-bearing			×
8	Ag-Fe-Ni sulfide	Argentopenitlandite; $\text{Ag}(\text{Fe},\text{Ni})_8\text{S}_8$				×
9	Zn sulfide	Sphalerite (and/or wurtzite); ZnS	Fe-Cd-bearing			×
10	Ag sulfide	Acanthite; Ag_2S				×
11	Ag telluride	Hessite; Ag_2Te				×
12	Pb telluride	Altaite; PbTe	Se-bearing			×
13	Pb selenide	Clausthalite; PbSe	S-bearing			×
14	Ni arsenide	Nickelinite NiAs				×
15	Au-Ag alloys	Native silver	Au-bearing			×
16		Native gold	Ag-bearing			×
17	Fe-Cr-Ti oxides	Chromite; FeCr_2O_4	Mg-(Ti)-bearing		×	
18		Magnetite; Fe_3O_4	Cr-(Ti)-bearing		×	
19		Ilmenite; FeTiO_3	Mg-Mn-bearing		×	
20	Zr silicate	Zircon; ZrSiO_4	Hf-bearing			×
21	Th silicate	Thorite; ThSiO_4	Solid solution with coffinite; $\text{U}(\text{SiO}_4)_{1-x}(\text{OH})_{4x}$			×
22	Zr oxide	Baddeleyite; ZrO_2	Hf-bearing			×
23	Zr-Ti oxide	Zirconolite; $(\text{Ca},\text{Y})\text{ZrTi}_2\text{O}_7$	Th-(Fe)-bearing			×
24	Th-U oxydes	Thorianite; ThO_2				×
25		Uraninite; UO_2	$\text{U}(\text{SiO}_4)_{1-x}(\text{OH})_{4x}$			×
26	Ce-REE phosphate	Monazite-(Ce); $(\text{Ce},\text{La},\text{Nd},\text{Th})\text{PO}_4$				×
27	A zirconolite-type oxide (Ca-dominant)	Unnamed $(\text{Ca},\text{Y},\text{REE})_2\text{Zr}_2\text{Ti}(\text{Ti},\text{Nb})_2\text{Fe}^{2+}\text{O}_{14}$				×
28	A zirconolite-type oxide (Y-dominant)	Unnamed $(\text{Y},\text{Ca},\text{REE})_2\text{Zr}_2\text{Ti}(\text{Ti},\text{Nb})_2\text{Fe}^{2+}\text{O}_{14}$				×
29	La-dominant carbonate-fluoride	Bastnäsite(?) $(\text{La},\text{Ce},\text{Y})\text{CO}_3\text{F}$				×
30	Pd-(Ag)-Pt tellurides, bismuthotellurides and bismuthides	Kotulskite; PdTe	Bi-Sb-bearing	×		

Table 3. *Cont.*

#	Speciation	Mineral	Compositional Variety	Main or Common	Subordinate	Minor or Rare
31		Sobolevskite; PdBi	Te-Sb-bearing	×		
32		Merenskyite; PdTe ₂	Pt-(Bi)-bearing		×	
33		Moncheite; PtTe ₂	Pd-(Bi)-bearing		×	
34		Michenerite; PdBiTe			×	
35		Froodite; PdBi ₂				×
36		Sopcheite; Ag ₄ Pd ₃ Te ₄				×
37	Pd-Pt stannides	Paolovite; Pd ₂ Sn	Pt-bearing	×		
38		Atokite; Pd ₃ Sn				×
39		Rustenburgite; Pt ₃ Sn	Pd-bearing			×
40		Niggliite; PtSn				×
41	Pd antimonides	Mertieite-II; Pd ₈ Sb ₃				×
42		Naldrettite; Pd ₂ Sb				×
43	Pd plumbides	Zvyagintsevite; Pd ₃ Pb				×
44		Plumbopalladinite; Pd ₃ Pb ₂				×
45	Pt arsenide	Sperrylite; PtAs ₂	Sb-bearing	×		
46	Pd-Ni arsenide	Majakite; PdNiAs				×
47	Pd germanide-arsenide	Unnamed Pd ₁₁ Ge ₃ As ₂				×
48	Pd stannoarsenide	Unnamed Pd ₆ Sn ₂ As			×	
49	Pt-Pd stannide	Unnamed (Pt, Pd) ₂ Sn	Pd-bearing		×	
50	Pt-Cu arsено-oxysulfide	Unnamed PtCu ₂ AsSO ₃				×

Note: The estimation of relative abundances of species of platinum group minerals (PGM), listed under numbers 30 to 50, is the reflectance of their encountered frequency observed among the entire population of PGM grains and not among all of the ore species listed.

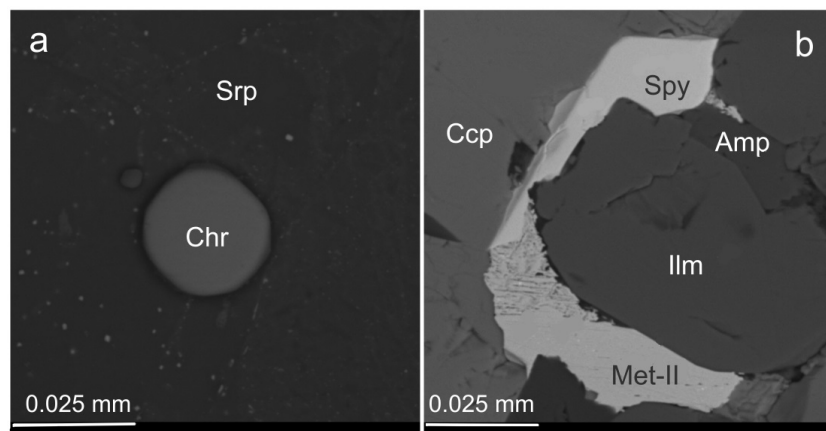


Figure 5. (a) (BSE) displays a globular grain of chromite (Chr) hosted by a member of the serpentine group (Srp). A grain of accessory ilmenite (Ilm), shown in (b) (BSE) in association with chalcopyrite (Ccp), is partially mantled by a rim of platinum group minerals (PGM): mertieite-II (Met-II) and sperrylite (Spy); a grain of calcic amphibole is labeled Amp. These BSE images were taken with the SEM.

Table 4. Compositions of grains of chromian spinels and ilmenite in the eastern portion of the Oktyabrsky ore deposit.

#	Sample		TiO ₂	Al ₂ O ₃	Cr ₂ O ₃	V ₂ O ₃	FeO Total	FeO Calc.	Fe ₂ O ₃ Calc.	MnO	MgO	Total (wt.%)	Mg#	Cr#	Fe ³⁺ #
1	EF0035-1534.1	Chr	3.24	2.15	13.43	0	71.19	28.91	46.98	0	3.32	98.04	17.0	80.7	59.4
2	EF0040-1706.4		3.37	2.68	16.28	0.97	71.19	32.38	43.13	0	1.76	100.57	8.8	80.3	54.5
3	EF0062-1597.4		2.94	1.70	1.77	0	87.13	32.33	60.90	0	1.34	100.98	6.9	41.1	62.9
4	EF0065-1713.3		4.50	4.84	26.44	1.00	55.20	32.12	25.65	0	2.19	96.74	10.8	78.6	41.8
5	EF0065-1714.8		1.87	16.02	39.07	0.53	33.22	22.45	11.97	0	9.15	101.06	42.1	62.1	32.4
6	EF0065-1714.8		2.02	15.46	39.96	0.46	33.55	22.63	12.14	0	9.24	101.91	42.1	63.4	32.6
7	EF0065-1714.8		3.90	12.77	36.47	0.71	37.50	24.87	14.03	0.43	8.19	101.38	36.6	65.7	33.7
8	EF0066-1684.4		2.05	16.68	38.98	0	31.79	21.80	11.10	0	9.57	100.18	43.9	61.1	31.4
9	EF0066-1684.4		2.32	15.72	38.07	0.38	32.74	22.24	11.67	0	9.22	99.62	42.5	61.9	32.1
10	EF0066-1684.4		1.02	10.62	34.07	0.47	47.33	27.29	22.27	0.54	4.39	100.67	21.9	68.3	42.3
11	EF0069-1743.6		1.37	19.42	37.12	0.35	31.27	22.08	10.22	0	9.19	99.74	42.6	56.2	29.4
12	EF0069-1743.6		1.40	20.03	37.87	0.28	31.30	22.11	10.21	0	9.62	101.52	43.7	55.9	29.4
13	EF0069-1743.6		2.49	15.19	38.34	0.53	32.91	22.21	11.89	0	9.37	100.02	42.9	62.9	32.5
14	EF0062-1615.4		3.74	10.58	24.44	0.26	53.98	30.71	25.86	0	3.81	99.40	18.1	60.8	43.1
15	EF-0040-1706.4	Ilm	54.01	0	0	0	42.34	0	0	0.89	4.26	101.50	14.9	-	-
16	EF0040-1706.4		47.64	0	0	0	49.25	0	0	0	2.11	99.00	7.1	-	-
17	EF0040-1706.4		48.07	0	0	0	47.00	0	0	0	3.66	98.73	12.2	-	-
18	EF0043-1764.3		51.23	0	0	1.24	43.52	0	0	0.65	2.5	99.14	9.2	-	-
19	EF0066-1726.05		52.44	0	0	0	46.70	0	0	1.10	0	100.24	0.0	-	-
20	EF67-1724.65		54.66	0	0	0	40.82	0	0	5.05	0	100.53	0.0	-	-
21	EF67-1724.65		54.20	0	0	0	42.21	0	0	4.52	0	100.93	0.0	-	-
22	EF8057-1572.3		54.83	0	1.15	0	40.58	0	0	0.71	5.42	102.69	19.0	-	-
23	EF0066-1717		53.08	0	0	0	46.73	0	0	0.62	0	100.43	0.0	-	-

Note: The indices Mg# = 100 Mg/(Mg + Fe²⁺ + Mn); Cr# = 100 Cr/(Cr + Al); and Fe³⁺# = 100 Fe^{3+)/(Fe³⁺ + Fe²⁺) all calculated on the basis of values expressed in atoms per formula unit (apfu).}

3.2. Amphiboles and Micas

The amphibole compositions in the ore-bearing specimens that we have investigated consist of members of the calcic, sodic-calcic and Fe-Mg groups (Table 5, Figure 7a). The mica compositions are annitic, unusually chlorine-rich (Table 6, Figure 7b), with up to 5–7 wt.% Cl, and display a close association with platinum group minerals. Amphiboles of series 1 are generally poor in Cl, except for a potassic variety of hastingsite (composition #5 in Table 5) that contains 4.06 wt.% Cl. The variations shown in Figure 8a yield a positive correlation of K with Cl in the amphiboles. Note the presence of a negative correlation of MgO vs. Cl ($R = -0.85$), along with a positive correlation of FeO vs. Cl ($R = 0.84$ for $n = 35$, in which R is the correlation coefficient calculated on the basis of 35 data-points), recorded in the mica compositions (Figure 8b,c).

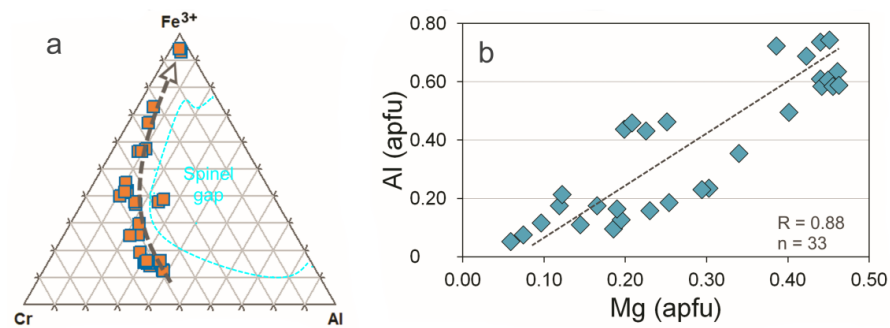


Figure 6. Compositional variations in grains of chromian spinel in the eastern portion of the Oktyabrsky ore deposit are shown in terms of the plots Cr-Al-Fe³⁺ (a) and Mg vs. Al (b), expressed in values of atoms per formula unit (apfu).

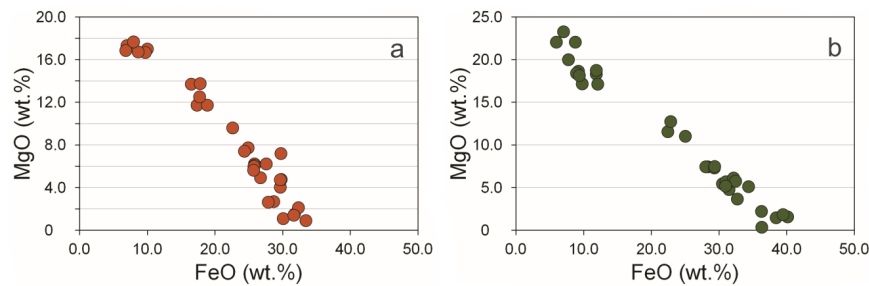


Figure 7. A plot of FeO vs. MgO (wt.%) shows compositional variations in the calcic, sodic-calcic and calcian Fe-Mg amphiboles (a) and in the micas (b).

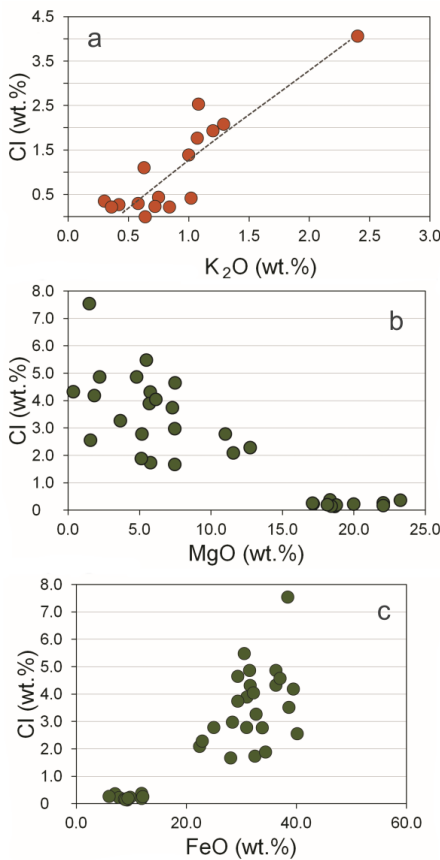


Figure 8. (a), a plot of K₂O vs. Cl (wt.%), shows a positive correlation of K with Cl in compositions of the calcic, sodic-calcic and calcian Fe-Mg amphiboles. (b,c) display a negative correlation of MgO vs. Cl (wt.%) and a positive correlation of FeO vs. Cl in the compositions of micas.

Table 5. Compositions of grains of calcic, sodic-calcic and calcian Fe-Mg amphiboles in the eastern portion of the Oktyabrsky ore deposit.

#	Group	Name	Sample	SiO ₂	TiO ₂	Al ₂ O ₃	Cr ₂ O ₃	FeO	MnO	MgO	CaO	Na ₂ O	K ₂ O	Cl	O ≡ Cl	Total
1	Calcic	Ferro-actinolite	EF0035-1553.75	51.39	0	0.83	0	27.57	0.40	6.22	11.98	0	0	0	0.00	98.39
2	Calcic	Ferro-actinolite	EF0035-1553.75	51.90	0	3.12	0	24.89	0	7.73	12.09	0	0.30	0.35	0.08	100.38
3	Calcic	Magnesio-hornblende	EF0040-1706.4	47.04	0.77	8.77	0	10.00	0	17.00	11.82	2.20	0.42	0.27	0.06	98.29
4	Calcic	Magnesio-hornblende	EF0040-1706.4	47.30	0.45	7.43	0	9.71	0	16.68	11.80	1.97	0.36	0.22	0.05	95.92
5	Calcic chloro potassic	Hastingsite	EF0043-1764.3	38.72	0.73	9.03	0	28.69	0.43	2.69	10.72	0.90	2.40	4.06	0.92	98.37
6	Calcic	Ferro-hornblende	EF0043-1764.3	44.93	0	7.10	0	27.85	1.42	2.64	10.34	0	0.75	0.44	0.10	95.47
7	Calcic chlorian	Ferro-hornblende	EF0043-1764.3	44.35	0.57	6.97	0	25.83	0	6.22	10.03	0	1.08	2.53	0.57	97.58
8	Calcic	Actinolite	EF0061-1603.3	54.17	0	0	0	16.48	0	13.71	13.17	0	0	0	0.00	97.53
9	Calcic	Ferro-hornblende	EF0061-1603.3	47.15	0	4.72	0	31.73	0.85	1.51	11.94	0	1.02	0.42	0.10	99.34
10	Calcic	Magnesio-hastingsite	EF0062-1597.41	44.80	3.20	8.71	0	8.65	0	16.72	11.46	2.76	0.64	0	0.00	96.94
11	Calcic	Edenite	EF0066-1684.4	47.73	2.27	9.33	1.36	6.97	0	17.31	11.36	3.68	0	0	0.00	100.01
12	Sodic-calcic	Barroisite	EF0066-1684.4	45.95	1.80	9.50	1.84	6.79	0	16.85	8.70	4.00	0	0	0.00	95.43
13	Calcic chlorian potassian	Ferro-hornblende	EF0066-1726.05	44.37	0	7.22	0	26.72	0.26	4.94	11.49	0.90	1.29	2.08	0.47	99.27
14	Calcic chlorian	Ferro-hornblende	EF0066-1726.05	45.65	0.30	6.08	0	25.81	0	6.09	11.43	0.74	1.07	1.77	0.40	98.94
15	Calcic chlorian	Ferro-hornblende	EF0066-1726.05	46.94	0	5.86	0	25.74	0.34	5.99	11.74	0.74	1.20	1.93	0.44	100.48
16	Calcic	Magnesio-hornblende	EF0069-1743.6	47.90	2.39	8.86	0	7.94	0	17.68	11.57	2.62	0	0.23	0.05	99.19
17	Calcic	Ferro-actinolite	EF0069-1757.8	50.06	0	2.63	0	29.64	0	4.05	12.33	0	0.45	0	0.00	99.16
18	Calcic	Ferro-actinolite	EF0069-1757.8	52.54	0	1.13	0	29.76	0.41	4.76	12.27	0	0	0	0.00	100.87
19	Na-Ca-Mg-Fe	Ferro-actinolite	EF0069-1757.8	47.07	0	3.44	0	29.71	0	7.20	8.48	0	0	0	0.00	95.90
20	Calcic	Ferro-actinolite	EF0057-1590.5	47.52	0	0	0	33.41	0.87	0.91	11.43	0	0	0	0.00	94.14
21	Calcic	Actinolite	EF0062-1615.4	53.85	0	0.72	0	17.35	0.67	11.72	13.85	0	0	0	0.00	98.16
22	Calcic	Actinolite	EF0062-1615.4	54.62	0	0.81	0	18.86	0.44	11.72	12.65	0	0	0	0.00	99.10
23	Calcic	Actinolite	EF0062-1615.4	51.92	0	2.85	0	17.79	0.49	13.75	11.57	0	0	0	0.00	98.37
24	Calcic	Ferro-actinolite	EF0066-1717	48.24	0	2.95	0	30.07	1.45	1.09	14.57	0	0.58	0.30	0.07	99.25
25	Calcic	Ferro-actinolite	EF0066-1717	50.23	0	1.62	0	32.32	0.61	2.12	11.64	0	0.36	0	0.00	98.90
26	Calcic	Magnesio-hornblende	EF0066-1717	47.60	1.18	5.31	0	17.73	0.52	12.50	10.48	1.62	0.84	0.22	0.05	98.00
27	Calcic chlorian	Ferro-hornblende	EF0066-1717	43.49	0.62	7.27	0	25.70	0.28	5.64	11.43	1.12	1.00	1.39	0.31	97.94
28	Calcic	Ferro-actinolite	EF0066-1717	46.89	0	4.29	0	31.62	0.30	1.41	11.49	0	0.72	0.23	0.05	96.95
29	Mg-Fe calcian	Ferro-gedrite	EF0066-1717	29.25	0	0.38	0	48.99	0.61	0	14.31	0	0	0	0.00	93.54
30	Mg-Fe calcian	Ferro-gedrite	EF0066-1717	29.97	1.35	0	0	49.63	0.70	0	14.01	0	0	0	0.00	95.66
31	Mg-Fe calcian	Ferro-gedrite	EF0066-1717	28.86	0	0.85	0	47.88	0.96	0	14.69	0	0	0	0.00	93.24
32	Mg-Fe calcian	Ferro-gedrite	EF0066-1717	29.29	0	0	0	49.71	0.74	0	14.19	0	0	0	0.00	93.93
33	Calcic	Ferro-actinolite	EF0056-1568.7	51.05	0	0.83	0	24.34	0.53	7.41	13.22	0	0	0	0.00	97.38
34	Calcic	Ferro-hornblende	EF0056-1568.7	49.93	0	5.27	0	22.59	0.40	9.60	11.64	0	0.63	1.10	0.25	101.16
35	Calcic	Ferro-actinolite	EF0056-1568.7	52.86	0	2.36	0	29.64	0.71	4.73	11.88	0	0	0	0.00	102.18

Table 6. Compositions of grains of micas in the eastern portion of the Oktyabrsky ore deposit.

#	Sample	SiO ₂	TiO ₂	Al ₂ O ₃	Cr ₂ O ₃	FeO	MnO	MgO	CaO	NiO	Na ₂ O	K ₂ O	Cl	O≡Cl	Total
1	EF0035-1534.1	39.66	2.30	13.64	0	7.01	0	23.25	0	0	0.78	9.48	0.36	0.08	96.48
2	EF0035-1546.2	37.22	1.83	12.11	0	22.42	0	11.56	0	0	0	11.03	2.09	0.47	98.26
3	EF0040-1706.4	38.49	4.15	13.40	0	7.76	0	19.98	0	0	0	11.14	0.22	0.05	95.14
4	EF0043-1748.4	38.96	6.52	12.22	0.50	9.24	0	18.66	0	0	0.98	9.77	0.14	0.03	96.99
5	EF044-1801.05	33.07	0.73	11.45	0	31.49	0	4.79	0	0	0	10.67	4.86	1.10	97.06
6	EF0061-1603.3	37.16	0.55	10.64	0	30.49	0	5.47	0	0	0	10.89	5.48	1.24	100.68
7	EF0061-1603.3	36.78	0	10.64	0	31.57	0.27	5.74	0.60	0	0	9.07	4.31	0.97	98.98
8	EF0062-1597.4	40.69	3.40	11.58	0	5.94	0	22.06	0	0	0.59	10.76	0.27	0.06	95.29
9	EF0062-1597.4	40.41	3.25	12.43	0	8.75	0	22.06	0	0	0	10.94	0.17	0.04	98.01
10	EF0063-1744.3	40.11	3.94	14.89	0	11.87	0	18.32	0	0	0	10.30	0.37	0.08	99.8
11	EF0065-1714.8	35.56	3.09	11.92	0.51	9.76	0	17.15	0	0	1.15	9.48	0.23	0.05	88.85
12	EF0065-1714.8	38.25	4.82	12.7	0.50	11.86	0	18.76	0	0	0	9.56	0.19	0.04	96.64
13	EF0066-1726.05	34.53	0.58	12.11	0	31.02	0	5.69	0	0	0	10.96	3.89	0.88	98.78
14	EF0066-1726.05	35.75	0	12.28	0	32.16	0	6.14	0	0	0	7.73	4.04	0.91	98.1
15	EF67-1707.8	37.87	4.65	12.34	0	12.07	0	17.11	0	0.46	0	11.84	0.25	0.06	96.59
16	EF67-1724.65	30.40	1.67	11.30	0	32.46	0.56	5.77	0	0	0	6.53	1.73	0.39	90.42
17	EF67-1724.65	33.31	2.09	11.79	0	36.29	0	0.36	0	0	0	10.49	4.32	0.98	98.65
18	EF67-1724.65	37.59	0	8.71	0	38.43	0.50	1.48	0	0	0	7.42	7.54	1.70	101.67
19	EF67-1724.65	34.64	0	11.20	0	36.25	0.35	2.21	0	0	0	10.23	4.86	1.10	99.74
20	EF67-1724.65	32.48	0	13.74	0	37.00	0.39	0	0	0.41	0	10.9	4.57	1.03	99.49
21	EF67-1724.65	31.28	1.42	12.64	0	38.65	0.37	0	0	0	0	8.14	3.52	0.79	96.02
22	EF67-1724.65	30.51	0.53	11.71	0	40.14	0.50	1.56	0	0.39	0	5.70	2.55	0.58	93.59
23	EF67-1724.65	35.51	0.25	12.58	0	28.35	0.25	7.46	0	0.51	0	11.18	2.98	0.67	99.07
24	EF67-1724.65	35.06	0	13.25	0	39.44	0.40	1.84	0.67	0	0	6.43	4.18	0.94	101.27
25	EF0069-1743.6	38.66	7.06	13.15	0.56	8.95	0	18.41	0	0	1.00	11.00	0.15	0.03	98.94
26	EF8057-1572.3	38.66	7.26	13.47	1.07	9.37	0	18.13	0	0	1.13	10.38	0.20	0.05	99.67
27	EF0066-1717	38.81	0	11.79	0	30.95	0	5.17	0	0	0	9.72	2.78	0.63	99.22
28	EF0066-1717	34.32	0.35	12.57	0	34.36	0.43	5.12	0	0	0	6.70	1.89	0.43	95.74
29	EF0066-1717	38.44	0.37	12.57	0	28.02	0	7.46	0	0	0	10.02	1.67	0.38	98.55
30	EF0066-1717	33.42	0	11.17	0	32.68	0	3.66	0	0	0	9.60	3.27	0.74	93.8
31	EF0056-1568.7	33.42	0	16.48	0	33.81	0.53	0	0	0	0	10.83	2.77	0.63	97.84
32	EF0056-1568.7	38.57	0.98	11.13	0	29.32	0	7.30	0	0	0	10.61	3.74	0.84	101.65
33	EF0056-1568.7	39.60	0	12.32	0	25.00	0	11.01	0	0	0	9.87	2.78	0.63	100.58
34	EF0056-1568.7	36.73	0	10.15	0	29.33	0	7.48	0	0	0	10.64	4.65	1.05	98.98
35	EF0056-1568.7	43.19	0	9.54	0	22.86	0	12.74	0	0	0	8.34	2.28	0.51	98.95

3.3. Compositional Variations of Apatite and Minerals of Zr, REE, Y, Th and U

Apatite is a fairly common accessory mineral in our suite of samples. Grains reach up to 0.5–1 mm in length; they exhibit various shapes, from anhedral or subhedral to nearly euhedral (Figure 9a,b and Figure 10a). High variability in the levels of halogens and hydroxyl (calculated) has been documented (Table 7; Figure 11). These variations were established in both intragranular and grain-to-grain patterns.

Baddeleyite grains (≤ 10 to $30 \mu\text{m}$) appear sporadically in various textural forms, such as (1) a peripheral rim-like aggregate deposited around a core of Mg-enriched ilmenite (hosted by pyrrhotite); (2) inclusions in grains of base metal sulfides (pyrrhotite and cubanite; close to their margins or contacts); and (3) a veinlet-like aggregate of twinned grains of Hf-bearing baddeleyite cutting a host grain of orthopyroxene close to its contact (Figure 10b). Additionally, subhedral grains of baddeleyite occur as composite inclusions enclosed by a grain of titanian phlogopite, in which it is intergrown with zirconolite (Figure 10c). The compositions of eight grains of baddeleyite correspond to ZrO_2 with minor incorporation of Ti, Fe and Hf (≤ 2 wt.% of the oxides each).

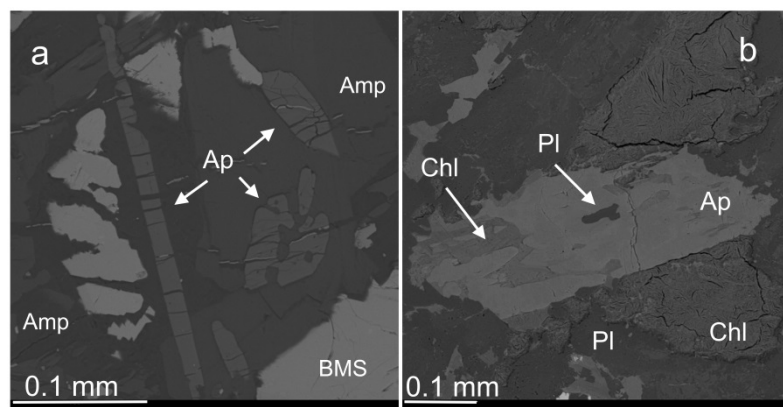


Figure 9. (a) is a BSE image of grains of apatite (Ap), which occur as elongate, partly subhedral or skeletal grains, enriched in Cl (3.87–5.93 wt.%), in association with grains of amphibole (Amp) and base metal sulfides (BMS). (b) (BSE) shows a grain of accessory apatite (Ap) that is strongly heterogeneous in the distribution of Cl (up to 5.34–6.74 wt.% Cl: brighter areas) and of F (2.48–3.15 wt.%). The associated minerals are a plagioclase (Pl) enriched in the Ab component and a Fe-enriched member of the chlorite group (Chl).

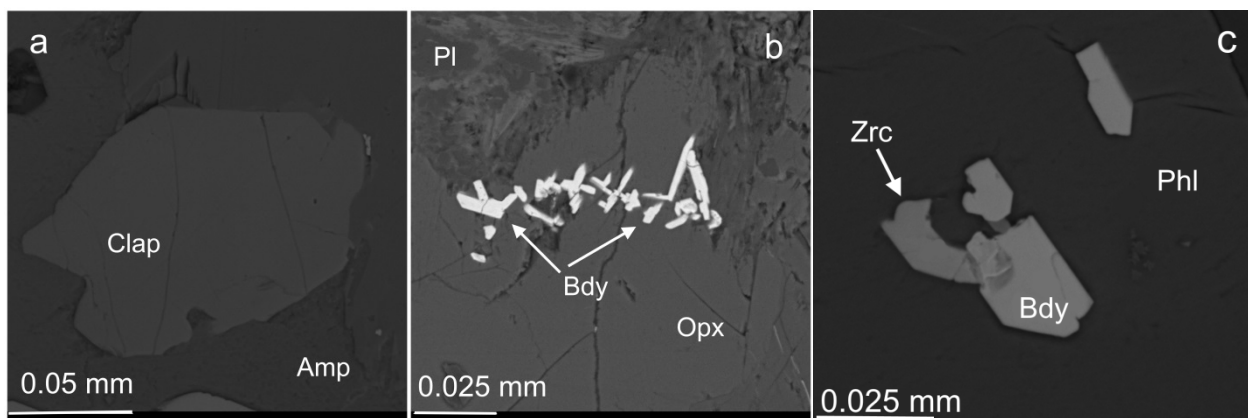


Figure 10. (a) (BSE) shows a subhedral grain of chlorapatite (Clap; 6.44–6.51 wt.% Cl) associated with a grain of calcic amphibole (Amp). A BSE image in (b) displays a veinlet-like aggregate of twinned grains of Hf-bearing baddeleyite (Bdy) that transects a host grain of orthopyroxene (Opx) close to its contact with plagioclase (Pl). (c) is a BSE image showing subhedral grains of baddeleyite (Bdy) intergrown with zirconolite (Zrc) hosted by a grain of titanian phlogopite (Phl).

Table 7. Compositions of accessory grains of apatite in the eastern portion of the Oktyabrsky ore deposit.

#	Sample	P ₂ O ₅	SiO ₂	Ce ₂ O ₃	La ₂ O ₃	FeO	CaO	Na ₂ O	F	Cl	O≡F	O≡Cl	Total (wt.%)	F (apfu)	Cl (apfu)	OH (calc.)
1	EF0035-1534.1	42.94	0	0	0	0	54.89	0	0	0.69	0.00	0.16	98.62	0.00	0.19	1.81
2	EF0035-1534.1	41.96	0.36	0.20	0	0	54.51	0	0.98	1.26	0.41	0.28	98.57	0.51	0.35	1.13
3	EF0035-1534.1	41.66	0	0	0.26	0	53.48	0	0	6.97	0.00	1.58	100.53	0.00	1.95	0.05
4	EF0035-1534.1	42.46	0	0	0	0	54.79	0	1.62	3.00	0.68	0.68	100.51	0.83	0.83	0.34
5	EF0035-1534.1	42.37	0	0	0	0	54.81	0	1.31	3.76	0.55	0.85	100.85	0.67	1.04	0.29
6	EF0035-1534.1	40.95	0	0	0	0	53.23	0	0	6.87	0.00	1.55	99.50	0.00	1.95	0.05
7	EF0035-1534.1	41.68	0.34	0	0	0.73	54.53	0	0	1.99	0.00	0.45	98.82	0.00	0.56	1.44
8	EF0035-1534.1	40.76	0	0.50	0	0.77	52.89	0	0	6.83	0.00	1.54	100.21	0.00	1.93	0.07
9	EF0035-1534.1	42.14	0.79	0	0	0.44	55.06	0	1.37	1.13	0.58	0.26	100.10	0.71	0.31	0.98
10	EF0035-1534.1	41.38	0	0.83	0	0	53.38	0	0	6.49	0.00	1.47	100.61	0.00	1.82	0.18
11	EF0035-1534.1	40.83	0.60	0	0	0	53.13	0	0	5.84	0.00	1.32	99.08	0.00	1.66	0.34
12	EF0035-1534.1	41.73	0.81	0	0	0.89	54.90	0	1.69	0.87	0.71	0.20	99.98	0.87	0.24	0.89
13	EF0035-1534.1	42.28	0	0	0		54.48	0	0	6.55	0.00	1.48	101.83	0.00	1.81	0.19
14	EF0035-1553.75	42.00	0.51	0	0	0	54.46	0	2.92	1.45	1.23	0.33	99.78	1.50	0.40	0.10
15	EF0035-1553.75	41.91	0.43	0	0	0.57	55.49	0	0.29	3.53	0.12	0.80	101.30	0.15	0.98	0.87
16	EF0035-1553.75	42.55	0.39	0	0	0	55.00	0	0.98	5.34	0.41	1.21	102.64	0.50	1.45	0.05
17	EF0035-1553.75	42.28	0	0	0	0	55.24	0	0	6.74	0.00	1.52	102.74	0.00	1.85	0.15
18	EF0035-1553.75	43.56	0	0	0	0	56.79	0	3.15	0.54	1.33	0.12	102.59	1.57	0.14	0.28
19	EF0040-1706.4	41.04	0	0	0	0.42	53.55	0	0	6.11	0.00	1.38	99.74	0.00	1.73	0.27
20	EF0040-1706.4	42.18	0.41	0	0	0.35	54.71	0	2.71	0.44	1.14	0.10	99.56	1.39	0.12	0.48
21	EF0040-1706.4	42.99	0	0	0	0	54.93	0	2.53	0.80	1.07	0.18	100.00	1.29	0.22	0.49
22	EF0040-1706.4	40.99	0.32	0	0	0	53.13	0	0	6.44	0.00	1.46	99.42	0.00	1.82	0.18
23	EF0040-1706.4	40.56	0	0	0	0	52.82	0	0	6.56	0.00	1.48	98.46	0.00	1.88	0.12
24	EF0043-1748.4	41.96	0.36	0.19	0	0.78	53.07	0.34	0.76	3.36	0.32	0.76	99.74	0.40	0.94	0.66
25	EF0043-1748.4	41.86	0.39	0.47	0	0.75	53.38	0.38	0	4.09	0.00	0.92	100.40	0.00	1.15	0.85
26	EF0043-1748.4	41.52	0.62	0.53	0	0.45	52.62	0.34	0.25	3.87	0.11	0.87	99.22	0.13	1.09	0.78
27	EF0043-1748.4	40.74	0.62	0.35	0	0.98	52.50	0.13	0	5.93	0.00	1.34	99.91	0.00	1.68	0.32
28	EF0061-1603.3	43.01	0	0	0	0.49	55.09	0	2.43	0.45	1.02	0.10	100.35	1.24	0.12	0.63
29	EF0061-1603.3	42.83	0	0	0	0.6	54.41	0	2.68	0.54	1.13	0.12	99.81	1.37	0.15	0.48
30	EF0061-1603.3	42.48	0	0	0	0.5	54.09	0	3.23	0.58	1.36	0.13	99.39	1.66	0.16	0.18
31	EF0061-1603.3	42.14	0	0	0	0.51	54.81	0	3.14	0.64	1.32	0.14	99.77	1.61	0.18	0.21
32	EF0062-1591.3	41.66	0	0	0	0.58	53.94	0	0	4.17	0.00	0.94	99.41	0.00	1.18	0.82
33	EF0065-1714.8	41.91	0.36	0	0	0	54.39	0	0.74	3.45	0.31	0.78	99.76	0.39	0.96	0.65
34	EF0065-1714.8	41.63	0.41	0.61	0	0	53.38	0	1.86	1.22	0.78	0.28	98.05	0.98	0.34	0.68
35	EF0065-1714.8	41.47	0.60	0	0	0.68	53.74	0	1.90	2.40	0.80	0.54	99.45	0.99	0.67	0.34

Table 7. Cont.

#	Sample	P ₂ O ₅	SiO ₂	Ce ₂ O ₃	La ₂ O ₃	FeO	CaO	Na ₂ O	F	Cl	O≡F	O≡Cl	Total (wt.%)	F (apfu)	Cl (apfu)	OH (calc.)
36	EF0065-1714.8	41.54	0.39	0	0	0.49	53.20	0	0.75	3.92	0.32	0.89	99.09	0.39	1.10	0.50
37	EF0066-1726.05	42.53	0	0	0	0	54.85	0	2.85	1.71	1.20	0.39	100.35	1.46	0.47	0.08
38	EF67-1707.8	41.38	0.60	1.07	0	0	52.32	0.44	0.80	2.99	0.34	0.68	99.09	0.42	0.84	0.73
39	EF67-1707.8	40.05	0.68	1.02	0	0.84	51.32	0.63	0.65	2.97	0.27	0.67	97.60	0.35	0.86	0.79
40	EF67-1724.65	42.07	0	0	0.5	0.98	53.24	0	2.55	1.75	1.07	0.40	99.12	1.32	0.49	0.19
41	EF0069-1743.6	41.41	0.73	0.84	0.38	0.36	52.54	0.32	1.45	3.09	0.61	0.70	99.43	0.76	0.86	0.38
42	EF0069-1743.6	41.36	0.73	0.80	0	0.57	52.50	0.34	0.97	3.12	0.41	0.71	99.28	0.51	0.88	0.61
43	EF0069-1743.6	41.80	0.58	1.00	0	1.00	53.00	0	0.44	3.71	0.19	0.84	100.51	0.23	1.04	0.73
44	EF0069-1743.6	41.93	0	0	0	0.91	53.21	0.39	0.38	4.80	0.16	1.08	100.38	0.20	1.34	0.46
45	EF0069-1757.8	42.67	0	0	0	0.64	54.58	0	3.51	0.31	1.48	0.07	100.16	1.79	0.08	0.13
46	EF0069-1757.8	42.48	0	0	0	0.58	54.79	0	3.40	0.37	1.43	0.08	100.10	1.74	0.10	0.16
47	EF8057-1572.3	43.17	0	0	0	0	54.30	0	2.05	1.74	0.86	0.39	100.00	1.05	0.48	0.47
48	EF8057-1572.3	43.15	0.34	0	0	0.45	54.72	0	1.32	2.48	0.56	0.56	101.34	0.67	0.68	0.65
49	EF8057-1572.3	42.41	0.32	0	0	0	53.93	0.27	0.98	3.94	0.41	0.89	100.55	0.51	1.09	0.41
50	EF8057-1572.3	41.45	0.58	0	0	0.4	53.14	0.36	0.66	4.47	0.28	1.01	99.77	0.34	1.25	0.40
51	EF0057-1590.5	41.82	0.17	0	0	0.48	53.24	0	3.43	0.21	1.44	0.05	97.86	1.79	0.06	0.16
52	EF0062-1615.4	42.85	0	0.64	0	0	53.73	0.53	2.97	0.70	1.25	0.16	100.01	1.52	0.19	0.29
53	EF0066-1717	42.67	0	0	0	0.50	54.67	0	3.47	0.76	1.46	0.17	100.44	1.77	0.21	0.03

Note: The formula proportions of F and Cl are based on 25 O atoms; values of OH (calc.) are estimated as 2 – (F + Cl) apfu assuming the full site occupancy.

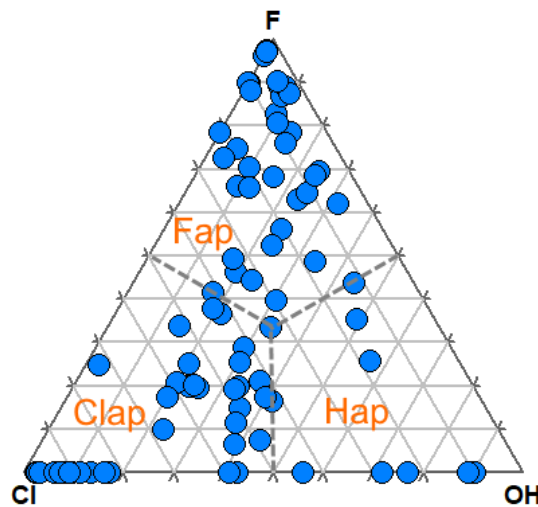


Figure 11. Triangular Cl-F-OH plot showing the overall compositional variations (based on a total of 83 data-points) in accessory grains of apatite in mineralized zones in the eastern portion of the Oktyabrsky ore deposit. The label Fap is fluorapatite, Clap is chlorapatite, and Hap is hydroxylapatite.

Several small grains of zirconolite were also analyzed. Elevated levels of Th and Fe are characteristic. The grain shown in Figure 10c has the following composition: Nb_2O_5 1.99, SiO_2 2.57, TiO_2 27.77, ZrO_2 35.58, ThO_2 8.55, UO_2 2.09, Y_2O_3 3.77, Ce_2O_3 1.15, Nd_2O_3 0.79, FeO 5.72, CaO 5.93, and total 95.91 wt.% (sample EF0069-1743.6). The formula calculated on the basis of seven oxygen atoms per formula unit is $(\text{Ca}_{0.45}\text{Fe}_{0.34}\text{Y}_{0.14}\text{Th}_{0.14}\text{Ce}_{0.03}\text{U}_{0.03}\text{Nd}_{0.02})_{\Sigma 1.15}\text{Zr}_{1.00}(\text{Ti}_{1.48}\text{Zr}_{0.23}\text{Nb}_{0.06})_{\Sigma 1.77}\text{O}_7$. Presumably, this phase is metamict, in view of its high Th and U contents. The associated baddeleyite (Figure 10c) gave ZrO_2 96.12, HfO_2 1.65, and TiO_2 1.37, for a total of 99.14 wt.%. The host grain of phlogopite has a high content of titanium: SiO_2 38.66, TiO_2 7.06, Al_2O_3 13.15, Cr_2O_3 0.56, FeO 8.95, MgO 18.41, Na_2O 1.0 and K_2O 11.0, and a total of 98.79 wt.%.

Zircon is rare, and close to being stoichiometric in composition; e.g., SiO_2 28.90, ZrO_2 64.37, HfO_2 1.69, and FeO 1.53, and a total of 96.49 wt.%. Its grains are typically less than 10 μm across; they display a close spatial association with grains of F-enriched apatite (4.44 wt.% F and 0.56 wt.% Cl) and Pd-based minerals of stannide and antimonide compositions, all hosted by a Cl-bearing chamosite-like silicate. The latter has the following composition: SiO_2 31.30, Al_2O_3 9.73, FeO 42.97, MnO 0.76, MgO 1.14, CaO 0.42, K_2O 0.63, and Cl 0.96 (or 0.19 apfu), for a total of 87.91 wt.%. Interestingly, tiny grains ($\leq 10 \mu\text{m}$) of monazite-(Ce), thorite-coffinite, thorianite and uraninite commonly display an intimate association with the highly Cl-enriched species chlorapatite, and the Cl-rich annite (Figure 12a,b and Figure 13a,b). Representative compositions of selected grains of these minerals are given in Table 8.

In addition, a single inclusion (~2 μm across) of a highly F-enriched composition was encountered, which likely represents bastnäsite-(La), although its composition somewhat deviates from the ideal formula, likely because of analytical difficulties caused by the very tiny grain-size. This grain is hosted by plagioclase ($\text{An}_{61.2}\text{Ab}_{37.5}\text{Or}_{1.4}$; sample EF0043-1764.3) and has the following composition: La_2O_3 47.03, Ce_2O_3 18.81, Pr_2O_3 6.73, F 12.01, O ≡ F 5.06, and CO_2 (by difference) 20.48, for a total of 100.0 wt.%.

Table 8. Compositions of grains of monazite-(Ce), thorite-coffinite, thorianite and uraninite in the eastern portion of the Oktyabrsky ore deposit.

#	Sample		P ₂ O ₅	SiO ₂	ThO ₂	UO ₂	Ce ₂ O ₃	La ₂ O ₃	Pr ₂ O ₃	Nd ₂ O ₃	Sm ₂ O ₃	Gd ₂ O ₃	Dy ₂ O ₃	Al ₂ O ₃	PbO	FeO	CaO	Total (wt.%)
1	EF0040-1706.4	Mnz-Ce	29.54	0	13.22	0	29.43	20.99	0	7.49	0	0	0	0	0	0	100.67	
2	EF0040-1706.4		31.07	0.47	0	0	32.96	15.11	4.15	13.83	1.53	1.26	0.55	0	0	0.71	101.64	
3	EF0062-1597.4		32.13	0.77	0	0	34.47	18.25	2.88	9.39	0	0	0	0	0.94	0.85	99.68	
4	EF67-1707.8		26.26	0	19.57	0	27.95	13.56	2.67	9.30	0	0	0	0	0	0.60	99.91	
5	EF0065-1714.8	Thr	5.25	14.80	68.37	0	5.55	2.33	0	1.89	0	0	0	0	1.96	1.44	101.59	
6	EF0065-1714.8		5.45	14.38	67.47	0	6.21	3.01	0	1.47	0	0	0	0	2.07	1.23	101.29	
7	EF67-1707.8		2.29	24.56	54.26	0	1.66	0	0	0	0	0	0	3.65	0	3.45	0	89.87
8	EF67-1724.65		0.76	17.59	53.72	23.64	0	0	0	0	0	0	0	0	0.41	1.93	0	98.05
9	EF67-1724.65		0	17.37	51.98	25.30	0	0	0	0	0	0	0	0	1.01	2.68	0	98.34
10	EF67-1707.8	Tho	0	0	91.29	3.90	0	0	0	0	0	0	0	0	0	0	0	95.19
11	EF67-1724.65	Urn	0	0	0	93.74	0	0	0	0	0	0	0	0	3.10	0	0	96.84
#		P (apfu)	Si	Th	U	Ce	La	Pr	Nd	Sm	Gd	Dy	Al	Pb	Fe	Ca	Σ	
1	Mnz-Ce	1.00	0.00	0.12	0.00	0.43	0.31	0.00	0.11	0.00	0.00	0.00	0.00	0.00	0.00	0.00	0.96	
2		1.01	0.00	0.00	0.00	0.46	0.21	0.06	0.19	0.02	0.02	0.01	0.00	0.00	0.00	0.03	1.00	
3		1.03	0.00	0.00	0.00	0.48	0.26	0.04	0.13	0.00	0.00	0.00	0.00	0.00	0.03	0.03	0.97	
4		0.94	0.00	0.19	0.00	0.43	0.21	0.04	0.14	0.00	0.00	0.00	0.00	0.00	0.00	0.03	1.04	
5	Thr	0.22	0.74	0.77	0	0.10	0.04	0.00	0.03	0.00	0.00	0.00	0.00	0.00	0.08	0.08	-	
6		0.23	0.72	0.77	0	0.11	0.06	0.00	0.03	0.00	0.00	0.00	0.00	0.00	0.09	0.07	-	
7		0.09	1.10	0.56	0	0.03	0.00	0.00	0.00	0.00	0.00	0.00	0.19	0.00	0.13	0.00	-	
8		0.04	0.96	0.67	0.29	0.00	0.00	0.00	0.00	0.00	0.00	0.00	0.00	0.01	0.09	0.00	-	
9		0	0.96	0.66	0.31	0.00	0.00	0.00	0.00	0.00	0.00	0.00	0.00	0.02	0.12	0.00	-	
10	Tho	0.00	0.00	0.96	0.04	0.00	0.00	0.00	0.00	0.00	0.00	0.00	0.00	0.00	0.00	0.00	-	
11	Urn	0.00	0.00	0	0.98	0.00	0.00	0.00	0.00	0.00	0.00	0.00	0.00	0.04	0.00	0.00	-	

Note: The atomic proportions of monazite-(Ce), labeled Mnz-Ce, and thorite (Thr) are based on four oxygen atoms apfu, and those of thorianite (Tho) and uraninite (Urn) are based on O = 2 apfu.

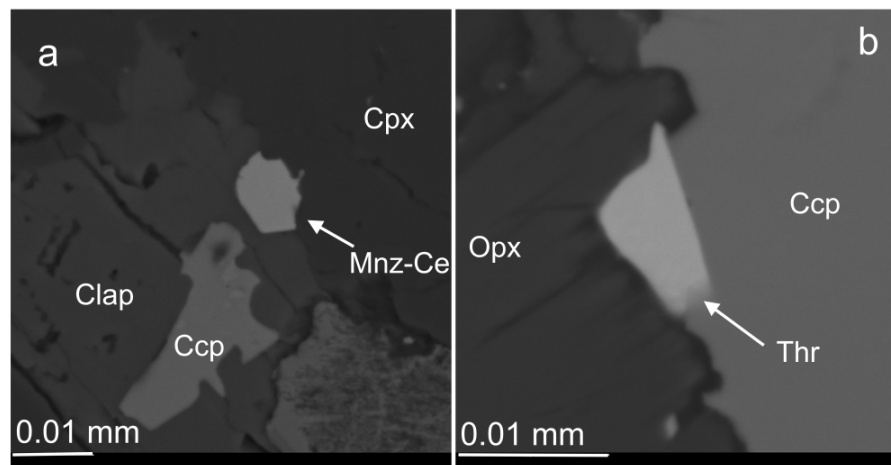


Figure 12. (a) (BSE) shows a grain of monazite-(Ce), labeled Mnz-Ce, located at the boundary of a grain of chlorapatite, Clap (6.11 wt.% Cl) with clinopyroxene (Cpx); Ccp is chalcopyrite. (b) (BSE) shows a tiny grain of thorite (Thr) at the contact of orthopyroxene (Opx) and chalcopyrite (Ccp) grains.

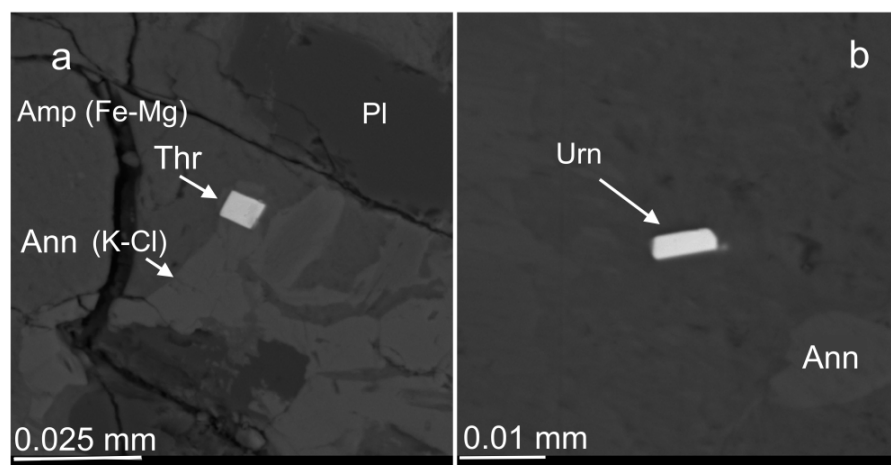


Figure 13. (a) (BSE) shows a tiny and subhedral grain of thorite-coffinite (Thr) associated with a Fe-Mg amphibole (Amp) and a Cl-rich mica related to annite, Ann (7.42 wt.% K₂O, 7.54 wt.% Cl); Pl is an Ab-rich plagioclase. (b) (BSE) shows a minute grain of uraninite (Urn) associated intimately with a grain of Cl-rich annite, Ann (10.23 wt.% K₂O, 4.86 wt.% Cl).

3.4. Unnamed $(Y,Ca,REE)_2Zr_2(Ti,Nb)_2TiFe^{2+}O_{14}$

Of particular interest are the documented occurrences of an unnamed, Y-dominant, zirconolite-related mineral, hitherto unreported, which occurs as elongate and platy grains commonly associated with the Cl-rich annite (Figure 14a). Representative results of selected analyses (#8 in Table 9) lead to the following formula based on 14 O apfu: $(Y_{0.90}Ca_{0.44}Nd_{0.14}Gd_{0.11}Ce_{0.08}Dy_{0.08}Sm_{0.05}Yb_{0.03}Th_{0.03})_{\Sigma 1.86}Zr_{2.16}Ti_{1.00}(Ti_{1.90}Nb_{0.10})_{\Sigma 2.00}Fe^{2+}_{1.03}O_{14}$. A minor excess in Zr, combined with a related deficit in the total content of cations at the Y site, imply that 0.16 Zr apfu could well be incorporated at the Y site. Yet another potentially new species in the series that is Ca-dominant, $(Ca,Y,REE)_2Zr_2Ti(Ti,Nb)_2Fe^{2+}O_{14}$, is present in this association (Table 9).

Table 9. Compositions of grains of a zirconolite-type mineral (Y-rich, unnamed) in the eastern portion of the Oktyabrsky ore deposit.

#	Sample	Nb ₂ O ₅	TiO ₂	ZrO ₂	ThO ₂	UO ₂	Y ₂ O ₃	Ce ₂ O ₃	Nd ₂ O ₃	Sm ₂ O ₃	Gd ₂ O ₃	Dy ₂ O ₃	Er ₂ O ₃	Yb ₂ O ₃	FeO	CaO	Total (wt.%)
1	EF00401706.4	0	30.68	33.50	2.22	2.16	9.65	1.17	1.85	1.01	0.67	1.61	1.25	0	9.58	4.84	100.19
2	EF0040-1706.4	0	29.67	33.27	1.31	4.57	6.20	0.40	0.62	0	0.35	0	0.67	0.73	8.12	6.37	92.28
3	EF0061-1603.3	3.99	28.74	33.35	0.89	0	10.50	1.93	3.57	1.06	1.18	0	0	0	8.74	4.07	98.02
4	EF0069-1743.6	1.99	27.77	35.58	8.55	2.09	3.77	1.15	0.79	0	0	0	0	0	5.72	5.93	93.34
5	EF0066-1717	0	28.71	34.81	1.15	0	8.90	2.79	3.52	1.11	0.68	1.62	0	1.17	9.51	3.71	97.68
6	EF0066-1717	0	29.57	34.54	1.31	0	8.83	2.64	3.58	0.80	0.56	1.39	0	1.22	9.49	3.74	97.67
7	EF0066-1717	3.49	27.24	32.16	1.70	1.36	11.86	1.71	2.44	1.16	1.37	2.10	0	1.43	9.39	2.78	100.19
8	EF0066-1717	1.70	28.57	32.76	0.90	0	12.47	1.52	2.96	1.11	1.29	1.84	0	0.84	9.10	3.06	98.12
9	EF0066-1717	1.97	31.48	34.74	1.18	0	7.20	3.91	3.16	0.79	0.21	0	0.51	0.54	8.49	5.41	99.59
10	EF0066-1717	1.93	30.01	35.12	1.08	0.36	5.51	4.71	2.67	0.77	0.39	0.50	0.61	0.71	9.17	5.26	98.80
#		Nb (apfu)	Ti	Zr	Th	U	Y	Ce	Nd	Sm	Gd	Dy	Er	Yb	Fe ²⁺	Ca	
1		0.00	3.05	2.16	0.07	0.06	0.68	0.06	0.09	0.05	0.06	0.07	0.05	0.00	1.06	0.69	-
2		0.00	3.13	2.28	0.04	0.14	0.46	0.02	0.03	0.00	0.03	0.00	0.03	0.03	0.95	0.96	-
3		0.24	2.87	2.16	0.03	0.00	0.74	0.09	0.17	0.05	0.10	0.00	0.00	0.00	0.97	0.58	-
4		0.13	2.96	2.46	0.28	0.07	0.28	0.06	0.04	0.00	0.00	0.00	0.00	0.00	0.68	0.90	-
5		0.00	2.95	2.31	0.04	0.00	0.65	0.14	0.17	0.05	0.06	0.07	0.00	0.05	1.08	0.54	-
6		0.00	3.01	2.28	0.04	0.00	0.64	0.13	0.17	0.04	0.05	0.06	0.00	0.05	1.08	0.54	-
7		0.21	2.76	2.12	0.05	0.04	0.85	0.08	0.12	0.05	0.12	0.09	0.00	0.06	1.06	0.40	-
8		0.10	2.90	2.16	0.03	0.00	0.90	0.08	0.14	0.05	0.11	0.08	0.00	0.03	1.03	0.44	-
9		0.12	3.08	2.20	0.03	0.00	0.50	0.19	0.15	0.04	0.02	0.00	0.02	0.02	0.92	0.75	-
10		0.12	2.99	2.27	0.03	0.01	0.39	0.23	0.13	0.04	0.03	0.02	0.03	0.03	1.02	0.75	-

Note: The formula proportions were calculated on the basis of 14 oxygen atoms pfu.

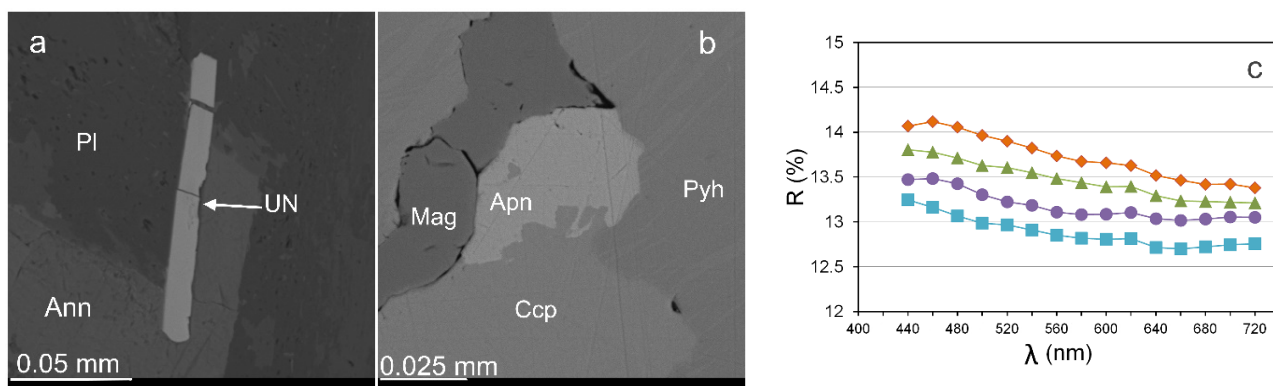


Figure 14. (a) (BSE) shows a platy grain of an unnamed (Y-rich) mineral labeled UN, which has an empirical formula $(\text{Y,Ca,REE})_2\text{Zr}_2(\text{Ti,Nb})_2\text{Ti Fe}^{2+}\text{O}_{14}$ and is associated closely with a Cl-rich annitic mica (Ann) with 10.89 wt.% K_2O and 5.48 wt.% Cl, at the boundary with a sodic plagioclase (Pl). (b) (BSE) displays an irregular grain of argentopentlandite (Apn) in association with chalcopyrite (Ccp), pyrrhotite (Pyh) and magnetite (Mag). Figure 14c shows reflectance spectra measured in air for grains of the zirconolite-type unnamed oxide (Y-dominant) from the Oktyabrsky ore deposit.

The potentially new Y-dominant mineral has a fairly low reflectance measured in air (Figure 14c, Table 10). Attempts were made to characterize its crystal structure; these failed because the mineral is metamict (I.V. Pekov, written communication), a reflection of its elevated content of Th and U. These phases at Norilsk appear to be related to stefanweissite, $(\text{Ca,REE})_2\text{Zr}_2(\text{Nb,Ti})(\text{Ti,Nb})_2\text{Fe}^{2+}\text{O}_{14}$, nöggerathite-(Ce), $(\text{Ce,Ca})_2\text{Zr}_2(\text{Nb,Ti})(\text{Ti,Nb})_2\text{Fe}^{2+}\text{O}_{14}$, and laachite, $(\text{Ca,Mn})_2\text{Zr}_2\text{Nb}_2\text{TiFeO}_{14}$, which are all zirconolite-related minerals discovered in the Eifel paleovolcanic region, Germany [13–15]. The low level of radioactive elements in the relatively young complexes of that region has ensured the preservation of their crystal structure.

Table 10. Reflectance values, measured in air, for a zirconolite-type mineral (Y-dominant, unnamed) from the Oktyabrsky ore deposit.

Λ, nm	R, %	R, %	R, %	R, %
440	13.8	14.1	13.5	13.2
460	13.8	14.1	13.5	13.2
480	13.7	14.1	13.4	13.1
500	13.6	14.0	13.3	13.0
520	13.6	13.9	13.2	13.0
540	13.5	13.8	13.2	12.9
560	13.5	13.7	13.1	12.9
580	13.4	13.7	13.1	12.8
600	13.4	13.7	13.1	12.8
620	13.4	13.6	13.1	12.8
640	13.3	13.5	13.0	12.7
660	13.2	13.5	13.0	12.7
680	13.2	13.4	13.0	12.7
700	13.2	13.4	13.1	12.7
720	13.2	13.4	13.1	12.8

3.5. Au-Ag Minerals and Variations in the System PbS-PbSe-PbTe

Argentopentlandite, the Fe-Ni-Ag sulfide (Figures 14b and 15a–c, Table 11), occurs sporadically in the samples investigated, along with other Ag-based species (hessite, acanthite, sopcheite (i.e., Ag-Pd telluride)), in grains varying from 2 μm to 50–70 μm across. Present as well are grains of Au-Ag alloys, in the range 5–15 μm ; they typically accompany grains of platinum group minerals. These alloys correspond to the minerals

silver (Ag-dominant) and gold (Au-dominant; Table 12), which display an extensive series of intermediate solid solutions (Figure 16).

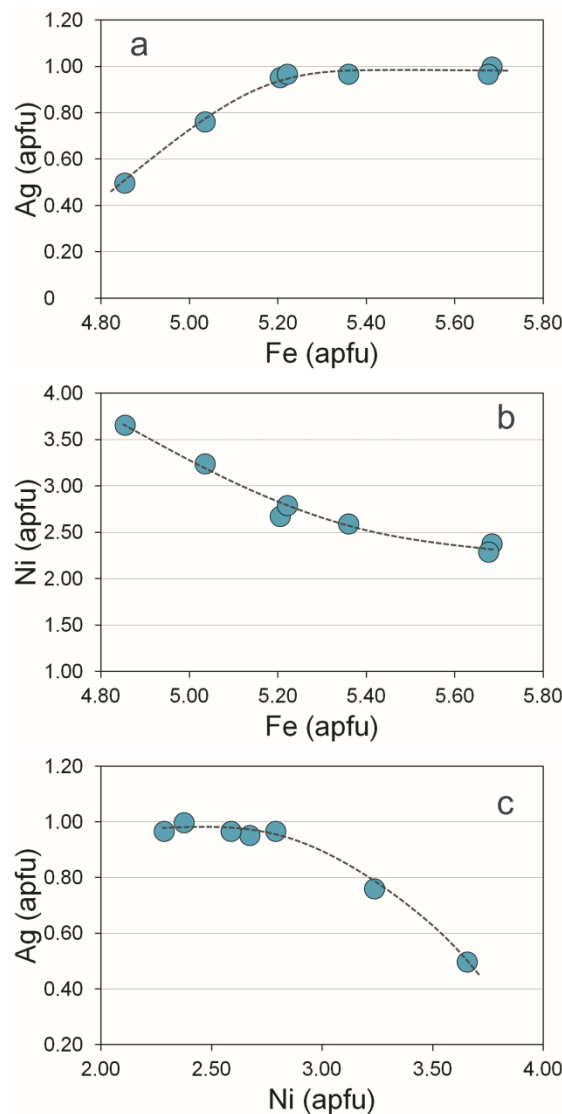


Figure 15. Plots of contents of Fe vs. Ag (a), Fe vs. Ni (b), and Ni vs. Ag (c) in argentopentlandite are presented in terms of apfu (for a total of 17 apfu).

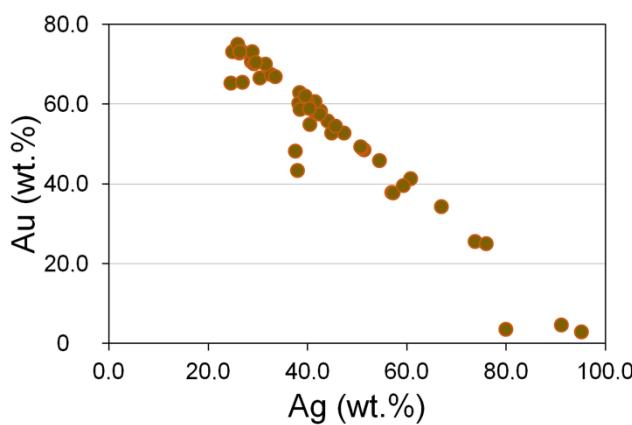


Figure 16. Compositional variations in Au vs. Ag in grains of Au-Ag alloys, expressed in weight %. A total of 69 data-points are plotted.

Table 11. Compositions of grains of argentopentlandite, hessite, acanthite and sopcite in the eastern portion of the Oktyabrsky ore deposit.

#	Sample		Pd	Fe	Ni	Ag	Cu	S	Te	Total (wt.%)	Pd (apfu)	Fe	Ni	Cu	Ag	Σ Me	S	Te
1	EF0057-1590.5	Sop	25.32	0	0	33.87	0	0	40.80	99.99	3.00	0.00	0.00	0.00	3.96	-	0.00	4.04
2	EF0061-1603.3		26.32	0	0	33.93	0	0	41.90	102.15	3.06	0.00	0.00	0.00	3.89	-	0.00	4.06
3	EF0035-1546.2	Apn	0	34.96	23.62	10.19	0	31.75	0	100.52	0.00	5.04	3.24	0.00	0.76	9.03	7.97	0.00
4	EF0042-1722.3		0	39.24	17.24	13.30	0	31.47	0	101.25	0.00	5.68	2.38	0.00	1.00	9.06	7.94	0.00
5	EF0061-1603.3		0	36.12	19.49	12.75	1.35	31.87	0	101.58	0.00	5.21	2.67	0.17	0.95	9.00	8.00	0.00
6	EF0063-1744.3		0	38.60	16.34	12.69	0	31.51	0	99.14	0.00	5.68	2.29	0.00	0.97	8.93	8.07	0.00
7	EF0069-1757.8		0	36.89	18.72	12.84	0	31.95	0	100.40	0.00	5.36	2.59	0.00	0.97	8.91	8.09	0.00
8	EF0069-1757.8		0	36.40	20.44	13.00	0	32.11	0	101.95	0.00	5.22	2.79	0.00	0.97	8.98	8.02	0.00
9	EF0069-1757.8		0	34.93	27.65	6.89	0	33.02	0	102.49	0.00	4.85	3.66	0.00	0.50	9.01	7.99	0.00
10	EF0040-1706.4	Hes	0	0	0	60.50	0	0	36.04	96.54	0.00	0.00	0.00	0.00	2.00	2.00	0.00	1.00
11	EF0043-1764.3		0	0	0	61.59	0	0	38.41	100.00	0.00	0.00	0.00	0.00	1.96	1.96	0.00	1.04
12	EF044-1801.05		0	0	0	59.78	0	0	37.80	97.58	0.00	0.00	0.00	0.00	1.95	1.95	0.00	1.05
13	EF0063-1744.3		0	0	0	62.73	0	0	37.27	100.00	0.00	0.00	0.00	0.00	2.00	2.00	0.00	1.00
14	EF0063-1744.3		0	0	0	62.70	0	0	37.78	100.48	0.00	0.00	0.00	0.00	1.99	1.99	0.00	1.01
15	EF0066-1726.05		0	0	0	63.74	0	0	37.91	101.65	0.00	0.00	0.00	0.00	2.00	2.00	0.00	1.00
16	EF0062-1597.4	Aca	0	0	0	85.83	0	13.70	0	99.53	0.00	0.00	0.00	0.00	1.95	1.95	1.05	0.00

Note: These formulae were calculated for a total of 11 apfu for sopcite (Sop) and 3 apfu for hessite (Hes) and acanthite (Aca).

Table 12. Compositions of grains of Au-Ag alloy minerals in the eastern portion of the Oktyabrsky ore deposit.

#	Sample	Au	Ag	Cu	Total (wt.%)	Au (at.%)	Ag	Cu
1	EF0035-1534.1	58.26	42.56	0	100.82	42.8	57.2	0.0
2	EF0035-1534.1	57.99	41.49	0	99.48	43.4	56.6	0.0
3	EF0035-1534.1	58.09	41.53	0	99.62	43.4	56.6	0.0
4	EF0035-1534.1	62.95	38.36	0	101.31	47.3	52.7	0.0
5	EF0042-1722.3	66.84	33.51	0	100.35	52.2	47.8	0.0
6	EF0042-1722.3	55.78	44.04	0	99.82	41.0	59.0	0.0
7	EF0043-1748.4	41.33	60.72	0	102.05	27.2	72.8	0.0
8	EF0043-1748.4	45.81	54.49	0	100.30	31.5	68.5	0.0
9	EF0043-1764.3	70.68	28.69	0	99.37	57.4	42.6	0.0
10	EF0043-1764.3	70.02	31.55	0	101.57	54.9	45.1	0.0
11	EF044-1801.05	73.14	25.94	0	99.08	60.7	39.3	0.0
12	EF044-1801.05	60.22	38.23	0	98.45	46.3	53.7	0.0
13	EF044-1801.05	73.66	25.50	0	99.16	61.3	38.7	0.0
14	EF0061-1603.3	72.83	26.25	0	99.08	60.3	39.7	0.0
15	EF0061-1603.3	73.14	28.85	0	101.99	58.1	41.9	0.0
16	EF0061-1603.3	70.10	29.23	0	99.33	56.8	43.2	0.0
17	EF0061-1603.3	70.42	29.49	0	99.91	56.7	43.3	0.0
18	EF0062-1597.4	0	98.98	0	98.98	0.0	100.0	0.0
19	EF0062-1597.4	60.58	41.46	0	102.04	44.5	55.5	0.0
20	EF0062-1597.4	0	99.88	0	99.88	0.0	100.0	0.0
21	EF0062-1597.4	0	100.55	0	100.55	0.0	100.0	0.0
22	EF0062-1597.4	0	101.71	0	101.71	0.0	100.0	0.0
23	EF0062-1597.4	0	100.86	0	100.86	0.0	100.0	0.0
24	EF0062-1597.4	0	98.46	0	98.46	0.0	100.0	0.0
25	EF0062-1597.4	0	99.81	0	99.81	0.0	100.0	0.0
26	EF0063-1744.3	60.48	39.92	0	100.40	45.3	54.7	0.0
27	EF0065-1713.3	39.61	59.26	1.74	100.61	25.9	70.6	3.5
28	EF0065-1713.3	0	98.74	0	98.74	0.0	100.0	0.0
29	EF0065-1713.3	52.74	44.85	0	97.59	39.2	60.8	0.0
30	EF0065-1713.3	34.34	66.98	0	101.32	21.9	78.1	0.0
31	EF0065-1714.8	58.90	40.38	0	99.28	44.4	55.6	0.0
32	EF0065-1714.8	62.06	39.51	0	101.57	46.2	53.8	0.0
33	EF0066-1726.05	2.88	95.11	0	97.99	1.6	98.4	0.0
34	EF67-1724.65	0	99.22	0	99.22	0.0	100.0	0.0
35	EF67-1724.65	25.55	73.71	0	99.26	16.0	84.0	0.0
36	EF67-1724.65	24.98	75.96	0	100.94	15.3	84.7	0.0
37	EF67-1724.65	0	100.62	0.28	100.90	0.0	99.5	0.5
38	EF0069-1757.8	73.18	24.92	1.29	99.39	59.7	37.1	3.3
39	EF0069-1757.8	74.98	25.94	0	100.92	61.3	38.7	0.0
40	EF0069-1757.8	73.12	26.37	0	99.49	60.3	39.7	0.0

Note: The atomic proportions were calculated for a total of 100 at.-%.

Our data on argentopentlandite (analyses #3–9, Table 11; Figure 15a–c) have interesting implications. These grains (~5–10 µm to 60 µm across; e.g., Figure 14b), hosted by chalcopyrite or pyrrhotite, or occurring at their boundaries, exhibit unusually high variations in Fe (4.85–5.68), Ni (2.29–3.66) and Ag (0.50–1.00), all quoted in apfu calculated for a total of 17 apfu (Table 11). On the basis of these observations, we infer that: (1) up to 0.5 apfu of Ag at the Ag site can be replaced by another cation, namely Ni; (2) nickel, not Fe, replaces Ag in the structure, and (3) a coupled mechanism (Ag + Fe) → Ni can be inferred, which suggests that a Ni-for-Ag substitution at the Ag site is combined with a Ni-for-Fe substitution at the Fe-Ni site. The presently observed variations in Ag extend those reported previously: $(\text{Fe}_5 \pm 0.6 \text{Ni}_3 \pm 0.4)\Sigma_8 + x\text{Ag}_1 - x\text{S}_8$ with $0 < x < 0.2$, from Mount Windarra, Australia [16,17], and $(\text{Fe}_5 \pm 0.77 \text{Ni}_3 \pm 0.75)\Sigma_8 + x\text{Ag}_1 \pm y\text{S}_8 \pm z$, with $0 < x < 0.30$, $0 < y < 0.23$, $0 < z < 0.30$ from El Charcón, Spain [18].

Grains of altaite and members of the galena-clausthalite series (Table 13) typically form small inclusions: <5–10 µm, occasionally 20–25 µm, and rarely up to 50 µm, hosted by chalcopyrite, cubanite or pyrrhotite, or associated with aggregates of grains of chalcopyrite and pentlandite within silicate minerals. A close association with the Cl-rich annite (3.89 wt.% Cl) is observed. In addition, these species of chalcogenides commonly occur in mutual intergrowths or accompany Pd-based bismuthotellurides and, in some instances, are associated with hessite. The analyzed members of the system PbS-PbSe-PbTe display the common Se-for-S substitution (Figure 17), whereas the Se-for-Te (or S-for-Te) exchanges are minor or virtually absent in these solid solutions.

Table 13. Compositions of grains of altaite and members of the galena-clausthalite series in the eastern portion of the Oktyabrsky ore deposit.

#	Sample		Pb	Fe	Te	Se	S	Total (wt.%)	Pb (apfu)	Fe	Te	Se	S	S + Se + Te
1	EF0040-1706.4	Alt	62.45	0	36.84	2.04	0	101.33	0.98	0.00	0.94	0.08	0.00	1.02
2	EF0040-1706.4		63.22	0	38.01	0	0	101.23	1.01	0.00	0.99	0.00	0.00	0.99
3	EF0040-1706.4		61.94	0	37.98	0	0	99.92	1.00	0.00	1.00	0.00	0.00	1.00
4	EF0040-1706.4		61.71	0	38.16	0	0	99.87	1.00	0.00	1.00	0.00	0.00	1.00
5	EF0043-1748.4		58.14	1.82	36.83	0	0	96.79	0.93	0.11	0.96	0.00	0.00	0.96
6	EF0043-1748.4	Gn	85.55	0	0	1.18	13.27	100.00	0.98	0.00	0.00	0.04	0.98	1.02
7	EF0043-1764.3	Cth-Gn	74.03	0	1.21	21.25	1.82	98.31	1.03	0.00	0.03	0.78	0.16	0.97
8	EF0061-1603.3		87.00	0	0	3.07	10.97	101.04	1.05	0.00	0.00	0.10	0.85	0.95
9	EF0061-1603.3		82.52	0	0	14.06	5.88	102.46	1.05	0.00	0.00	0.47	0.48	0.95
10	EF0063-1744.3	Gn	86.14	0	0	0	11.79	97.93	1.06	0.00	0.00	0.00	0.94	0.94
11	EF0065-1714.8		87.62	0	0	0	12.03	99.65	1.06	0.00	0.00	0.00	0.94	0.94
12	EF0066-1726.05		82.41	1.71	0	5.09	9.75	98.96	1.00	0.08	0.00	0.16	0.76	0.93
13	EF67-1707.8		83.85	1.99	0	2.28	11.01	99.13	1.00	0.09	0.00	0.07	0.85	0.92
14	EF0069-1743.6		85.68	0	0	0	14.32	100.00	0.96	0.00	0.00	0.00	1.04	1.04
15	EF0069-1757.8	Gn-Cth	78.89	0	0.69	14.37	5.84	99.79	1.01	0.00	0.01	0.49	0.49	0.99
16	EF0069-1757.8	Gn	88.93	0	0	0	12.78	101.71	1.04	0.00	0.00	0.00	0.96	0.96
17	EF0069-1757.8	Gn-Cth	80.84	0	0.81	13.87	5.90	101.42	1.03	0.00	0.02	0.46	0.49	0.97
18	EF0069-1757.8		79.73	0	0.95	14.62	5.20	100.50	1.04	0.00	0.02	0.50	0.44	0.96
19	EF0069-1757.8	Gn	87.73	0	0	0	12.43	100.16	1.04	0.00	0.00	0.00	0.96	0.96
20	EF0069-1757.8	Cth-Gn	81.50	0	0.34	12.03	6.45	100.32	1.05	0.00	0.01	0.41	0.54	0.95

Note: The atomic proportions are based on a total of 2 atoms per formula unit, apfu. The label Alt is altaite, Gn is galena, and Cth is clausthalite.

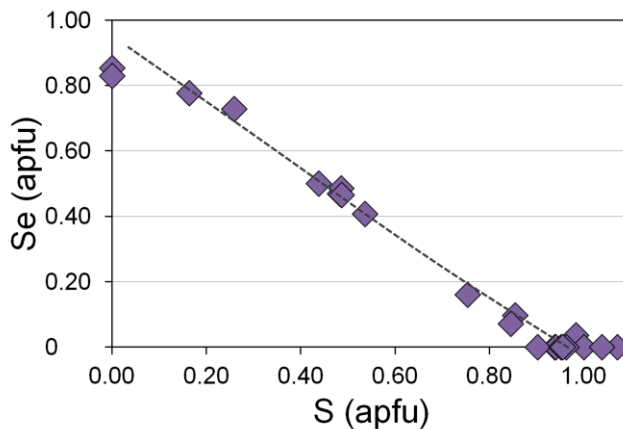


Figure 17. Compositional variations in Se vs. S, expressed in values of atoms per formula unit (apfu; calculated for Σ atoms = 2), in grains of members of the galena-clausthalite series. A total of 32 data-points are plotted.

3.6. Base Metal Sulfides and Nickeline

As noted, base metal sulfide mineralization typically develops in the form of large, primary grains with droplet-like or angular shapes, or interstitial disseminations (Figure 3a). It is composed of varying proportions of chalcopyrite, pyrrhotite, troilite, and pentlandite, with lesser amounts of cubanite and rare bornite.

The grains of chalcopyrite-type minerals, analyzed in all of the ore-bearing specimens, display notable variations in Cu and Fe. The overall ranges observed for a total n of 119 data-points are: Cu 0.84–1.10 (mean 0.99), Fe 0.95–1.18 (1.02), and S 1.90–2.06 (2.00), calculated

for a total of 4 apfu; the Cu/Fe ratio is in the range 0.75–1.15 (mean 0.97). In the absence of structural data, we cannot specify whether or not the chalcopyrite-derivative sulfides talnakhite $\text{Cu}_{18}(\text{Fe},\text{Ni})_{16}\text{S}_{32}$, mooihoekite $\text{Cu}_9\text{Fe}_9\text{Si}_{16}$, and haycockite $\text{Cu}_4\text{Fe}_5\text{S}_8$ [19–22] are present. In experimental systems, wide variations in Cu/Fe values were reported: 0.67–1.03 in tetragonal chalcopyrite, 0.68–0.92 in cubic haycockite, and 0.93–1.04 in mooihoekite [23].

Compositional series of pyrrhotite and troilite vary greatly (Table 14), as is shown in Figure 18, in comparison with ideal compositions of the known polytypes: orthorhombic pyrrhotite-11C ($\text{Fe}_{10}\text{S}_{11}$), hexagonal pyrrhotite-11H ($\text{Fe}_{10}\text{S}_{11}$), monoclinic pyrrhotite-4C (Fe_7S_8), and monoclinic pyrrhotite-5C (Fe_9S_{10}) (e.g., [24] and references therein).

Table 14. Compositions of grains of pyrrhotite and troilite in the eastern portion of the Oktyabrsky ore deposit.

#	Sample	Fe	Ni	S	Total (wt.%)	Fe (at.%)	Ni	Fe + Ni	S
1	EF0035-1534.1	60.01	0	38.77	98.78	47.0	0.00	47.0	53.0
2	EF0035-1534.1	60.33	0	40.33	100.66	46.2	0.00	46.2	53.8
3	EF0035-1546.2	60.63	0	39.14	99.77	47.1	0.00	47.1	52.9
4	EF0035-1546.2	60.75	0.78	39.98	101.51	46.3	0.57	46.9	53.1
5	EF0035-1553.75	60.71	0.42	39.35	100.48	46.8	0.31	47.1	52.9
6	EF0035-1553.75	60.54	0	39.39	99.93	46.9	0.00	46.9	53.1
7	EF0035-1553.75	60.93	0	39.33	100.26	47.1	0.00	47.1	52.9
8	EF0040-1706.4	63.44	0	36.38	99.82	50.0	0.00	50.0	50.0
9	EF0040-1706.4	63.41	0	35.93	99.34	50.3	0.00	50.3	49.7
10	EF0040-1706.4	63.38	0	36.68	100.06	49.8	0.00	49.8	50.2
11	EF0042-1722.3	61.85	0	39.14	100.99	47.6	0.00	47.6	52.4
12	EF0042-1722.3	61.54	0	38.38	99.92	47.9	0.00	47.9	52.1
13	EF0043-1748.4	62.79	0	38.25	101.04	48.5	0.00	48.5	51.5
14	EF0043-1764.3	60.23	0	39.30	99.53	46.8	0.00	46.8	53.2
15	EF0043-1764.3	60.72	0	39.46	100.18	46.9	0.00	46.9	53.1
16	EF0043-1764.3	60.41	0	38.08	98.49	47.7	0.00	47.7	52.3
17	EF044-1801.05	60.69	0.83	38.64	100.16	47.1	0.61	47.7	52.3
18	EF0061-1603.3	60.90	0.62	39.35	100.87	46.8	0.45	47.3	52.7
19	EF0061-1603.3	60.28	0	39.94	100.22	46.4	0.00	46.4	53.6
20	EF0062-1591.3	63.45	0	36.84	100.29	49.7	0.00	49.7	50.3
21	EF0062-1591.3	60.32	0	38.32	98.64	47.5	0.00	47.5	52.5
22	EF0062-1591.3	64.37	0	36.11	100.48	50.6	0.00	50.6	49.4
23	EF0062-1597.4	61.75	1.78	35.52	99.05	49.3	1.35	50.6	49.4
24	EF0062-1597.4	64.37	0	36.52	100.89	50.3	0.00	50.3	49.7
25	EF0062-1597.4	63.54	0	36.76	100.30	49.8	0.00	49.8	50.2
26	EF0063-1744.3	62.05	0	38.59	100.64	48.0	0.00	48.0	52.0
27	EF0063-1744.3	63.78	0	36.91	100.69	49.8	0.00	49.8	50.2
28	EF0065-1713.3	64.20	0	36.84	101.04	50.0	0.00	50.0	50.0
29	EF0065-1714.8	63.41	0	36.63	100.04	49.8	0.00	49.8	50.2
30	EF0065-1714.8	64.34	0	36.67	101.01	50.2	0.00	50.2	49.8
31	EF0066-1684.4	64.07	0	36.90	100.97	49.9	0.00	49.9	50.1
32	EF67-1712.0	60.50	0.75	39.67	100.92	46.4	0.55	47.0	53.0
33	EF0069-1743.6	63.14	0	36.71	99.85	49.7	0.00	49.7	50.3
34	EF0069-1743.6	63.93	0	36.80	100.73	49.9	0.00	49.9	50.1
35	EF0069-1743.6	63.35	0	36.65	100.00	49.8	0.00	49.8	50.2
36	EF0069-1757.8	61.02	0.71	39.51	101.24	46.8	0.52	47.3	52.7
37	EF0069-1757.8	60.68	0.79	40.30	101.77	46.1	0.57	46.7	53.3
38	EF8057-1572.3	63.66	0	36.68	100.34	49.9	0.00	49.9	50.1

Note: The atomic proportions were calculated for a total of 100 at.%.

Nickeline was observed as a tiny grain (2–3 μm across) analyzed in a polymimetic intergrowth of Pd-Sn-(As) and Pd-Te-Bi compounds. The results of the analysis are Ni 48.20, and As 51.92, for a total of 100.12 wt.%, thus corresponding to $\text{Ni}_{1.08}\text{As}_{0.92}$.

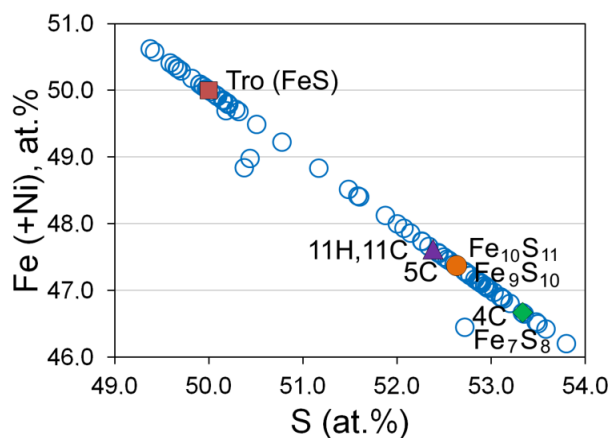


Figure 18. Compositional variations in Fe (+Ni) vs. S, expressed in values of atomic percent (calculated for Σ atoms = 100 at.-%), in grains of troilite (Tro) and pyrrhotite. A total of 79 data-points are plotted. For comparison, ideal compositions of pyrrhotite polytypes are shown (i.e., orthorhombic 11C, $\text{Fe}_{10}\text{S}_{11}$; hexagonal 11H, $\text{Fe}_{10}\text{S}_{11}$; monoclinic 4C, Fe_7S_8 ; and monoclinic 5C Fe_9S_{10}).

A total of sixty-nine grains ($n = 69$) of pentlandite analyzed in all of the collected specimens (Table 15, Figure 19) gave broad variations: Fe 3.56–5.64, with a mean of 4.70 apfu, and Ni 3.11–5.28, with a mean of 4.18 apfu (and up to 2.18 wt% Co); the average values of the total contents of metals and S are 8.97 and 8.03 apfu, respectively.

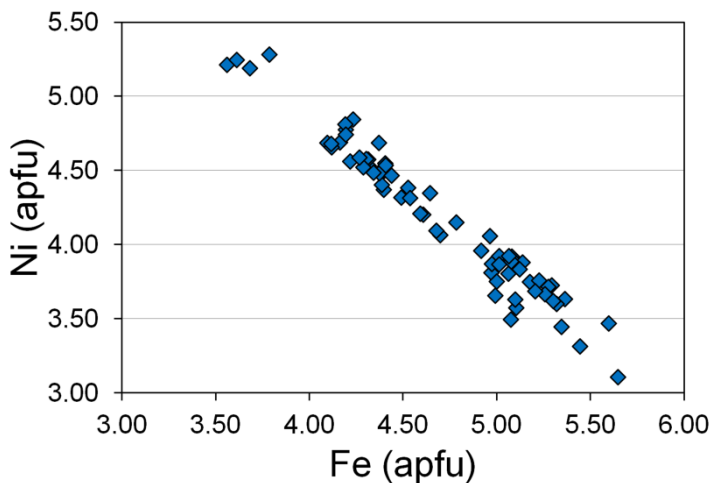


Figure 19. Compositional variations in Ni vs. Fe, expressed in values of apfu (calculated for Σ atoms = 17 apfu), in grains of pentlandite sampled in the eastern portion of the Oktyabrsky ore deposit. A total of 69 data-points are plotted.

Compositional variations in cubanite or isocubanite (or both) were examined on the basis of 33 data-points. A fairly strong negative correlation of Cu vs. Fe ($R = -0.95$) is recorded. The observed ranges, expressed in weight %, are: Fe 37.08–42.76 (mean 41.12), Cu 22.43–29.28 (23.69), and S 34.51–36.35 (35.45), for a total of 98.37–101.86 (100.25) wt %. The corresponding variations in apfu are: Fe 1.78–2.04 (mean 1.99), Cu 0.95–1.24 (1.01), and S 2.98–3.04 (3.00); the Cu + Fe values, 2.96–3.02, agree well with the stoichiometry.

The compositions of bornite ($n = 3$) are stoichiometric, with the possibility of minor Fe-for-Cu substitution, as implied from the observed variations: Fe 11.64–12.71, Cu 62.67–63.35, and S 25.48–25.91, for a total of 100.77–100.90 wt.%, or $\text{Cu}_{4.91-4.95}\text{Fe}_{1.04-1.13}\text{S}_{3.96-4.01}$ (for a total of 10 apfu).

Tiny grains of sphalerite or wurtzite ($n = 8$) are Cd-bearing (0.69–2.71 wt.% Cd). The results of a representative analysis are as follows: Zn 56.64, Cd 2.71, Fe 8.41, and S 34.19,

for a total of 101.96 wt.%, leading to the formula $(\text{Zn}_{0.84}\text{Fe}_{0.14}\text{Cd}_{0.02})_{\Sigma 1.00}\text{S}_{1.00}$ (for a total of 2 apfu).

Table 15. Compositions of grains of pentlandite in the eastern portion of the Oktyabrsky ore deposit.

#	Sample	Fe	Ni	Co	Cu	S	Total (wt.%)	Fe (apfu)	Ni	Co	Cu	ΣM	S
1	EF0035-1534.1	32.00	34.40	0	0	33.83	100.23	4.40	4.50	0.00	0.00	8.90	8.10
2	EF0035-1546.2	30.55	36.18	1.76	0	33.38	101.87	4.16	4.69	0.23	0.00	9.08	7.92
3	EF0035-1546.2	29.85	35.49	2.17	0	33.03	100.54	4.12	4.66	0.28	0.00	9.06	7.94
4	EF0035-1553.75	31.87	35.91	0	0	33.24	101.02	4.37	4.69	0.00	0.00	9.06	7.94
5	EF0035-1553.75	30.38	36.36	0	0	33.39	100.13	4.19	4.78	0.00	0.00	8.97	8.03
6	EF0035-1553.75	31.01	37.32	0	0	33.31	101.64	4.23	4.85	0.00	0.00	9.08	7.92
7	EF0040-1706.4	37.09	30.07	0	0	33.53	100.69	5.08	3.92	0.00	0.00	9.00	8.00
8	EF0040-1706.4	35.89	28.94	1.15	0	33.44	99.42	4.97	3.81	0.15	0.00	8.93	8.07
9	EF0042-1722.3	33.81	33.28	0	0	33.47	100.56	4.64	4.35	0.00	0.00	8.99	8.01
10	EF0042-1722.3	33.00	33.58	1.04	0	33.29	100.91	4.53	4.38	0.14	0.00	9.04	7.96
11	EF0042-1722.3	33.36	31.99	1.46	0	33.24	100.05	4.61	4.20	0.19	0.00	9.00	8.00
12	EF0043-1748.4	36.93	30.23	0	0	34.11	101.27	5.02	3.91	0.00	0.00	8.93	8.07
13	EF0043-1748.4	37.75	28.74	0	0	33.80	100.29	5.18	3.75	0.00	0.00	8.93	8.07
14	EF0043-1764.3	32.01	33.45	1.45	0	33.62	100.53	4.40	4.37	0.19	0.00	8.96	8.04
15	EF0043-1764.3	32.27	34.91	0	0	33.87	101.05	4.41	4.54	0.00	0.00	8.94	8.06
16	EF044-1801.05	30.85	33.49	2.18	0	32.14	98.66	4.34	4.49	0.29	0.00	9.12	7.88
17	EF044-1801.05	31.18	34.57	1.82	0	33.20	100.77	4.29	4.52	0.24	0.00	9.05	7.95
18	EF0061-1603.3	30.48	36.23	0	0	33.66	100.37	4.19	4.74	0.00	0.00	8.93	8.07
19	EF0061-1603.3	30.62	34.8	1.55	0	33.42	100.39	4.22	4.56	0.20	0.00	8.98	8.02
20	EF0062-1591.3	37.29	27.44	0	2.09	33.86	100.68	5.10	3.57	0.00	0.25	8.93	8.07
21	EF0062-1597.4	36.25	28.64	0	0.87	33.00	98.76	5.06	3.80	0.00	0.11	8.97	8.03
22	EF0062-1597.4	36.88	29.27	0	0	32.90	99.05	5.14	3.88	0.00	0.00	9.02	7.98
23	EF0062-1597.4	35.97	27.69	0	2.39	33.34	99.39	4.99	3.66	0.00	0.29	8.94	8.06
24	EF0063-1744.3	33.35	32.14	1.41	0	33.42	100.32	4.59	4.21	0.18	0.00	8.99	8.01
25	EF0063-1744.3	34.79	31.72	1.17	0	33.05	100.73	4.78	4.15	0.15	0.00	9.08	7.92
26	EF0065-1713.3	36.92	26.73	0	3.46	33.45	100.56	5.08	3.50	0.00	0.42	8.99	8.01
27	EF0065-1714.8	36.54	29.64	0	1.14	33.42	100.74	5.01	3.87	0.00	0.14	9.02	7.98
28	EF0065-1714.8	36.08	31.02	0	0	33.31	100.41	4.96	4.06	0.00	0.00	9.02	7.98
29	EF0065-1714.8	36.76	29.93	0	0	33.41	100.10	5.06	3.92	0.00	0.00	8.98	8.02
30	EF0066-1684.4	38.75	28.41	0.95	0	33.68	101.79	5.26	3.67	0.12	0.00	9.04	7.96
31	EF0066-1684.4	38.47	28.65	0.80	0	33.97	101.89	5.20	3.69	0.10	0.00	8.99	8.01
32	EF0066-1684.4	38.30	27.26	0	0	33.42	98.98	5.32	3.60	0.00	0.00	8.92	8.08
33	EF0066-1726.05	32.01	33.86	0	0	33.53	99.40	4.44	4.47	0.00	0.00	8.90	8.10
34	EF67-1724.65	26.24	40.08	1.38	0	33.22	100.92	3.61	5.25	0.18	0.00	9.04	7.96
35	EF67-1724.65	26.81	39.33	0	0	32.24	98.38	3.79	5.28	0.00	0.00	9.07	7.93
36	EF67-1724.65	27.04	40.07	1.34	0	33.54	101.99	3.68	5.19	0.17	0.00	9.05	7.95
37	EF0069-1743.6	39.71	25.88	0	0	32.31	97.90	5.60	3.47	0.00	0.00	9.07	7.93
38	EF0069-1743.6	38.93	27.95	0	0	34.08	100.96	5.30	3.62	0.00	0.00	8.92	8.08
39	EF0069-1757.8	31.53	35.63	1.51	0	33.73	102.40	4.27	4.59	0.19	0.00	9.05	7.95
40	EF8057-1572.3	41.61	24.08	1.26	0	34.21	101.16	5.64	3.11	0.16	0.00	8.92	8.08

Note: The atomic proportions are based on a total of 17 atoms per formula unit, apfu.

3.7. Platinum Group Minerals

A total of 20 species of PGM were recognized in the specimens we examined, including some uncommon or potentially unnamed compounds. They can be grouped into the following families: (1) Pd-Pt tellurides, bismuthotellurides and bismuthides (kotulskite PdTe ; sobolevskite PdBi ; merenskyite PdTe_2 ; moncheite PtTe_2 ; michenerite PdBiTe , and froodite PdBi_2); (2) Pd-Ag telluride (sopcheite $\text{Ag}_4\text{Pd}_3\text{Te}_4$); (3) Pd-Pt stannides, members of the palovite $\text{Pd}_2\text{Sn}-(\text{Pt},\text{Pd})_2\text{Sn}$ series; atokite Pd_3Sn ; rustenburgite Pt_3Sn , and niggliite PtSn ; (3) Pd antimonides (mertieite-II Pd_8Sb_3 ; naldrettite Pd_2Sb); (4) Pd plumbides (zvyagintsevite Pd_3Pb ; plumbopalladinite Pd_3Pb_2); (5) Pt arsenide (sperrylite PtAs_2); (6) Pd-Ni arsenide (majakite PdNiAs); (7) Pd germanide-arsenide (unnamed $\text{Pd}_{11}\text{Ge}_3\text{As}_2$).

or an As-rich variety of palladogermanide $\text{Pd}_2(\text{Ge},\text{As})$; and 8) Pt-Cu arseno-oxysulfide (unnamed $\text{PtCu}_2\text{AsSO}_3$).

Several hundreds of PGM grains were analyzed. They are dominantly located at the boundaries of grains of base metal sulfides (BMS) with silicate minerals (in many cases with the Cl-enriched annite), or are hosted entirely by chalcopyrite or, less commonly, by other BMS. The Pd-Pt tellurides, bismuthotellurides, Pd-Pt stannides and sperrylite are most abundant in the ore-bearing zones. The other species of PGM (#30–50 in Table 3) are subordinate or rare.

The bulk of the PGM grains are characteristically tiny, ranging from ≤ 1 – 2 to 10 – 15 μm for most grains (on the order of 80%). We estimate that about 10–15% of the examined grains exceed $20 \mu\text{m}$, whereas $\leq 5\%$ of the grains attain or exceed 0.1 mm in the longest dimension.

Characteristic textures, associations and compositional variations of PGM are displayed in Figures 20–28. Representative analytical results are presented in Tables 16–20. Extensive solid solutions are evident in the kotulskite-sobolevskite series, merenskyite-moncheite series, paolovite-unnamed ($\text{Pt},\text{Pd})_2\text{Sn}$ series, and a subordinate series of sperrylite toward PtSb_2 (Tables 16–18, Figure 21a,b, Figures 25 and 26) that also has a pyrite-type structure [25].

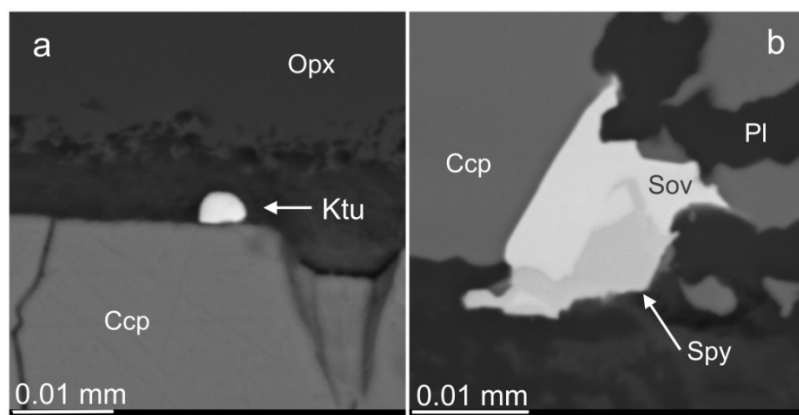


Figure 20. (a) BSE image of a tiny and roundish grain of a member of the kotulskite-sobolevskite series (Ktu) associated with a narrow zone of secondary alteration (dark in the BSE) developed along the contact of chalcopyrite (Ccp) and orthopyroxene (Opx) grains. (b) (BSE) shows Rh-bearing sperrylite (3.47 wt.% Rh) in intergrowth with a grain of sobolevskite (Sov); Ccp is chalcopyrite, and Pl is a sodic plagioclase.

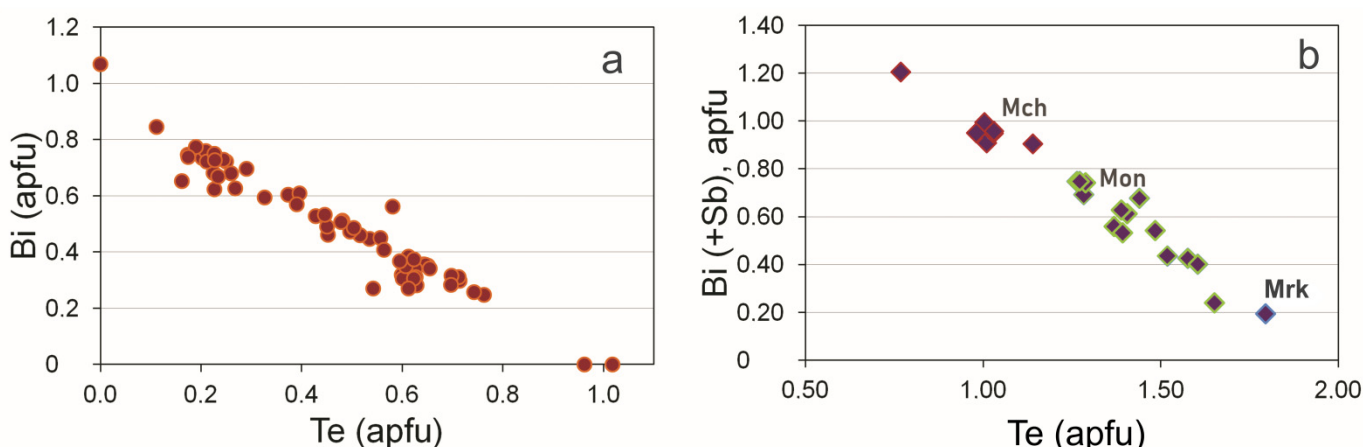


Figure 21. Compositional variations in Bi vs. Te, expressed in apfu (calculated for a total of 2 and 3 apfu in Figure 21a,b, respectively), in grains of members of the kotulskite-sobolevskite series (a) and of the merenskyite-moncheite series (Mrk-Mon) and michenerite (Mch) (b). Totals of 61 and 24 data-points are plotted in Figure 21a,b, respectively.

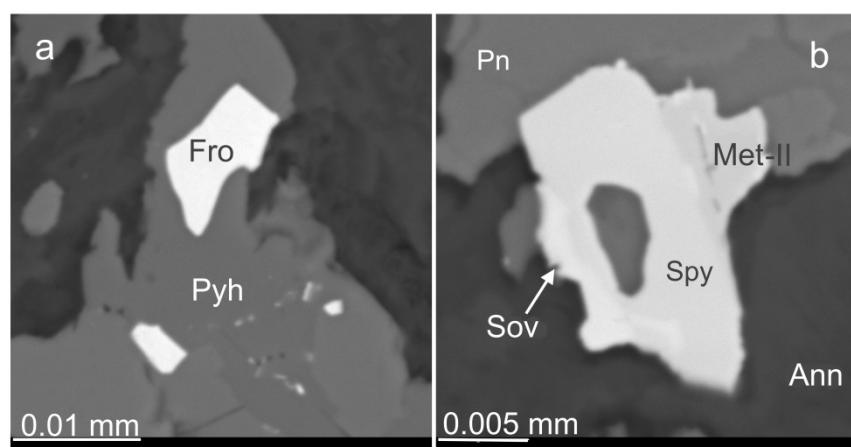


Figure 22. BSE images show grains of froodite (Fro) hosted by pyrrhotite (Pyh) in (a), and in (b), a grain of sperrylite (with 2.28 wt.% Sb) having a narrow rim of sobolevskite (Sov), also Sb-bearing (3.73 wt.%), intergrown with a mertieite-II-related phase (Met-II). Ann is a grain of Cl-rich annite with 10.67 wt.% K₂O and 4.86 wt.% Cl.

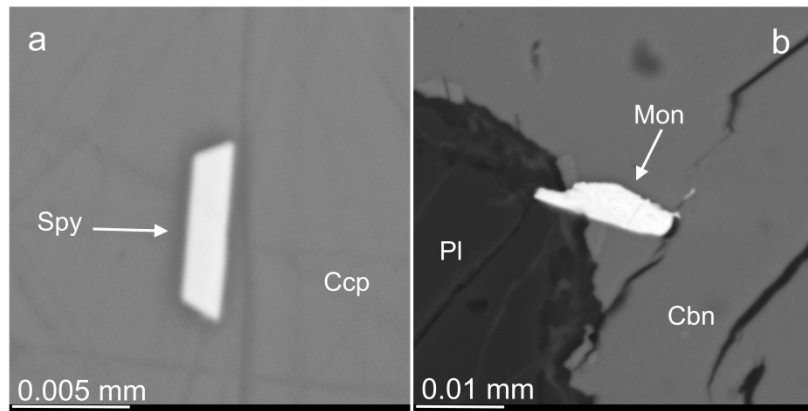


Figure 23. BSE images of a euhedral grain of Sb-rich sperrylite (with 7.79 wt.% Sb; Spy), enclosed within chalcopyrite (Ccp) in (a) and, in (b), a grain of moncheite (Mon) located at the contact of plagioclase rich in Ab (Pl) and cubanite (Cbn).

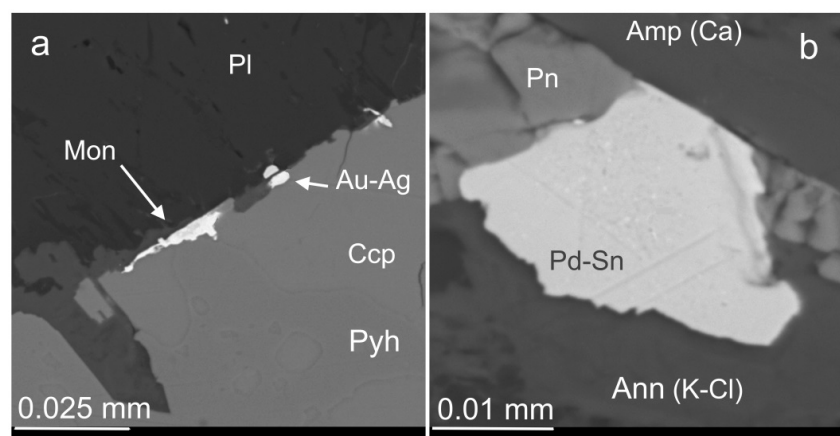


Figure 24. (a) BSE image of a rim-like aggregate of grains of moncheite (Mon) and Au-Ag alloy located along the boundary of the composite grain chalcopyrite (Ccp)-pyrrhotite (Pyh) with plagioclase rich in Ab (Pl). (b) BSE image of a Pd-Sn-(As) alloy grain (with submicrometric inclusions of a bright phase in the center), which occurs in contact with pentlandite (Pn), we see a grain of calcic amphibole, labeled Amp, and a grain of annite containing K (9.60 wt.% K₂O) and Cl (3.27 wt.% Cl), labeled Ann.

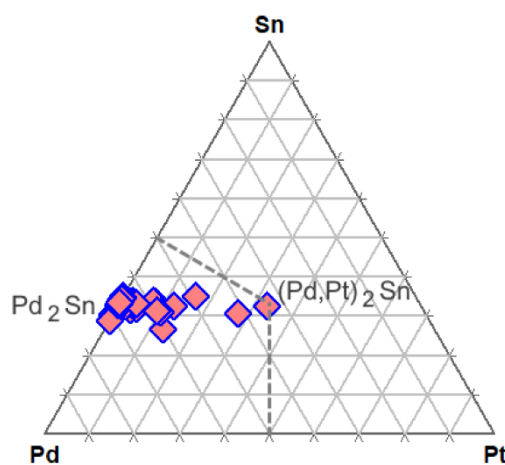


Figure 25. A triangular plot of Pd-Pt-Sn (apfu) shows the series paolovite-unnamed $(Pt,Pd)_2Sn$ from the eastern portion of the Oktyabrsky ore deposit.

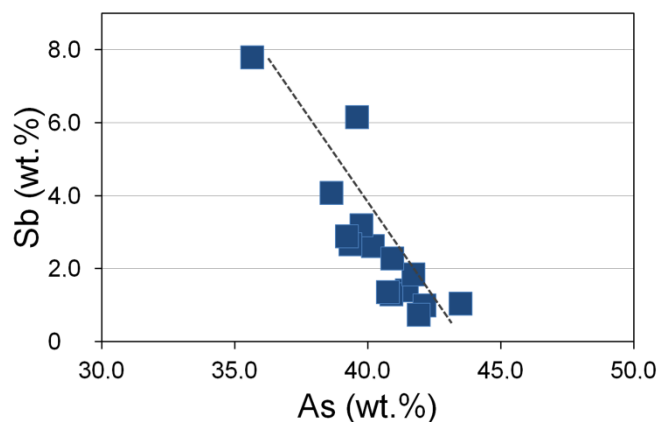


Figure 26. A plot of Sb vs. As, expressed in weight %, in compositions of sperrylite from the eastern portion of the Oktyabrsky ore deposit.

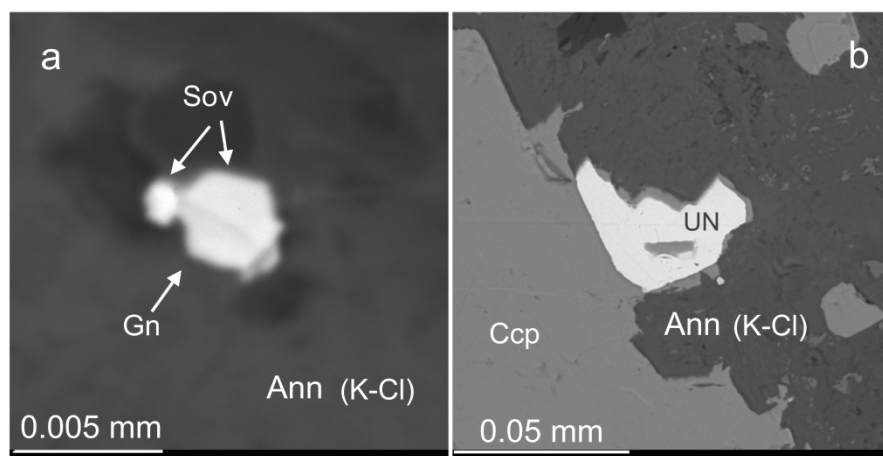


Figure 27. (a) BSE image of a two-phase grain of galena (Gn) and sobolevskite-kotulskite (Sov) included in Cl-enriched annite, with 7.73 wt.% K_2O and 4.04 wt.% Cl, labeled Ann. (b) BSE image of the unnamed Pd_6Sn_2As (labeled UN), which occurs at the contact of grains of chalcopyrite (Ccp) and annitic mica (Ann) containing 10.49 wt.% K_2O and 4.32 wt.% Cl.

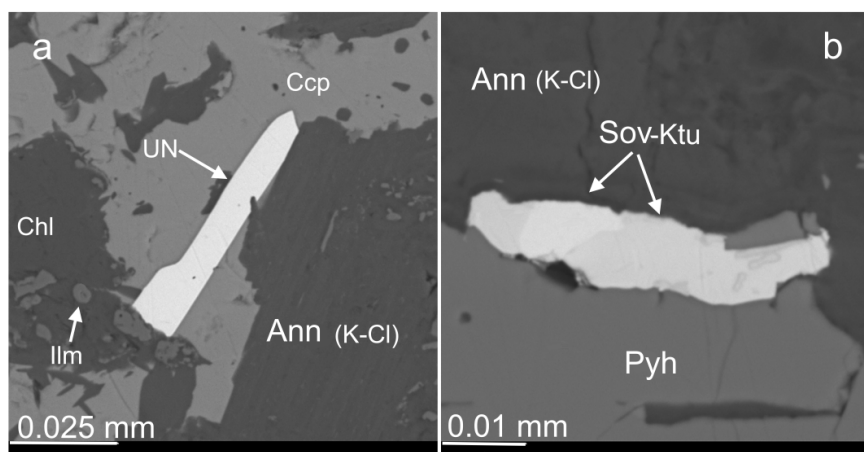


Figure 28. (a) (BSE) displays a platy grain of unnamed $\text{Pd}_6\text{Sn}_2\text{As}$ (UN) associated with chalcopyrite (Ccp), a Fe-rich member of the chlorite group (Chl), Mn-rich ilmenite (5.45 wt.% MnO) and annitic mica (Ann) containing 8.14 wt.% K_2O and 3.52 wt.% Cl. (b) (BSE) shows a composite grain of the sobolevskite-kotulskite series (Sov-Ktu) located along the boundary of pyrrhotite (Pyh) with annitic mica (Ann) containing 10.64 wt.% K_2O and 4.65 wt.% Cl.

Table 16. Compositions of grains of members of the kotulskite-sobolevskite series in the eastern portion of the Oktyabrsky ore deposit.

#	Sample	Pd	Te	Bi	Sb	Total (wt.%)	Pd (apfu)	Te	Bi	Sb	Te + Bi + Sb
1	EF0035-1534.1	38.54	29.12	29.84	1.50	99.00	0.97	0.61	0.38	0.03	1.03
2	EF0035-1546.2	37.37	8.82	52.37	1.44	100.00	1.03	0.20	0.73	0.03	0.97
3	EF0040-1706.4	44.09	29.22	25.45	0	98.76	1.08	0.60	0.32	0.00	0.92
4	EF0040-1706.4	40.79	31.38	28.40	0	100.57	1.00	0.64	0.36	0.00	1.00
5	EF0040-1706.4	41.20	32.20	27.49	0	100.89	1.00	0.65	0.34	0.00	1.00
6	EF0042-1722.3	39.15	14.96	44.57	2.51	101.19	1.02	0.33	0.59	0.06	0.98
7	EF0043-1748.4	40.21	24.29	35.50	0	100.00	1.02	0.52	0.46	0.00	0.98
8	EF0043-1748.4	37.55	10.95	51.79	0	100.29	1.03	0.25	0.72	0.00	0.97
9	EF0043-1748.4	38.53	16.84	44.58	0	99.95	1.02	0.37	0.60	0.00	0.98
10	EF044-1801.05	37.39	12.86	50.40	0	100.65	1.01	0.29	0.70	0.00	0.99
11	EF044-1801.05	38.02	9.27	54.96	0	102.25	1.03	0.21	0.76	0.00	0.97
12	EF044-1801.05	39.22	12.37	47.34	3.73	102.66	1.02	0.27	0.63	0.08	0.98
13	EF0061-1603.3	41.38	38.24	20.39	0	100.01	0.99	0.76	0.25	0.00	1.01
14	EF0061-1603.3	40.36	34.24	25.40	0	100.00	0.99	0.70	0.32	0.00	1.01
15	EF0061-1603.3	44.94	55.85	0	0	100.79	0.98	1.02	0.00	0.00	1.02
16	EF0061-1603.3	40.92	23.59	36.82	0	101.33	1.03	0.50	0.47	0.00	0.97
17	EF0062-1591.3	42.87	21.40	35.73	0	100.00	1.09	0.45	0.46	0.00	0.91
18	EF0062-1591.3	38.12	25.61	33.85	0	97.58	0.99	0.56	0.45	0.00	1.01
19	EF0063-1744.3	39.21	11.51	49.28	0	100.00	1.06	0.26	0.68	0.00	0.94
20	EF0063-1744.3	37.48	7.57	53.20	2.02	100.27	1.03	0.17	0.75	0.05	0.97
21	EF0066-1684.4	39.96	29.81	29.32	0	99.09	1.00	0.62	0.37	0.00	1.00
22	EF0066-1684.4	41.86	34.31	22.88	0	99.05	1.02	0.70	0.28	0.00	0.98
23	EF0066-1726.05	37.41	8.22	54.84	0	100.47	1.04	0.19	0.77	0.00	0.96
24	EF0066-1726.05	37.75	10.02	54.20	0	101.97	1.02	0.23	0.75	0.00	0.98
25	EF67-1712.0	37.94	18.06	45.56	0	101.56	1.00	0.40	0.61	0.00	1.00
26	EF67-1712.0	37.75	7.69	53.47	2.70	101.61	1.02	0.17	0.74	0.06	0.98
27	EF67-1724.65	40.03	26.32	31.22	0	97.57	1.03	0.56	0.41	0.00	0.97
28	EF0069-1743.6	39.86	20.85	40.83	0	101.54	1.02	0.45	0.53	0.00	0.98
29	EF0069-1743.6	39.18	22.12	38.41	0	99.71	1.02	0.48	0.51	0.00	0.98
30	EF8057-1572.3	39.51	23.64	37.35	0	100.50	1.01	0.50	0.49	0.00	0.99
31	EF8057-1572.3	39.56	17.82	42.63	0	100.01	1.04	0.39	0.57	0.00	0.96

Note: The atomic proportions are based on a total of 2 atoms per formula unit, apfu.

Table 17. Compositions of grains of members of the moncheite-merenskyite series, michenerite and froodite in the eastern portion of the Oktyabrsky ore deposit.

#	Sample		Pt	Pd	Te	Bi	Sb	Total (wt.%)	Pt (apfu)	Pd	Pt + Pd	Te	Bi	Sb	Te + Bi + Sb
1	EF0042-1722.3	Mch	0	23.75	34.00	38.74	3.16	99.65	0.00	0.96	0.96	1.14	0.79	0.11	2.04
2	EF0042-1722.3		19.19	12.08	20.21	46.48	3.15	101.11	0.48	0.55	1.03	0.77	1.08	0.13	1.97
3	EF0043-1764.3	Mon	39.33	0	32.20	28.47	0	100.00	1.02	0.00	1.02	1.28	0.69	0.00	1.98
4	EF044-1801.05	Mch	0	24.12	28.92	46.95	0	99.99	0.00	1.00	1.00	1.00	0.99	0.00	2.00
5	EF044-1801.05		0	24.99	30.19	45.58	0	100.76	0.00	1.02	1.02	1.03	0.95	0.00	1.98
6	EF0061-1603.3		0	24.81	30.25	46.05	0	101.11	0.00	1.01	1.01	1.03	0.96	0.00	1.99
7	EF0061-1603.3	Mrk	0	28.83	61.31	10.85	0	100.99	0.00	1.01	1.01	1.79	0.19	0.00	1.99
8	EF0057-1590.5		0	30.01	71.65	0	0	101.66	0.00	1.00	1.00	2.00	0.00	0.00	2.00
9	EF0061-1603.3	Mch	0	25.47	29.87	47.15	0	102.49	0.00	1.03	1.03	1.00	0.97	0.00	1.97
10	EF0061-1603.3		0	24.44	29.35	45.76	0	99.55	0.00	1.02	1.02	1.02	0.97	0.00	1.98
11	EF0062-1597.4	Mon	30.66	7.76	42.67	20.10	0	101.19	0.71	0.33	1.04	1.52	0.44	0.00	1.96
12	EF0065-1713.3		38.06	0	35.60	25.46	0	99.12	0.98	0.00	0.98	1.40	0.61	0.00	2.02
13	EF0065-1714.8		39.03	0	38.91	23.36	0	101.30	0.97	0.00	0.97	1.48	0.54	0.00	2.03
14	EF0065-1714.8		38.37	0	35.41	26.27	0	100.05	0.98	0.00	0.98	1.39	0.63	0.00	2.02
15	EF0065-1714.8		37.98	0	32.95	31.13	0	102.06	0.97	0.00	0.97	1.29	0.74	0.00	2.03
16	EF0069-1743.6		37.13	2.43	42.99	19.11	0	101.66	0.89	0.11	1.00	1.58	0.43	0.00	2.00
17	EF0069-1743.6		37.87	1.72	43.33	17.83	0	100.75	0.92	0.08	0.99	1.60	0.40	0.00	2.01
18	EF0069-1743.6		37.31	0	31.20	30.27	0	98.78	0.99	0.00	0.99	1.26	0.75	0.00	2.01
19	EF0069-1743.6		38.12	0	32.32	31.20	0	101.64	0.98	0.00	0.98	1.27	0.75	0.00	2.02
20	EF044-1801.05	Fro	0	21.82	0	79.10	0	100.92	0.00	1.05	1.05	0.00	1.95	0.00	1.95
21	EF044-1801.05		0	21.53	0	80.92	0	102.45	0.00	1.03	1.03	0.00	1.97	0.00	1.97
22	EF0063-1744.3		7.87	17.16	0	72.86	0	97.89	0.22	0.88	1.10	0.00	1.90	0.00	1.90

Note: The atomic proportions for moncheite (Mon), merenskyite (Mrk), michenerite (Mch) and froodite (Fro) are based on a total of 3 atoms per formula unit (apfu).

Table 18. Compositions of grains of members of the paolovite (Pd_2Sn)-unnamed ($Pt,Pd)_2Sn$ series and of unnamed Pd_6Sn_2As in the eastern portion of the Oktyabrsky ore deposit.

#	Sample		Pt	Pd	Au	Sn	Sb	As	Total (wt.%)	Pt (apfu)	Pd	Pd + Pt	Au	Sn	Sb	As	Sn + Sb + As
1	EF0035-1546.2	Plv- Unnamed (Pt, Pd) $_2Sn$	5.43	59.36	0	32.11	3.19	0	100.09	0.09	1.90	1.99	0.00	0.92	0.09	0.00	1.01
2	EF0035-1546.2		7.21	57.80	0	32.61	1.72	0	99.34	0.13	1.88	2.00	0.00	0.95	0.05	0.00	1.00
3	EF0040-1706.4		0	64.27	0	36.18	0	0	100.45	0.00	1.99	1.99	0.00	1.01	0.00	0.00	1.01
4	EF0043-1764.3		0	64.05	0	36.59	0	0	100.64	0.00	1.98	1.98	0.00	1.02	0.00	0.00	1.02
5	EF0043-1764.3		1.98	62.59	0	35.28	0	0	99.85	0.03	1.97	2.00	0.00	1.00	0.00	0.00	1.00
6	EF044-1801.05		4.48	60.53	0	34.98	0	0	99.99	0.08	1.93	2.00	0.00	1.00	0.00	0.00	1.00
7	EF044-1801.05		4.59	59.87	0	35.54	0	0	100.00	0.08	1.91	1.99	0.00	1.01	0.00	0.00	1.01
8	EF0061-1603.3		0	63.75	0	36.23	0	0	99.98	0.00	1.99	1.99	0.00	1.01	0.00	0.00	1.01
9	EF0061-1603.3		0	64.90	0	36.22	0	0	101.12	0.00	2.00	2.00	0.00	1.00	0.00	0.00	1.00
10	EF0063-1744.3		11.94	51.86	0	33.27	0.49	0.41	97.97	0.22	1.74	1.96	0.00	1.00	0.01	0.03	1.04
11	EF0063-1744.3		5.52	57.99	0	33.47	0	0	96.98	0.10	1.91	2.01	0.00	0.99	0.00	0.00	0.99
12	EF0065-1713.3		19.92	48.38	0	31.89	0	0	100.19	0.37	1.65	2.02	0.00	0.98	0.00	0.00	0.98
13	EF0065-1713.3		0	65.31	0	36.52	0	0	101.83	0.00	2.00	2.00	0.00	1.00	0.00	0.00	1.00
14	EF0065-1714.8		15.28	53.35	0	31.37	0	0	100.00	0.28	1.78	2.06	0.00	0.94	0.00	0.00	0.94
15	EF0065-1714.8		46.18	26.11	0	27.70	0	0	99.99	0.99	1.03	2.02	0.00	0.98	0.00	0.00	0.98
16	EF0065-1714.8		25.21	41.59	0	33.20	0	0	100.00	0.48	1.47	1.95	0.00	1.05	0.00	0.00	1.05
17	EF0066-1726.05		0	64.94	0	36.29	0	0	101.23	0.00	2.00	2.00	0.00	1.00	0.00	0.00	1.00
18	EF67-1707.8		39.24	32.06	0	26.44	0	0	97.74	0.83	1.25	2.08	0.00	0.92	0.00	0.00	0.92
19	EF67-1707.8		0	64.49	0	35.51	0	0	100.00	0.00	2.01	2.01	0.00	0.99	0.00	0.00	0.99
20	EF0035-1546.2	UN Pd_6Sn_2As	0	65.39	0	27.99	0	6.21	99.59	0.00	5.93	0.00	2.27	0.00	0.80	0.00	
21	EF0043-1748.4		68.11	0	21.64	0	10.25	100.00	0.00	6.01	0.00	1.71	0.00	1.28	0.00		
22	EF0061-1603.3		68.96	0	22.71	0	8.46	100.13	0.00	6.12	0.00	1.81	0.00	1.07	0.00		
23	EF67-1724.65		67.74	0.71	24.16	0	7.51	100.12	0.00	6.07	0.03	1.94	0.00	0.96	0.00		
24	EF67-1724.65		66.58	1.00	24.56	0	7.12	99.26	0.00	6.04	0.05	2.00	0.00	0.92	0.00		
25	WDS		0.22	65.76	1.20	24.30	0	7.58	99.06	0.01	5.97	0.06	1.98	0.00	0.98	0.00	

Note: The atomic proportions for members of the series of paolovite (Plv) to unnamed (Pt, Pd) $_2Sn$ are based on a total of 3 atoms per formula unit (apfu). Compositions of unnamed Pd_6Sn_2As were recalculated on the basis of a total of 9 apfu. Analysis #25 represents results of the test (i.e., repeat analysis) performed using a mode of wavelength-dispersive spectrometry (WDS). The presence of essential amounts of Au was thus confirmed.

Table 19. Compositions of grains of members of the atokite-rustenburgite series, niggliite, naldrettite, zvyagintsevite, plumbopalladinite and palladium antimonides related to mertieite-II in the eastern portion of the Oktyabrsky ore deposit.

#	Sample	Pt	Pd	Au	Sn	Pb	Sb	Bi	Te	As	Total (wt.%)	Pt (apfu)	Pd	Au	Pd + Pt (+Au)	Sn	Pb	Sb	Bi	Te	As	Sn + Sb (+Bi + As)	
1	EF0065-1714.8	Ato-Rsb	48.44	28.07	2.41	21.08	0	0	0	0	100.00	1.42	1.50	0.07	2.99	1.01	0.00	0.00	0.00	0.00	0.00	1.01	
2	EF0065-1714.8		48.42	30.26	0	21.32	0	0	0	0	100.00	1.39	1.60	0.00	2.99	1.01	0.00	0.00	0.00	0.00	0.00	1.01	
3	EF0065-1714.8		41.57	35.75	0	22.68	0	0	0	0	100.00	1.15	1.82	0.00	2.97	1.03	0.00	0.00	0.00	0.00	0.00	1.03	
4	EF0069-1743.6	Nig	63.66	0	0	33.25	0	3.09	0	0	100.00	1.03	0.00	0.00	1.03	0.89	0.00	0.08	0.00	0.00	0.00	0.97	
5	EF0063-1744.3		63.55	0	0	36.45	0	0	0	0	100.00	1.03	0.00	0.00	1.03	0.97	0.00	0.00	0.00	0.00	0.00	0.97	
6	EF0065-1714.8		58.92	0	0	28.78	0	2.58	9.73	0	100.01	0.99	0.00	0.00	0.99	0.79	0.00	0.07	0.15	0.00	0.00	1.01	
7	EF0042-1722.3	Nld	0	64.80	0	0	22.99	8.93	3.87	2.35	102.94	0.00	2.02	0.00	2.02	0.00	0.00	0.63	0.14	0.10	0.10	0.97	
8	EF0069-1743.6	Zv	0	60.43	0	0	39.57	0	0	0	100.00	0.00	2.99	0.00	0.00	0.00	1.01	0.00	0.00	0.00	0.00	0.00	
9	EF8057-1572.3		0	61.94	0	0	38.88	0	0	0	100.82	0.00	3.02	0.00	0.00	0.00	0.98	0.00	0.00	0.00	0.00	0.00	
10	EF8057-1572.3		0	60.65	0	0	36.81	0	0	0	97.46	0.00	3.05	0.00	0.00	0.00	0.95	0.00	0.00	0.00	0.00	0.00	
11	EF8057-1572.3	Ppdn	0	42.21	0	0	58.05	0	0	0	100.26	0.00	2.93	0.00	0.00	0.00	2.07	0.00	0.00	0.00	0.00	0.00	
12	EF8057-1572.3		0	40.32	0	0	58.30	0	0	0	98.62	0.00	2.87	0.00	0.00	0.00	2.13	0.00	0.00	0.00	0.00	0.00	
13	EF044-1801.05	Met-II	0	71.07	0	4.69	0	22.36	0	0	2.35	101.78	0.00	7.77	0.00	0.00	0.46	0.00	2.14	0.00	0.00	2.96	
14	EF0061-1603.3		0	70.93	0	0	0	25.11	0	0	3.58	99.62	0.00	7.96	0.00	0.00	0.00	0.00	2.46	0.00	0.00	0.57	3.04
15	EF0061-1603.3		0	71.90	0	0	0	24.73	0	0	2.98	101.84	0.00	7.75	0.00	0.00	0.00	0.00	2.33	0.00	0.00	0.46	2.79
16	EF0062-1591.3		0	69.84	0	0	0	29.68	0	0	0	99.52	0.00	8.02	0.00	0.00	0.00	2.98	0.00	0.00	0.00	2.98	
17	EF0062-1591.3		0	69.73	0	0	0	30.08	0	0	0.76	100.57	0.00	7.90	0.00	0.00	0.00	2.98	0.00	0.00	0.12	3.10	
18	EF0062-1591.3		0	68.85	0	0	0	29.39	0	0	0.67	98.91	0.00	7.93	0.00	0.00	0.00	2.96	0.00	0.00	0.11	3.07	
19	EF0062-1591.3		0	68.11	0	0	0	29.43	0	0	0	98.43	0.00	7.84	0.00	0.00	0.00	2.96	0.00	0.00	0.00	2.96	
20	EF0066-1726.05		0	68.72	0	0	0	30.28	0	0	0.86	99.86	0.00	7.84	0.00	0.00	0.00	3.02	0.00	0.00	0.14	3.16	
21	EF67-1724.65		0	70.28	0	9.12	0	16.48	0	0	3.30	99.18	0.00	7.93	0.00	0.00	0.92	0.00	1.62	0.00	0.00	0.53	3.07
22	EF67-1724.65		0	67.15	0	14.4	0	11.41	0	0	3.12	96.08	0.00	7.82	0.00	0.00	1.50	0.00	1.16	0.00	0.00	0.52	3.18

Note: The atomic proportions of members of the series of atokite-rustenburgite (Ato-Rsb) and zvyagintsevite (Zv) are based on a total of 4 apfu, those of niggliite (Nig) are based on 2 apfu, naldrettite (Nld) on 3 apfu, and plumbopalladinite (Ppdn) on 5 apfu, and mertieite-II (Met-II) on a total of 11 apfu. Totals include the following values of minor elements: 1.31 wt.% Fe in analysis #13, 2.23 wt.% Fe in analysis #15, and 0.89 wt.% Fe in analysis #19.

Table 20. Compositions of grains of sperrylite (Sb-bearing), majakite and unnamed $Pd_{11}Ge_3As_2$ in the eastern portion of the Oktyabrsky ore deposit.

#	Sample		Pt	Pd	Ni	As	Sb	Ge	Total (wt.%)	Pt (apfu)	Pd	Ni	As	Sb	As + Sb	Ge
1	EF0035-1546.2	Spy	56.36	0	0	41.47	1.41	0	99.24	1.01	0.00	0.00	1.94	0.04	1.98	0.00
2	EF0035-1546.2		57.86	0	0	42.12	0.99	0	100.97	1.03	0.00	0.00	1.95	0.03	1.98	0.00
3	EF044-1801.05		53.68	1.20	0	40.88	1.30	0	97.06	0.98	0.04	0.00	1.94	0.04	1.98	0.00
4	EF044-1801.05		56.17	0	0	40.19	2.62	0	98.98	1.02	0.00	0.00	1.90	0.08	1.98	0.00
5	EF0062-1591.3		57.74	0	0	39.76	3.19	0	100.69	1.04	0.00	0.00	1.87	0.09	1.96	0.00
6	EF0063-1744.3		55.74	0	0	35.66	7.79	0	99.19	1.04	0.00	0.00	1.73	0.23	1.96	0.00
7	EF0063-1744.3		57.28	0	0	38.64	4.08	0	100.00	1.05	0.00	0.00	1.84	0.12	1.96	0.00
8	EF0066-1684.4		57.34	0	0	41.92	0.74	0	100.00	1.03	0.00	0.00	1.95	0.02	1.97	0.00
9	EF67-1712.0		57.97	0	0	43.48	1.04	0	102.49	1.01	0.00	0.00	1.96	0.03	1.99	0.00
10	EF67-1724.65	Mjk	0	43.50	20.57	31.18	0	0	95.25	0.00	1.04	0.89	1.06	0.00	-	0.00
11	EF67-1724.65	UN	0	75.44	0	10.12	0	14.06	99.62	0.00	10.93	0.00	2.08	0.00	2.08	2.99
12	EF67-1724.65	$Pd_{11}Ge_3As_2$	0	72.60	0	10.46	0	14.23	97.29	0.00	10.72	0.00	2.19	0.00	2.19	3.08

Note: Atomic proportions in compositions of sperrylite (Spy) and majakite (Mjk) are based on a total of 3 atoms per formula unit (apfu), and for unnamed $Pd_{11}Ge_3As_2$ they are based on a total of 16 apfu.

Three of the analyzed compounds are noteworthy. The first is unnamed $\text{Pd}_6\text{Sn}_2\text{As}$ (Table 18), which commonly occurs in direct contact or adjacent to grains of the Cl-rich annite (Figures 27b and 28a). A phase having this formula was previously reported in the Norilsk complex [26]. The likely existence of a separate site for As seems reasonable because of the known differences in the crystal-chemical properties of Sn and As. On the other hand, the possibility of a palovite structure tending towards a formula $\text{Pd}_2(\text{Sn},\text{As})$ cannot be excluded. Insufficient grain sizes precluded a structural study.

The second compound, unnamed $\text{Pd}_{11}\text{Ge}_3\text{As}_2$ (#11, 12 in Table 20), forms minute grains (10 μm across) associated with majakite, at the boundary of a chalcopyrite grain. Alternatively, this arsenide-germanide could represent $\text{Pd}_2(\text{Ge},\text{As})$ as an As-enriched variant of palladogermanide (Pd_2Ge), discovered at the Marathon deposit, Coldwell complex, Ontario, Canada [27,28].

The third phase is the most uncommon and may well represent the first documented example of a Pt-rich arsено-oxysulfide. Its composition is: Pt 34.20, Cu 30.84, Fe 1.29, As 18.57, S 5.23, and O 9.97, for a total of 100.10 wt.%; this can satisfactorily be recalculated to a formula of $(\text{Pt}_{0.82}\text{Fe}_{0.11})\text{Cu}_{2.26}\text{As}_{1.15}\text{S}_{0.76}\text{O}_{2.90}$, based on a total of 8 apfu. The simplified formula is $\text{PtCu}_2\text{AsSO}_3$. As can be seen in Figure 29, this phase formed as a result of the replacement of the precursor sperrylite, which has a notably “pure” and stoichiometric composition ($\text{Pt}_{1.01}\text{As}_{1.99}$); it is also associated with an intermediate member of the kotulskite-sobolevskite solid solution: $\text{Pd}_{1.01}(\text{Te}_{0.50}\text{Bi}_{0.49})$. Note that the observed texture (Figure 29) clearly points to the late formation of the entire grain of intergrown PGM, deposited along the boundary, presumably after the associated grain of Cu-bearing troilite: $(\text{Fe}_{0.97}\text{Cu}_{0.01-0.02})\text{S}_{1.00}$.

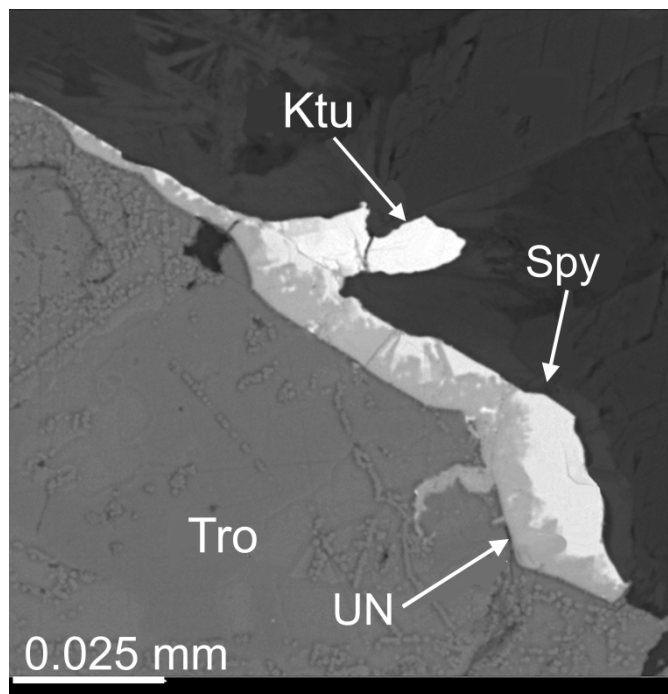


Figure 29. BSE image shows the development of a Pt-Cu arsено-oxysulfide (unnamed $\text{PtCu}_2\text{AsSO}_3$), labeled UN, which replaces sperrylite (Spy) along the boundary of a grain of troilite (Tro) with silicate minerals (dark gray and black in BSE). The label Ktu is kotulskite.

4. Discussion

4.1. Evidence for Extensive Differentiation in the Ore-Bearing Sequences

The associations of ore-forming elements, which are atypical owing to differences in their geochemical nature (cf. Pd-Pt vs. REE, Y, U, Th), are attributed to their incompatible behavior and mutual accumulation at late stages of crystallization in a system that had

attained a high degree of magmatic differentiation. Extensive variations are observed in the compositions of all rock-forming minerals in the eastern portion of the ore deposit (Tables 1 and 2). The overall variations in the ore-bearing sequences are as follows: olivine Mg# 79.8 → 74.1, orthopyroxene Mg# 77.7 → 65.3, clinopyroxene 79.9 → 9.2, and plagioclase An 79.0 → to 3.7 (Ab 96.3). The oxide mineralization also displays extensive ranges, from the most strong in magnesian chromite (MgO 9.62 wt.%; Mg# 43.9) to Cr-bearing magnetite. Compositions of the associated ilmenite evolved from being relatively enriched in Mg (MgO 5.42%) to showing a buildup in Mn (MnO 5.05%), i.e., from geikielite- to pyrophanite-enriched varieties (Table 4).

The observed trends and ranges of compositions of plagioclase and clinopyroxene (Figure 4a,b) greatly exceed those of olivine and orthopyroxene. This contrast is ascribed to a longer-lasting interval of crystallization of the plagioclase and clinopyroxene, from magmatic down to subsolidus conditions of crystallization in the intercumulus (interstitial) parageneses. In contrast, crystallization of the pair of Ol and Opx was confined to an early magmatic stage. Additionally, considerable variations in Mg and Fe are recorded in the amphibole and mica series, with a progressive decrease in Mg content during crystallization (Figure 6a,b).

Thus, we infer that the early parageneses involved grains of magnesian olivine (Mg# 79.8), orthopyroxene (Mg# 77.7) and clinopyroxene (Mg# 79.9), along with calcic plagioclase (An_{79.0}) plus accessory amounts of magnesian chromite (Mg# 43.9). Interestingly, grains of An_{79.0} in the eastern Oktyabrsky area nearly coincide in composition with primocrysts of calcic plagioclase reported from layered intrusions: An₇₈ in the Bushveld complex in South Africa [29], An_{77.6–78.2} in the Sopcha-Nyud-Poaz suite of the Monchepluton complex in the Kola Peninsula [30], and An_{79.2} in the Kivakka layered intrusion, northern Karelia, Russia [31]. Compositions of crystallizing plagioclase (Figure 4b) evolved normally and gradually toward Na-enrichment to attain the minimum An_{3.7} in microvolumes of late interstitial melt.

The compositions of chromian spinel display a common trend of increasing Fe^{3+} (Figure 6a) with a decrease in Mg#, which implies a progressive rise in levels of oxygen fugacity ($f\text{O}_2$) during crystallization. The inferred buildup in $f\text{O}_2$ in a portion of late fluid was likely important to forming the arseno-oxysulfide phase $\text{PtCu}_2\text{AsSO}_3$, under subsolidus conditions, by the oxidation of a precursor grain of sperrylite (Figure 29). The associated grain of Cu-bearing troilite, $(\text{Fe}_{0.97}\text{Cu}_{0.01–0.02})\text{S}_{1.00}$, crystallized prior to the arseno-oxysulfide, thus implying a more reduced environment at the earlier stage.

The positive Mg-Al correlation (Figure 6b) in the spinel phases reflects variations in the spinel *sensu stricto* component, which coexists with forsterite at high temperatures [32]; these values are expected to decrease during crystallization. The same correlation is characteristic of the chromian spinel from the subvolcanic komatiitic complexes in the Pados-Tundra complex and related intrusions of the Serpentinite Belt, Kola Peninsula, Russia [33].

Notable variations are recorded in compositions of the base metal sulfides. The observed ranges in compositions of pyrrhotite, troilite and pentlandite are especially prominent (Figures 18 and 19). The Fe content of pyrrhotite tends to correlate positively with the Fe:Ni ratio of the coexisting pentlandite, as previously reported in other deposits [34,35]. The observed trend of Ni-enrichment in pentlandite (Figure 19) may reflect a progressive rise in the level of sulfur fugacity, $f\text{S}_2$ (cf. [36,37]).

The observed variations in cubanite (or isocubanite, or both) are notable: Fe 1.78–2.04 (mean 1.99), Cu 0.95–1.24 (1.01), and S 2.98–3.04 (3.00), with Cu + Fe 2.96–3.02 apfu. The documented series thus extends toward nonstoichiometric compositions with an excess of Cu. The extent of the excess (1.24 apfu) surpasses that recorded in specimens of nonstoichiometric isocubanite ($\text{Cu}_{1.1}\text{Fe}_{2.0}\text{S}_{3.0}$) in the system Cu-Fe-S [38]. The results of the latter study show that isocubanite is able to crystallize directly from the melt and does not necessarily represent the result of a solid-phase reaction during the transformation of the intermediate solid solution.

Our textural observations of argentopentlandite (e.g., Figure 14b) imply its crystallization from pockets of a residual sulfide melt at late stages. Our results (Figure 15a–c) show that Ni can substitute up to a half of the Ag site, and is incorporated via a coupled mechanism ($\text{Ag} + \text{Fe} \rightarrow \text{Ni}$, in which the Ni-for-Ag substitution at the Ag site is combined with the Ni-for-Fe substitution at the Fe,Ni site). On the basis of a structural analogy with pentlandite, one can expect that levels of $f\text{S}_2$ play an important role in controlling the Ni:Fe ratio in argentopentlandite. Another example of coupled substitution, involving Rh and Co, was reported for pentlandite at Bolshoy Khailyk, western Sayans, Russia: $\text{Rh}^{3+} + \text{Co}^{3+} + \square \rightarrow 3 \text{Fe}^{2+}$ [39]. Related schemes of coupled substitution may well be common in pentlandite-type phases in other deposits.

4.2. Evidence for Cl-Enrichment in Ore-Forming Fluids

The occurrences of atypical mineralization that we investigated are related to moderately low-sulfide zones that developed relatively close to the external contacts of the Oktyabrsky ore deposit (Figure 1). This mineralization involves diverse assemblages of minerals of Pd-Pt, Au-Ag, REE, Y, Zr, Th, and U, which coexist with Cl- and F-enriched species. The ore minerals are associated with Cl-enriched hastingsite (4.06 wt.% Cl; #5, Table 5), ferro-hornblende (2.53 wt.% Cl; #7, Table 5), the chlorine-rich annitic mica (up to 7.54 wt.% Cl; #18, Table 6), chlorapatite (>6 wt.% Cl; Table 7, Figure 11), Cl-bearing members of the chlorite group (chamosite; up to 0.96 wt.% Cl), and a Cl-bearing serpentine (up to 0.79 wt.% Cl).

The Cl-enriched species coexist with assemblages rich in REE, Y, Zr, U, Th, Au-Ag and Pd-Pt. Note, for example, the documented associations of monazite-(Ce) with chlorapatite (Figure 12a), thorite and uraninite, of the unnamed zirconolite-related phase with grains of Cl-rich annite (Figures 13a,b and 14a), and of the platinum group minerals (sobolevskite-kotulskite, mertieite, Pd-Sn-(As) alloy and sperrylite) with the Cl-rich annite (Figures 22b, 24b, 27a,b and 28a,b). In addition, the veinlet-like grains of sperrylite display an intimate association with a Cl-rich apatite (4.17 wt.% Cl). These findings point to the existence of high levels of Cl in the fluid medium during the crystallization of the ore-bearing sequences.

The compositional variations (Tables 5 and 6 and Figure 7a–c) show a clear relationship between the Cl-enrichment and corresponding enrichments in K and Fe in compositions of the amphiboles and micas. These relationships are consistent with crystallochemical concepts [40]. The positive Fe vs. Cl correlation (Figure 8c) and the observed relationships of Cl with K indicate that Cl efficiently accumulated in a fluid phase associated with portions of late interstitial melts rich in Fe and K.

A close association of Pd-Ag tellurides with a Cl-rich amphibole, i.e., the Cl-dominant analogue of ferro-pargasite (up to 4.5 wt.% Cl; 1.2 Cl apfu), was previously reported from the Lukkulaisvaara layered intrusion, Kola Peninsula, Russia. Pods of plagioclase-bearing orthopyroxenite rich in Cu-Fe-Ni sulfide mineralization and rich in Pd, Pt and Ag probably formed by the in situ crystallization of isolated volumes of H_2O -saturated melt at Lukkulaisvaara [41,42]. Inclusions of lukkulaisvaaraite, $\text{Pd}_{14}\text{Ag}_2\text{Te}_9$ [43], hosted by grains of ferro-chloro-pargasite, clearly formed in a Cl-rich environment [41]. Another occurrence of ferro-chloro-pargasite (4.1 wt.% Cl), reported at Mount Poaz in the Monchepluton layered complex, Kola Peninsula, Russia, formed as a result of an autometasomatic reaction involving a hydrous fluid with plagioclase and pyroxene [30]. This rare species of amphibole, containing up to 6.34 wt.% Cl and 1.74 Cl apfu, was also described in the Tudor gabbroic complex, north of Madoc, Ontario, Canada [44]. Interestingly, notable amounts of Cl are present in shoshonite-type (K-enriched) silicate melt inclusions hosted by PGE alloys [45].

A strong Cl-enrichment in the medium also accounts for the abundance of Cl-rich apatite in the ore zones. Extensive solid solutions involving the components chlorapatite, fluorapatite and hydroxylapatite are documented in the F-Cl-OH diagram (Figure 11). These variations extend to the end member chlorapatite and involve compositionally heterogeneous, cryptically zoned grains, as well as grain-to-grain variations present in the

same sample (Table 7, Figure 10). These characteristics are consistent with data on apatite compositions from the Monchepluton layered complex, in which the degassing of the crystallizing melt caused a decoupling of Cl and F [30]. Fluorine mostly remained in the melt; in contrast, Cl was partitioned efficiently into an H₂O-bearing fluid phase. Consequently, the early-stage apatite incorporated combinations of OH and F, with a low content of Cl. At a late stage, chlorapatite crystallized from a Cl-rich fluid, and ferro-chloro-pargasite formed at Poaz [30]. The geochemical behavior of Cl was traced on the basis of findings related to apatite from layered intrusions. The maximum Cl recorded in compositions of apatite, close to the level of the Pd-Pt horizon, likely corresponds to the first appearance and the massive crystallization of plagioclase primocrysts at Kivakka, Karelia, Russia [31,46]. Similarly, a relationship exists between the stratigraphic levels of the crystallization of chlorapatite and zones of relative Pd-Pt enrichments at Kläppsjö, Sweden [47]. Especially high contents of Cl are present in a compound of Pb-Cl-(OH) composition associated with PGM in the Merensky Reef, Bushveld complex, South Africa [48]. Occurrences of bowlesite, PtSnS [49], are present in the Reef. In layered intrusions, chlorapatite typically tends to occur in lower units of ultramafic cumulates [50–52]. However, no definite relationships have been found at Monchepluton, Russia, between extents of magnesium enrichment and levels of Cl in the apatite [30].

Our study reveals the presence of apatite grains of varying compositions, which can range from fluorapatite to chlorapatite in the same sample (Table 7). These variations are attributed to the process of the degassing of the crystallizing melt, with the decoupling of Cl and F. The presence of micrometric inclusion of a La-dominant carbonate-fluoride phase, related to basträsite (hosted by plagioclase), is consistent with the inferred decoupling of F from Cl. The likely source of Cl at Norilsk is thus presumably intrinsic and related to magmatic differentiation. This inference is consistent with the exotic occurrences of Pd-Bi chlorides documented in the ore of this complex [53].

4.3. Characteristic Features of Pd-Pt Mineralization

The zones of noble metal mineralization investigated in the eastern part of the Oktyabrsky deposit bear some notable similarities to the classic deposits at Norilsk. For instance, the major species of PGM, i.e., Pd-(Ag)-Pt tellurides, bismuthotellurides and Pd-Pt stannides (Table 3), are generally common in the massive or high-grade deposits rich in sulfides of the Norilsk complex (cf. [2,26]). Furthermore, a close association with Au-Ag alloys is present, as is very typical at Norilsk.

On the other hand, there are certain prominent and distinctive characteristics, based on our findings. (1) The mean dimension of PGM grains is micrometer-sized ($\leq 10 \mu\text{m}$ across) in the ore assemblages examined. (2) The majority of the PGM exhibit evidence of late crystallization, commonly taking place after the deposition of grains of the associated base metal sulfides (BMS). As a result, these PGM phases typically occur at the boundary of the BMS with silicate minerals (Figures 20a,b, 22a,b, 23a,b, 27a,b and 29). (3) The documented association of PGM with the Cl-enriched species is important, including representatives of the series of chlorine-enriched micas and amphiboles (Figures 22b, 24b, 27a,b and 28a,b). (4) The atypical association of PGM with various species enriched in REE, Y, Zr, Th, U, and Cl-F is a prominent feature. (5) Species of Pd-Pt-Cu stannides, i.e., taimyrite, cabriite and tatyanaite, which are very abundant in the massive sulfide ores [2,54–57], are virtually absent in our specimens. (6) The occurrence of a Ge-bearing phase of PGM, i.e., the unnamed Pd₁₁Ge₃As₂ or Pd₂(Ge,As), is a distinctive feature. The Ge-based species of PGM occur very rarely worldwide, with a type locality known in the Marathon Cu-Pd deposit of the Coldwell alkaline complex in Canada [27,28]. They are also found in the Yoko-Dovyren pluton, Baikal region, Russia [58]. (7) The appearance of an arseno-oxysulfide phase, PtCu₂AsSO₃ hitherto unreported, was a result of a local buildup of *fO₂* during a late fluid and subsolidus reaction with the precursor sperrylite (Figure 29). Copper was likely remobilized and contributed by the fluid, and was likely released from the associated chalcopyrite, whereas the S was contributed by the associated troilite.

Several PGE-based oxides have been described in different settings and complexes, including Pb-, Sb-, Bi-, and Tl-bearing oxides, which reflect the compositions of the precursor PGM grains [59–64]. However, at least some of these grains could be composed of cryptic mixtures. No bonding was found to occur between platinum and oxygen in a Pt-Fe oxide grain studied by X-ray absorption spectroscopy [65], and so this likely corresponds to a mixture rather than a single mineral species.

The textural relations (Figures 20a,b, 22a,b, 23a,b, 27a,b and 29) are indicative of the late crystallization of the complex mineralization of Pd-Pt-Au-Au and associated species enriched in REE, Y, Zr, U, and Th (Figures 12a,b, 13a,b and 14a) from batches of Cl-enriched fluid under submagmatic conditions of crystallization. The low temperatures of the deposition of the PGM are consistent with experimental results. The values of the upper limit of stability are low for synthetic analogues of sopcheite $\text{Ag}_4\text{Pd}_3\text{Te}_4$ (383°C), froodite PdBi_2 ($\sim 480^\circ\text{C}$), michenerite Pd-Te-Bi (501°C), sobolevskite PdBi and kotulskite PdTe ($\sim 750^\circ\text{C}$) [66–69]. In addition, synthetic specimens of kotulskite, merenskyite PdTe_2 , atokite Pd_3Sn and palovite Pd_2Sn are stable at 400°C in the systems Pd-Sn and Pd-Te [70]. It is likely that a high-temperature crystallization ($>800^\circ\text{C}$) of sperrylite can proceed directly from a silicate melt [71], as was proposed in the case of this PGM in a low-sulfide horizon of the Noril'sk 1 intrusion, Russia [10]. However, this mode of origin appears highly unlikely in our case. Indeed, veinlets or rim-like grains of sperrylite have formed in the specimens examined, such as those shown in Figures 5b and 29. These conclusively point to the late formation of the entire ore assemblage in the presence of Cl and other volatiles in the growth medium at a low temperature during a submagmatic stage of crystallization. This inference is corroborated by the occurrence of hydrothermally formed sperrylite in the Imandra layered complex, Kola Peninsula, Russia [72]. In addition, sperrylite is the main species of PGM in the Copper Cliff South mine associated with the Sudbury structure, Ontario, Canada, at which the existence of Cl-bearing fluids is inferred [73].

5. Conclusions

1. The compositional variations described here document the extensive differentiation of the primary melt attained in ore-bearing zones close to the eastern contact of the Oktyabrsky ore deposit. As a result, a great variety of ore constituents (e.g., Pd-Pt, Au-Ag, REE, Y, Zr, U and Th), all rather incompatible, accumulated in that zone. Involved as well were chalcogens (S, Se, Te, O), semimetals (Sb, As, Ge) and metals (Bi, Pb, Sn), which can form ligands with the PGE in a Cl-rich fluid.
2. The newly recognized style of complex mineralization enriched in the incompatible constituents represents a variant of ore at Norilsk, the potential value of which may be enhanced by the complexity and diversity of the ore constituents.
3. We suppose that the abundance of Cl and other volatiles in the fluid-enriched system has promoted the remobilization and deposition of polycomponent mineralization in zones of deuteritic alteration, likely controlled by faults, or in ore zones of contact type, or possibly even in detached zones hosted by wallrocks in the exocontact of the Norilsk complex. One can expect such zones to resemble the Kirrakkajuppura PGE mineralization of the Penikat complex in Finland, which has huge grades of Pd and Pt that developed in virtually BMS-free rocks [60,61].

Author Contributions: The authors wrote the article together. A.Y.B., interpretations, conclusions, writing; I.I.N., investigations, sampling, writing; A.A.N., writing, diagrams, discussions; B.M.L., observations, analytical results, writing; S.A.S., analytical results, reflectance measurements, diagrams, writing; R.F.M., discussions, conclusions, writing. All authors have read and agreed to the published version of the manuscript.

Funding: This research received no specific grant.

Data Availability Statement: The data are available upon reasonable request (from A.Y.B.).

Acknowledgments: We thank the Editorial board members and three anonymous reviewers for their constructive comments. We are grateful to Igor V. Pekov for his attempts to study the zirconolite-related mineral via single-crystal diffraction. Support from the Cherepovets State University is acknowledged (A.Y.B. and A.A.N.).

Conflicts of Interest: The authors declare no conflict of interest.

References

1. Nikulin, I.I. *Geology of the Norilsk Metallogenic Province*; The Public Joint Stock Company “Mining and Metallurgical Company “NORILSK NICKEL”; OOO Maks Press: Moscow, Russia, 2020; p. 524. (In Russian)
2. Genkin, A.D.; Distler, V.V.; Gladyshev, D.G.; Filimonova, A.A.; Evstigneeva, T.L.; Kovalenker, V.A.; Laputina, I.P.; Smirnov, A.V.; Grokhovskaya, T.L. *Sulphide Copper-Nickel Ores of the Noril’sk Deposits*; Publishing House Nauka: Moscow, Russia, 1981; p. 238. (In Russian)
3. Campbell, I.H.; Czamanske, G.K.; Fedorenko, V.A.; Hill, R.J.; Stepanov, V. Synchronism of the Siberian traps and the Permian-Triassic boundary. *Science* **1992**, *258*, 1760–1763. [[CrossRef](#)]
4. Naldrett, A.J. A model for the Ni-Cu-PGE ores of the Noril’sk region and its application to other areas of flood basalt. *Econ. Geol.* **1992**, *87*, 1945–1962. [[CrossRef](#)]
5. Naldrett, A.J. World-class Ni-Cu-PGE deposits: Key factors in their genesis. *Mineral. Depos.* **1999**, *34*, 227–240. [[CrossRef](#)]
6. Sobolev, A.V.; Krivolutskaya, N.A.; Kuzmin, D.V. Petrology of the parental melts and mantle sources of Siberian trap magmatism. *Petrology* **2009**, *17*, 253–286. [[CrossRef](#)]
7. Cabri, L.J.; Wilson, J.M.D.; Distler, V.V.; Kingston, D.; Nejedlý, Z.; Sluzhenikin, S.F. Mineralogical distribution of trace platinum group elements in the disseminated sulphide ores of Noril’sk 1 layered intrusion. *Appl. Earth Sci.* **2002**, *111*, 15–22. [[CrossRef](#)]
8. Arndt, N.T.; Czamanske, G.K.; Walker, R.J.; Chauvel, C.; Fedorenko, V.A. Geochemistry and origin of the intrusive hosts of the Noril’sk-Talnakh Cu-Ni-PGE sulfide deposits. *Econ. Geol.* **2003**, *98*, 495–515. [[CrossRef](#)]
9. Sluzhenikin, S.F.; Mokhov, A.V. Gold and silver in PGE-Cu-Ni and PGE ores of the Noril’sk deposits, Russia. *Mineral. Depos.* **2015**, *50*, 465–492. [[CrossRef](#)]
10. Tolstykh, N.D.; Zhitova, L.M.; Shapovalova, M.O.; Chayka, I.F. The evolution of the ore-forming system in the low sulfide horizon of the Noril’sk 1 intrusion, Russia. *Mineral. Mag.* **2019**, *83*, 673–694. [[CrossRef](#)]
11. Morimoto, N. Nomenclature of pyroxenes. *Can. Mineral.* **1989**, *27*, 143–156. [[CrossRef](#)]
12. Barnes, S.J.; Kunilov, V.Y. Spinels and Mg ilmenites from the Noril’sk 1 and Talnakh intrusions and other mafic rocks of the Siberian Flood Basalt Province. *Econ. Geol.* **2000**, *95*, 1701–1717. [[CrossRef](#)]
13. Chukanov, N.V.; Zubkova, N.V.; Pekov, I.V.; Vigasina, M.F.; Polekhovsky, Y.S.; Ternes, B.; Schüller, W.; Britvin, S.N.; Pushcharovsky, D.Y. Stefanweissite, $(\text{Ca},\text{REE})_2\text{Zr}_2(\text{Nb},\text{Ti})(\text{Ti},\text{Nb})_2\text{Fe}^{2+}\text{O}_{14}$, a new zirconolite-related mineral from the Eifel paleovolcanic region, Germany. *Mineral. Mag.* **2019**, *83*, 607–614. [[CrossRef](#)]
14. Chukanov, N.; Zubkova, N.; Britvin, S.; Pekov, I.; Vigasina, M.; Schäfer, C.; Ternes, B.; Schüller, W.; Polekhovsky, Y.; Ermolaeva, V.; et al. Nöggerathite-(Ce), $(\text{Ce},\text{Ca})_2\text{Zr}_2(\text{Nb},\text{Ti})(\text{Ti},\text{Nb})_2\text{Fe}^{2+}\text{O}_{14}$, a new zirconolite-related mineral from the Eifel volcanic region, Germany. *Minerals* **2018**, *8*, 449. [[CrossRef](#)]
15. Chukanov, N.V.; Krivovichev, S.V.; Pakhomova, A.S.; Pekov, I.V.; Schäfer, C.; Vigasina, M.F.; Van, K.V. Laachite, $(\text{Ca},\text{Mn})_2\text{Zr}_2\text{Nb}_2\text{TiFeO}_{14}$, a new zirconolite-related mineral from the Eifel volcanic region, Germany. *Eur. J. Mineral.* **2014**, *26*, 103–111. [[CrossRef](#)]
16. Hall, S.R.; Stewart, J.M. The crystal structure of argentian pentlandite $(\text{Fe},\text{Ni})_8\text{AgS}_8$, compared with the refined structure of pentlandite $(\text{Fe},\text{Ni})_9\text{S}_8$. *Can. Mineral.* **1973**, *12*, 169–177.
17. Groves, D.I.; Hall, S.R. Argentian pentlandite with parkerite, josite A and the probable Bi-analogue of ullmannite from Mount Windarra, Western Australia. *Can. Mineral.* **1978**, *16*, 1–7.
18. Morales-Ruano, S.; Hach-Alí, P.F. Hydrothermal argentopentlandite at El Charcón, southeastern Spain: Mineral chemistry and conditions of formation. *Can. Mineral.* **1996**, *34*, 939–947.
19. Bud’ko, I.A.; Kulagov, E.A. The new mineral talnakhite, a cubic variety of chalcopyrite. *Zap. Vses. Mineral. Obshch* **1968**, *97*, 63. (In Russian)
20. Cabri, L.J.; Hall, S. Mooihoekeite and haycockite, two new copper-iron sulfides, and their relationship to chalcopyrite and talnakhite. *Am. Mineral.* **1972**, *57*, 5–6.
21. Rowland, J.F.; Hall, S.R. Haycockite, $\text{Cu}_4\text{Fe}_5\text{S}_8$: A superstructure in the chalcopyrite series. *Acta Crystallogr. B* **1975**, *31*, 2105–2112. [[CrossRef](#)]
22. Cabri, L.J.; Harris, D.C. New compositional data for talnakhite, $\text{Cu}_{18}(\text{Fe},\text{Ni})_{16}\text{S}_{32}$. *Econ. Geol.* **1971**, *66*, 673–675. [[CrossRef](#)]
23. Kravchenko, T.A.; Nenasheva, S.N. An experimental investigation of phase co#position in areas of crystallization of the chalcopyrite solid solution. *Vestn. Otd. Nauk Zemle RAN* **2012**, *4*, NZ9001. [[CrossRef](#)]
24. Makovicky, E. Crystal structures of sulfides and other chalcogenides. *Rev. Mineral. Geochem.* **2006**, *61*, 7–125. [[CrossRef](#)]
25. Brese, N.E.; von Schnerring, H.G. Bonding trends in pyrites and a reinvestigation of the structures of PdAs_2 , PdSb_2 , PtSb_2 and PtBi_2 . *Z. Anorg. Allg. Chem.* **1994**, *620*, 393–404. [[CrossRef](#)]
26. Genkin, A.D.; Evstigneeva, T.L. Associations of platinum group minerals of the Noril’sk copper-nickel sulfide ores. *Econ. Geol.* **1986**, *81*, 1203–1212. [[CrossRef](#)]

27. McDonald, A.M.; Ames, D.E.; Kjarsgaard, I.M.; Cabri, L.J.; Zhe, W.; Ross, K.C.; Good, D.J. Marathonite, $Pd_{25}Ge_9$, and palladogermanide, Pd_2Ge , two new platinum group minerals from the Marathon deposit, Coldwell Complex, Ontario, Canada: Descriptions, crystal chemical considerations and genetic implications. *Can. Mineral.* **2021**, *59*, in press.
28. Ames, D.E.; Kjarsgaard, I.M.; McDonald, A.M.; Good, D.J. Insights into the extreme PGE enrichment of the W horizon, Marathon Cu-Pd deposit, Coldwell alkaline complex, Canada: Platinum group mineralogy, compositions and genetic implications. *Ore Geol. Rev.* **2017**, *90*, 723–747. [[CrossRef](#)]
29. Cawthorn, R.G.; Ashwal, L.D. Origin of anorthosite and magnetitite layers in the Bushveld Complex, constrained by major element compositions of plagioclase. *J. Petrol.* **2009**, *50*, 1607–1637. [[CrossRef](#)]
30. Barkov, A.Y.; Sharkov, E.V.; Nikiforov, A.A.; Korolyuk, V.N.; Silyanov, S.A.; Lobastov, B.M. Compositional variations of apatite and REE-bearing minerals in relation to crystallization trends in the Monchepluton layered complex (Kola Peninsula). *Russ. Geol. Geophys.* **2021**, *62*, 427–444. [[CrossRef](#)]
31. Barkov, A.Y.; Nikiforov, A.A. Compositional variations of apatite, fractionation trends, and a PGE-bearing zone in the Kivakka layered intrusion, northern Karelia, Russia. *Can. Mineral.* **2016**, *54*, 475–490. [[CrossRef](#)]
32. Jamieson, H.E.; Roeder, P.L. The distribution of Mg and Fe^{2+} between olivine and spinel at 1300 °C. *Am. Mineral.* **1984**, *69*, 283–291.
33. Barkov, A.Y.; Nikiforov, A.A.; Barkova, L.P.; Korolyuk, V.N.; Martin, R.F. Zones of PGE-chromite mineralization in relation to crystallization of the Pados-Tundra ultramafic complex, Serpentinite Belt, Kola Peninsula, Russia. *Minerals* **2021**, *11*, 68. [[CrossRef](#)]
34. Harris, D.C.; Nickel, E.H. Pentlandite compositions and associations in some mineral deposits. *Can. Mineral.* **1972**, *11*, 861–878.
35. Harney, D.M.W.; Merkle, R.K.W. Sulfide mineralogy at the main magnetite layer, Upper Zone, eastern Bushveld Complex, and the effect of hydrothermal processes on pentlandite composition. *Eur. J. Mineral.* **1992**, *4*, 557–570. [[CrossRef](#)]
36. Kolonin, G.R.; Orsoev, D.A.; Sinyakova, E.F.; Kislov, E.V. The use of Ni: Fe ratio in pentlandite for estimation of sulfur fugacity during the formation of PGE-bearing sulfide mineralization of Yoko-Dovyren Massif. *Dokl. Earth Sci.* **2000**, *370*, 75–79. (In Russian)
37. Tolstykh, N.; Shvedov, G.; Polonyankin, A.; Korolyuk, V. Geochemical features and mineral associations of differentiated rocks of the Norilsk 1 intrusion. *Minerals* **2020**, *10*, 688. [[CrossRef](#)]
38. Kosyakov, V.I.; Sinyakova, E.F. Study of crystallization of nonstoichiometric isocubanite $Cu_{1.1}Fe_{2.0}S_{3.0}$ from melt in the system Cu–Fe–S. *J. Therm. Anal. Calorim.* **2017**, *129*, 623–628. [[CrossRef](#)]
39. Barkov, A.Y.; Shvedov, G.; Silyanov, S.; Martin, R.F. Mineralogy of platinum group elements and gold in the ophiolite-related placer of the River Bolshoy Khailyk, western Sayans, Russia. *Minerals* **2018**, *8*, 247. [[CrossRef](#)]
40. Oberti, R.; Ungaretti, L.; Cannillo, E.; Hawthorne, F.C. The mechanism of Cl incorporation in amphibole. *Am. Mineral.* **1993**, *78*, 746–752.
41. Barkov, A.Y.; Martin, R.F.; Tarkian, M.; Poirier, G.; Thibault, Y. Pd–Ag tellurides from a Cl-rich environment in the Lukkulaisvaara layered intrusion, northern Russian Karelia. *Can. Mineral.* **2001**, *39*, 639–653. [[CrossRef](#)]
42. Barkov, A.Y.; Martin, R.F.; Laajoki, K.V.O.; Alapieti, T.T.; Iljina, M.J. Paragenesis and origin of staurolite from a palladium-rich gabbronorite: An unusual occurrence from the Lukkulaisvaara layered intrusion, Russian Karelia. *Neues Jahrb. Mineral. Abh.* **1999**, *175*, 191–222. [[CrossRef](#)]
43. Vymazalová, A.; Grokhovskaya, T.L.; Laufek, F.; Rassulov, V.A. Lukkulaisvaaraite, $Pd_{14}Ag_2Te_9$, a new mineral from Lukkulaisvaara intrusion, northern Russian Karelia, Russia. *Min. Mag.* **2014**, *78*, 1743–1754. [[CrossRef](#)]
44. Duesterhoeft, E.; Raase, P.; Gremler, P. A new occurrence of extremely rare ferro-chloro-pargasite in Tudor, Ontario. *Int. J. Earth Sci.* **2017**, *106*, 2815–2816. [[CrossRef](#)]
45. Belkin, H.E.; Grosz, A.E. Platinum and gold placer from Tugidak Island, Alaska: Platinum group minerals and their inclusions, gold, and chromite mineralogy. *Can. Mineral.* **2021**, *59*, 667–712. [[CrossRef](#)]
46. Barkov, A.Y.; Nikiforov, A.A. A new criterion of searching for zones of PGE mineralization of the Kivakka Reef type. *Vestnik VGU Geol.* **2015**, *4*, 75–83. (In Russian)
47. Meurer, W.P.; Hellström, F.A.; Claeson, D.T. The relationship between chlorapatite and PGE-rich cumulates in layered intrusions: The Kläppsjö gabbro, north-central Sweden, as a case study. *Can. Mineral.* **2004**, *42*, 279–289. [[CrossRef](#)]
48. Barkov, A.Y.; Martin, R.F.; Kaukonen, R.J.; Alapieti, T.T. The occurrence of Pb–Cl–(OH) and Pt–Sn–S compounds in the Merensky Reef, Bushveld layered complex, South Africa. *Can. Mineral.* **2001**, *39*, 1397–1403. [[CrossRef](#)]
49. Vymazalová, A.; Zaccarini, F.; Garuti, G.; Laufek, F.; Mauro, D.; Stanley, C.J.; Biagioni, C. Bowlesite, $PtSnS$, a new platinum group mineral (PGM) from the Merensky Reef of the Bushveld Complex, South Africa. *Mineral. Mag.* **2020**, *84*, 468–476. [[CrossRef](#)]
50. Boudreau, A.E.; McCallum, I.S. Investigations of the Stillwater Complex. V. Apatites as indicators of evolving fluid composition. *Contrib. Mineral. Petrol.* **1989**, *102*, 138–153. [[CrossRef](#)]
51. Boudreau, A.E.; Mathez, E.A.; McCallum, I.S. Halogen geochemistry of the Stillwater and Bushveld complexes: Evidence for transport of the platinum group elements by Cl-rich fluids. *J. Petrol.* **1986**, *27*, 967–986. [[CrossRef](#)]
52. Cawthorn, R.G. Formation of chlor- and fluorapatite in layered intrusions. *Mineral. Mag.* **1994**, *58*, 299–306. [[CrossRef](#)]
53. Karpenkov, A.M.; Rudashevsky, N.S.; Shumskaya, N.I. Natural palladium bismuth chloride phase of $Pd_4Bi_5Cl_3$ composition. *Zap. Vses. Mineral. Obshch.* **1981**, *110*, 86–91. (In Russian) [[CrossRef](#)]
54. Estignevea, T.L.; Genkin, A.D. Cabriite, Pd_2SnCu , a new mineral species in the mineral group of palladium, tin and copper compounds. *Can. Mineral.* **1983**, *21*, 481–487.

55. Barkov, A.Y.; Martin, R.F.; Poirier, G.; Yakovlev, Y.N. The taimyrite-tatyanaite series and zoning in intermetallic compounds of Pt, Pd, Cu, and Sn from Noril'sk, Siberia, Russia. *Can. Mineral.* **2000**, *38*, 599–609. [[CrossRef](#)]
56. Barkov, A.Y.; Martin, R.F.; Poirier, G.; Tarkian, M.; Pakhomovskii, Y.A.; Men'shikov, Y.P. Tatyanaite, a new platinum group mineral, the Pt analogue of taimyrite, from the Noril'sk complex (northern Siberia, Russia). *Eur. J. Mineral.* **2000**, *12*, 391–396. [[CrossRef](#)]
57. Barkov, A.Y.; Martin, R.F. Compositional variations in natural intermetallic compounds of Pd, Pt, Cu, and Sn: New data and implications. *Can. Mineral.* **2016**, *54*, 453–460. [[CrossRef](#)]
58. Spiridonov, E.M.; Orsoev, D.A.; Ariskin, A.A.; Kislov, E.V.; Korotaeva, N.N.; Nikolaev, G.S.; Yapaskurt, V.O. Germanium-rich palladium minerals of palladogermanide Pd_2Ge , paolovite $Pd_2(Sn, Ge)$, and zvyagintsevite in sulfide-bearing anorthosites of the Yoko-Dovyren pluton, Baikal area. *Geochem. Int.* **2019**, *57*, 600–603. [[CrossRef](#)]
59. Augé, T.; Legendre, O. Platinum group element oxides from the Pirogues ophiolitic mineralization, New Caledonia; origin and significance. *Econ. Geol.* **1994**, *89*, 1454–1468. [[CrossRef](#)]
60. Barkov, A.Y.; Halkoaho, T.A.A.; Roberts, A.C.; Criddle, A.J.; Martin, R.F.; Papunen, H. New Pd-Pb and Pb-V oxides from a bonanza-type PGE-rich, nearly BMS-free deposit in the Penikat layered complex, Finland. *Can. Mineral.* **1999**, *37*, 1507–1524.
61. Barkov, A.Y.; Fleet, M.E.; Martin, R.F.; Halkoaho, T.A.A. New data on “bonanza”-type PGE mineralization in the Kirakkajuppura PGE deposit, Penikat layered complex, Finland. *Can. Mineral.* **2005**, *43*, 1663–1686. [[CrossRef](#)]
62. Tolstykh, N.D.; Krivenko, A.P.; Lavrent'ev, Y.G.; Tolstykh, O.N.; Korolyuk, V.N. Oxides of the Pd-Sb-Bi system from the Chiney massif (Aldan Shield, Russia). *Eur. J. Mineral.* **2000**, *12*, 431–440. [[CrossRef](#)]
63. Shcheka, G.G.; Lehmann, B.; Solianik, A.N. Pd-bearing oxides and hydrated oxides in mertieite-II crystals from alluvial sediments of the Darya river, Aldan Shield, Russia. *Mineral. Mag.* **2005**, *69*, 981–994. [[CrossRef](#)]
64. Barkov, A.Y.; Shvedov, G.I.; Polonyankin, A.A.; Martin, R.F. New and unusual Pd-Tl-bearing mineralization in the Anomal'nyi deposit, Kondyor concentrically zoned complex, northern Khabarovskiy kray, Russia. *Mineral. Mag.* **2017**, *81*, 679–688. [[CrossRef](#)]
65. Hattori, K.H.; Takahashi, Y.; Augé, T. Mineralogy and origin of oxygen-bearing platinum–iron grains based on an X-ray absorption spectroscopy study. *Am. Mineral.* **2010**, *95*, 622–630. [[CrossRef](#)]
66. Kim, W.S.; Chao, G.Y.; Cabri, L.J. Phase relations in the Pd–Te system. *J. Less Common Met.* **1990**, *162*, 61–74. [[CrossRef](#)]
67. Hoffman, E.L.; MacLean, W.H. Phase relations of michenerite and merenskyite in the Pd–Bi–Te system. *Econ. Geol.* **1976**, *71*, 1461–1468. [[CrossRef](#)]
68. Kristavchuk, A.V.; Zabolotskaya, A.V.; Voronin, M.V.; Chareev, D.A.; Osadchii, E.G. Temperature dependence of tellurium fugacity for the kotulskite ($PdTe$)—merenskyite ($PdTe_2$) equilibrium determined by the method of a solid-state galvanic cell. *Phys. Chem. Miner.* **2021**, *48*, 16. [[CrossRef](#)]
69. Vymazalová, A.; Laufek, F.; Kristavchuk, A.V.; Chareev, D.A.; Drábek, M. The system Ag–Pd–Te: Phase relations and mineral assemblages. *Mineral. Mag.* **2015**, *79*, 1813–1832. [[CrossRef](#)]
70. Vymazalová, A.; Drábek, M. The system Pd–Sn–Te at 400 °C and mineralogical implications. I. The binary phases. *Can. Mineral.* **2010**, *48*, 1041–1050. [[CrossRef](#)]
71. Bai, L.; Barnes, S.-J.; Baker, D.R. Sperrylite saturation in magmatic sulfide melts: Implications for formation of PGE-bearing arsenides and sulfarsenides. *Am. Mineral.* **2017**, *102*, 966–974. [[CrossRef](#)]
72. Barkov, A.Y.; Fleet, M.E. An unusual association of hydrothermal platinum group minerals from the Imandra layered complex, Kola Peninsula, northwestern Russia. *Can. Mineral.* **2004**, *42*, 455–467. [[CrossRef](#)]
73. Magyarosi, Z.; Watkinson, D.H.; Jones, P.C. Mineralogy of Ni-Cu-platinum group element sulfide ore in the 800 and 810 orebodies, Copper Cliff South mine, and P-T-X conditions during the formation of platinum group minerals. *Econ. Geol.* **2002**, *97*, 147–1486. [[CrossRef](#)]